Journal of Computational Physics 276 (2014) 691–728

Contents lists available at ScienceDirect

Journal of Computational Physics

www.elsevier.com/locate/jcp

An efficient algorithm for incompressible N-phase flows

S. Dong

Center for Computational and Applied Mathematics, Department of Mathematics, Purdue University, United States

ARTICLE INFO

Article history:
Received 7 November 2013
Received in revised form 17 April 2014
Accepted 2 August 2014
Available online 7 August 2014

Keywords:
N-phase flow
Large density contrast
Large viscosity contrast
Phase field
Multiphase flow
Pairwise surface tensions

ABSTRACT

We present an efficient algorithm within the phase field framework for simulating the motion of a mixture of N ($N \geqslant 2$) immiscible incompressible fluids, with possibly very different physical properties such as densities, viscosities, and pairwise surface tensions. The algorithm employs a physical formulation for the N-phase system that honors the conservations of mass and momentum and the second law of thermodynamics. We present a method for uniquely determining the mixing energy density coefficients involved in the N-phase model based on the pairwise surface tensions among the N fluids. Our numerical algorithm has several attractive properties that make it computationally very efficient: (i) it has completely de-coupled the computations for different flow variables, and has also completely de-coupled the computations for the $(N-1)$ phase field functions; (ii) the algorithm only requires the solution of linear algebraic systems after discretization, and no nonlinear algebraic solve is needed; (iii) for each flow variable the linear algebraic system involves only constant and time-independent coefficient matrices, which can be pre-computed during pre-processing, despite the variable density and variable viscosity of the N-phase mixture; (iv) within a time step the semi-discretized system involves only individual *de-coupled* Helmholtz-type (including Poisson) equations, despite the strongly-coupled phase–field system of fourth spatial order at the continuum level; (v) the algorithm is suitable for large density contrasts and large viscosity contrasts among the N fluids. Extensive numerical experiments have been presented for several problems involving multiple fluid phases, large density contrasts and large viscosity contrasts. In particular, we compare our simulations with the de Gennes theory, and demonstrate that our method produces physically accurate results for multiple fluid phases. We also demonstrate the significant and sometimes dramatic effects of the gravity, density ratios, pairwise surface tensions, and drop sizes on the N-phase configurations and dynamics. The numerical results show that the method developed herein is capable of dealing with N-phase systems with large density ratios, large viscosity ratios, and pairwise surface tensions, and that it can be a powerful tool for studying the interactions among multiple types of fluid interfaces.

© 2014 Elsevier Inc. All rights reserved.

1. Introduction

The current work concerns the simulation of a mixture of N ($N \geqslant 2$) immiscible incompressible fluids, with possibly very different physical properties such as densities, viscosities and inter-fluid surface tensions. Such incompressible N-phase

---

E-mail address: sdong@math.purdue.edu.

http://dx.doi.org/10.1016/j.jcp.2014.08.002
0021-9991/© 2014 Elsevier Inc. All rights reserved.

flows admit multiple types of fluid interfaces and three-phase lines or junctures, and they underline many phenomena and processes of practical engineering significance and fundamental physical interest.

From the applications perspective, the N-phase problem has particular relevance and importance in light of the present issues on the environment and energy. A dramatic example in this regard is the BP oil spill in the Gulf of Mexico in 2010 (involving at least three fluid phases: oil, water, gas/air), which released an estimated 4.9 million barrels of oil into the ocean [1], causing enormous and extensive damage to the environment, marine and wild life habitats, fishing and tourism industries. Another example is in the enhanced oil recovery and geological CO_2 storage in depleted oil/gas reservoirs. Most enhanced oil-recovery techniques involve multiple fluid phases, where a gas, which could be air, natural gas or CO_2, is injected into a reservoir containing oil and water. The use of CO_2 injected into mature oil fields is likely to become increasingly common and important not only to improve oil recovery but for carbon sequestration. Emulsions and foams are other examples of applications, where one or more fluid phases are dispersed in another continuous phase [49,54]. These problems are also encountered in our everyday environment such as showers, kitchens, pharmaceutical sprays, rain drops, air bubbles and ocean waves. Oftentimes the bubble/droplet generation, coalescence, and breakup are involved.

From the fundamental physics perspective, the dynamics of N-phase flows probes a wide range of fundamental physical properties such as multiple pairwise surface tensions, three-phase lines, viscosity contrasts, and density contrasts. It involves the interactions among multiple types of fluid interfaces, and the formation of contact angles among multiple materials. N-phase flows are associated with many important physical phenomena such as wetting, spreading, and contact lines [15].

While the method developed herein equally applies to two-phase systems, our main focus in the paper will be on situations involving more than two fluid phases ($N \geqslant 3$). For two-phase flows, we will refer to e.g. [3,32,44,48,51,52,55] and the references therein for related reviews and more detailed expositions.

While we concentrate on the hydrodynamic interactions of multiple fluid components or phases, some of the issues encountered can be analogous to those facing the materials community for multi-component materials, whose history can be traced to the early work in the 1960s; we refer to e.g. [4,6,12–14,21–23,28,29,47] and the references therein for the work in multicomponent materials. For N-phase ($N \geqslant 3$) flows, while a significant portion of the existing work is based on the phase field (or diffuse interface) approach [9–11,34–37,40], there also exist sizable efforts utilizing other techniques such as level set or volume of fluids [8,30,46,50,53,56,58,59,61]. We focus on the phase field approach in the current paper.

With the phase field approach, the sharp interface between two immiscible incompressible fluids is replaced by a thin smooth transition layer (diffuse interface). The state of the system is represented by one or more phase field variables (or order parameters), which vary continuously over the thin transition layer and are mostly uniform in the bulk phases. The system is characterized by, besides the kinetic energy, the free energy density function, which represents the effects due to the interfacial tensions between the fluids. The free energy density function contains component terms whose effect tends to mix the fluids, and other component terms whose effect tends to separate the fluids [43,44]. The interplay between these two opposite tendencies determines the dynamic profiles of the interfaces. The chemical potentials characterize the change in the system free energy as the phase field variables are varied, and play an important role in the evolution of the phase field variables.

A foremost issue confronting N-phase simulations is how to formulate the system in a physically consistent manner. Most existing efforts have largely avoided this question and just combined e.g. the Navier–Stokes equations with a system of phase field equations. Thermodynamic consistency in the physical formulation has been taken to heart in only a handful of studies, most notably [27,38] (for two-phase systems, see also e.g. [2,44]). In these works the governing equations for the N-phase system have been derived based on the conservations of mass, momentum and energy, and the constitutive relations involved therein are determined based on a thermodynamic framework such as the second law of thermodynamics or the maximization of the rate of entropy production. We would also like to mention [45], in which a set of governing equations for multiple phases, without the dissipation terms, have been obtained based on a variational principle.

Another crucial outstanding issue with regard to phase field formulations, for situations with more than three fluid phases, concerns how to determine the mixing energy density coefficients (see Section 2 for definition) involved in the model from the pairwise surface tensions. In the case of two-phase flows, the mixing energy density coefficient can be determined by relating the surface tension to the integral of the free energy over the equilibrium interfacial profile; see [57] for details. For three fluid phases, in existing studies the three pairwise surface tensions are usually decomposed symmetrically into three phase-specific surface-tension coefficients (or equivalently the mixing energy density coefficients); see e.g. [9,10,34–36,38]. However, this decomposition encounters difficulties in cases of four or more fluid phases, because the number of pairwise surface tensions ($\frac{N(N-1)}{2}$) would be greater than the number of mixing energy density coefficients (N) to be determined [35,38]. To avoid this solvability problem, a phenomenological continuum surface tension force is discussed in [35].

Apart from the above issues regarding the physical formulations, one also faces several significant algorithmic challenges when numerically simulating the N-phase system. First, the density and the dynamic viscosity of the N-phase mixture are both field variables and vary over time. With usual algorithmic formulations, these field variables go inside the coefficient matrices for the linear algebraic systems for the pressure and the velocity after discretization (see e.g. [10,36,40]). Consequently, these coefficient matrices will be time-dependent and need to be re-computed *every time step*. This creates a severe performance bottleneck, because of the high cost associated with the coefficient matrix re-computation. This is perhaps in part why matched density or matched viscosity among the multitude of fluids has been assumed in a number of existing simulations [34,36,38,40]. The computational challenges induced by the variable density and variable viscosity of the

N-phase mixture are analogous to those encountered for two-phase flows [20]. Second, different flow variables (velocity, pressure, and phase field functions) are coupled with one another, which poses solution difficulties. Third, the $(N-1)$ phase field functions are strongly coupled with one another (see Section 2). Usual algorithmic formulations will result in a set of 4th-order semi-discretized nonlinear equations, which may further be coupled with one another, and each 4th-order equation would give rise to two coupled 2nd-order nonlinear equations. These will result in a set of coupled nonlinear algebraic equations after discretization, and require expensive Newton-type nonlinear algebraic solvers; see e.g. [9–11,34,38,40]. Fourth, large density ratios (e.g. air/water ~ 1000) and large viscosity ratios among the multitude of fluids will pose significant stability difficulties.

In the current paper, we aim to overcome the above issues with several techniques. Specifically, we present the following three aspects:

- A physical formulation for incompressible N-phase flows. The formulation (iso-thermal) honors the conservations of mass and momentum, and the second law of thermodynamics. In such a sense, it is thermodynamically consistent. Our physical formulation differs from those of [27,38] in an essential way: the velocity in our formulation is the *volume-averaged mixture velocity* and therefore is *divergence free*, while those of [27,38] are the *mass-averaged mixture velocity* and therefore are *not divergence free*. Our physical formulation is a generalization of the approach of [2] (for two-phase flows) to N fluid phases.
- A method to uniquely determine the mixing energy density coefficients involved in the N-phase model based on the $\frac{N(N-1)}{2}$ pairwise surface tensions. Our method consists of two key components: (i) a free-energy form for the N-phase system that involves $\frac{N(N-1)}{2}$ mixing energy density coefficients, and (ii) the requirement on the N-phase formulation that, if only a pair of two fluids (for any such pair) is present in the N-phase system, then the N-phase formulation shall reduce to an equivalent two-phase formulation consisting of these two fluids. Our method leads to an explicit form of a system of $\frac{N(N-1)}{2}$ linear algebraic equations, with the pairwise surface tensions on the right hand sides. This linear algebraic system can be solved for the $\frac{N(N-1)}{2}$ mixing energy density coefficients.
- An efficient numerical algorithm for simulating incompressible N-phase flows that has overcome the several aforementioned algorithmic issues. For example, with our algorithm the computations for different flow variables (velocity, pressure, phase field functions) are completely de-coupled, and the computations for the $(N-1)$ phase field functions have also been completely de-coupled. Only linear algebraic equations need to be solved after discretization, and no nonlinear algebraic solver is needed. In addition, for each flow variable the linear algebraic system involves only *constant* and *time-independent* coefficient matrices, which can be pre-computed during pre-processing, despite the variable and time-dependent nature of the mixture physical properties such as density and dynamic viscosity. The algorithm therefore effectively overcomes the performance bottleneck in N-phase flows caused by variable coefficient matrices associated with variable mixture density and variable mixture viscosity. Moreover, our algorithm is suitable for large density ratios and large viscosity ratios among the multitude of fluids, which will be demonstrated using numerical simulations.

The novelties of this paper lie in the following aspects: the physical formulation for the incompressible N-phase flows, the method for determining the mixing energy density coefficients based on the pairwise surface tensions, and the algorithm for solving the $(N-1)$ strongly-coupled phase field equations. Our algorithm for dealing with the variable mixture density and variable mixture viscosity is also new in the context of N-phase flows. But the essential strategies for achieving this are developed previously in two-phase flows [20]. On the other hand, the rotational velocity-correction type strategy employed here to de-couple the pressure and velocity computations for N-phase flows has been used previously in other contexts; see e.g. [19,25].

For spatial discretizations we employ the spectral element technique [33,60] in the current paper. However, we would like to point out that the numerical algorithm presented here is general, and can also be used with other spatial discretization schemes such as finite difference, finite element, or finite volume.

The structure of the rest of this paper is as follows. Section 2.1 and Appendix A describe the physical formulations of N-phase flows. In particular, Appendix A outlines the derivation of a general phase-field formulation for N fluid phases based on the mass conservation, momentum conservation, the second law of thermodynamics, and Galilean invariance. Section 2.1, on the other hand, presents a specific N-phase formulation obtained from the general formulation by choosing a specific form for the free energy density function and by assuming constant model parameters. This specific N-phase formulation serves as the starting point for the algorithmic development in later sections. Section 2.2 describes a method on how to compute the mixing energy density coefficients from the pairwise surface tensions among the N fluids. Sections 2.3 to 2.5 describe our numerical algorithm for simulating the incompressible N-phase flows. In particular, Section 2.3 provides the overall algorithmic formulation, while Sections 2.4 and 2.5 provide more details on the implementation and on how to compute the phase field functions and the flow variables. In Section 3 we present numerical tests for several equilibrium or dynamic problems involving three to five fluid phases, to demonstrate the capabilities and performance of the presented physical model and numerical algorithm. In particular, we compare our simulation results with de Gennes' theory to demonstrate that our method produces physically accurate results for multiple fluid phases. Finally, in Section 4 we summarize our discussions and provide some concluding remarks.

2. Algorithm for incompressible N-phase flows

2.1. Physical formulation

Consider a mixture of N ($N \geqslant 2$) immiscible incompressible fluids. One can formulate the governing equations that describe the motion of this mixture by considering the mass balance of the N individual fluid phases, the momentum balance, Galilean invariance, and the second law of thermodynamics. In Appendix A of this paper, we present a detailed discussion of this process, and derive a general formulation within the phase field framework for describing the motion of the N-phase mixture. The general formulation involves $(N-1)$ order parameters (or interchangeably, phase field variables) and the free energy density function of the system that are yet to be specified.

We employ a special set of order parameters in order to simplify the phase field equations in the general formulation. Then, by choosing a specific form for the free energy density function and by assuming constant model parameters, we arrive at a specific formulation for describing the N-phase system. Presented in the following is this specific N-phase formulation. It is the basis for the algorithmic development in the subsequent sections. The development discussed in Appendix A is an essential part of this paper, and we refer the reader to Appendix A for detailed derivations of the general N-phase formulation, on which the following specific formulation is based.

Let Ω denote the flow domain in two or three dimensions, and $\partial\Omega$ denote the domain boundary. Consider the mixture of N immiscible incompressible fluids contained in Ω. Let $\tilde{\rho}_i$ ($1 \leqslant i \leqslant N$) denote the constant densities of the N pure fluids (no mixing), and $\tilde{\mu}_i$ ($1 \leqslant i \leqslant N$) denote the constant dynamic viscosities of these pure fluids. Then the motion of the mixture can be described by the following system of equations (see Appendix A for details),

$$\rho\left(\frac{\partial \mathbf{u}}{\partial t} + \mathbf{u}\cdot\nabla\mathbf{u}\right) + \tilde{\mathbf{J}}\cdot\nabla\mathbf{u} = -\nabla p + \nabla\cdot\left[\mu\mathbf{D}(\mathbf{u})\right] - \sum_{i,j=1}^{N-1}\nabla\cdot(\lambda_{ij}\nabla\phi_i\nabla\phi_j) + \mathbf{f}(\mathbf{x},t) \tag{1a}$$

$$\nabla\cdot\mathbf{u} = 0 \tag{1b}$$

$$\frac{\partial\phi_i}{\partial t} + \mathbf{u}\cdot\nabla\phi_i = m_i\nabla^2\left[-\sum_{j=1}^{N-1}\lambda_{ij}\nabla^2\phi_j + \frac{\beta^2}{\eta^2}h_i(\vec{\phi})\right] + g_i(\mathbf{x},t), \quad 1 \leqslant i \leqslant N-1, \tag{1c}$$

where $\mathbf{u}(\mathbf{x},t)$ is the velocity, $p(\mathbf{x},t)$ is pressure, $\mathbf{D}(\mathbf{u}) = \nabla\mathbf{u} + \nabla\mathbf{u}^T$, $\mathbf{f}$ is an external body force, and $\mathbf{x}$ denotes the spatial coordinate and t denotes time. $\phi_i(\mathbf{x},t)$ ($1 \leqslant i \leqslant N-1$) denotes the $(N-1)$ independent phase field variables (or order parameters) that characterize this N-phase system, and $-1 \leqslant \phi_i \leqslant 1$. $\vec{\phi} = (\phi_1, \phi_2, \ldots, \phi_{N-1})$ denotes the vector of these $(N-1)$ phase field functions. The constants m_i ($m_i > 0$), $1 \leqslant i \leqslant N-1$, are the mobilities associated with ϕ_i. The constant β^2 denotes a characteristic energy scale, and $\eta > 0$ denotes a characteristic scale of the interfacial thickness. The parameters λ_{ij} ($1 \leqslant i, j \leqslant N-1$) are the mixing energy density coefficients and are assumed to be constant in the current paper. These parameters are such that the matrix

$$\mathbf{A} = [\lambda_{ij}]_{(N-1)\times(N-1)} \tag{2}$$

is symmetric positive definite (SPD). λ_{ij} can be determined from the pairwise surface tensions among the N fluids, which will be discussed subsequently in Section 2.2. g_i ($1 \leqslant i \leqslant N-1$) in Eq. (1c) are prescribed source terms for the purpose of numerical testing only, and they will be set to $g_i = 0$ in actual simulations.

The free energy density of this N-phase system is

$$W(\vec{\phi}, \nabla\vec{\phi}) = \sum_{i,j=1}^{N-1}\frac{\lambda_{ij}}{2}\nabla\phi_i\cdot\nabla\phi_j + \frac{\beta^2}{2\eta^2}H(\vec{\phi}) = \sum_{i,j=1}^{N-1}\frac{\lambda_{ij}}{2}\nabla\phi_i\cdot\nabla\phi_j + \frac{\beta^2}{2\eta^2}\sum_{k=1}^{N}c_k^2(1-c_k)^2, \tag{3}$$

where $c_k(\vec{\phi})$ ($1 \leqslant k \leqslant N$) denotes the volume fraction of the k-th fluid, and is given by

$$c_k(\vec{\phi}) = \tilde{\gamma}_k\rho_k(\vec{\phi}), \quad 1 \leqslant k \leqslant N, \tag{4}$$

and $\rho_k(\vec{\phi})$ is the density of the k-th fluid in the *mixture*,

$$\rho_k(\vec{\phi}) = \begin{cases} \frac{1}{\Gamma} - \sum_{i=1}^{N-1}\frac{\tilde{\gamma}_i}{\Gamma}[\frac{1}{2}(\tilde{\rho}_i - \tilde{\rho}_N) + \frac{1}{2}(\tilde{\rho}_i + \tilde{\rho}_N)\phi_i], & k = N, \\ \rho_N(\vec{\phi}) + [\frac{1}{2}(\tilde{\rho}_k - \tilde{\rho}_N) + \frac{1}{2}(\tilde{\rho}_k + \tilde{\rho}_N)\phi_k], & 1 \leqslant k \leqslant N-1 \end{cases} \tag{5}$$

and

$$\begin{cases} \tilde{\gamma}_k = \dfrac{1}{\tilde{\rho}_k}, \quad 1 \leqslant k \leqslant N \\ \Gamma = \displaystyle\sum_{k=1}^{N}\tilde{\gamma}_k. \end{cases} \tag{6}$$

Note that the above volume fractions satisfy the relation

$$\sum_{k=1}^{N} c_k = c_1 + c_2 + \ldots + c_N = 1. \tag{7}$$

$h_i(\vec{\phi})$ in Eq. (1c) is given by

$$h_i(\vec{\phi}) = \frac{1}{2}\frac{\partial H}{\partial \phi_i} = \frac{\tilde{\rho}_i + \tilde{\rho}_N}{2}\sum_{k=1}^{N}\left(\tilde{\gamma}_k \delta_{ki} - \frac{\tilde{\gamma}_k\tilde{\gamma}_i}{\Gamma}\right)c_k(1-c_k)(1-2c_k), \quad 1 \leqslant i \leqslant N-1, \tag{8}$$

where δ_{ij} is the Kronecker delta. In Eq. (1a), $\tilde{\mathbf{J}}$ is given by

$$\tilde{\mathbf{J}} = -\sum_{i=1}^{N-1}\left(1 - \frac{N}{\Gamma}\tilde{\gamma}_i\right)\frac{\tilde{\rho}_i + \tilde{\rho}_N}{2} m_i \nabla\left[-\sum_{j=1}^{N-1}\lambda_{ij}\nabla^2\phi_j + \frac{\beta^2}{\eta^2}h_i(\vec{\phi})\right]. \tag{9}$$

The mixture density $\rho(\vec{\phi})$ in Eq. (1a) is given by

$$\rho(\vec{\phi}) = \sum_{k=1}^{N}\rho_k(\vec{\phi}) = \frac{N}{\Gamma} + \sum_{i=1}^{N-1}\left(1 - \frac{N}{\Gamma}\tilde{\gamma}_i\right)\left[\frac{1}{2}(\tilde{\rho}_i - \tilde{\rho}_N) + \frac{1}{2}(\tilde{\rho}_i + \tilde{\rho}_N)\phi_i\right]. \tag{10}$$

The dynamic viscosity of the mixture, $\mu(\vec{\phi})$, is given by

$$\mu(\vec{\phi}) = \sum_{k=1}^{N}\tilde{\mu}_k c_k(\vec{\phi}). \tag{11}$$

In the above system, Eqs. (1a)–(1c) correspond to Eqs. (157a)–(157c) in the general N-phase formulation in Appendix A. Among them, Eq. (1a) reflects the momentum balance of the N-phase mixture. The phase field equations (1c) (with $g_i = 0$) reflect the mass balance of the individual fluid phases. The velocity $\mathbf{u}$ denotes the *volume-averaged* mixture velocity, which can be shown to be divergence free (see Appendix A). The term $\tilde{\mathbf{J}} \cdot \nabla\mathbf{u}$ results from the requirement for Galilean invariance of the formulation.

The set of $(N-1)$ phase field variables ϕ_i in the above system are not arbitrary order parameters. They are particularly chosen to simplify the form of the resulting phase field equations. Specifically, they are chosen such that

$$\rho_i(\vec{\phi}) - \rho_N(\vec{\phi}) = \frac{1}{2}(\tilde{\rho}_i - \tilde{\rho}_N) + \frac{1}{2}(\tilde{\rho}_i + \tilde{\rho}_N)\phi_i, \quad \phi_i \in [-1, 1], \ 1 \leqslant i \leqslant N-1, \tag{12}$$

where $\rho_i(\vec{\phi})$ $(1 \leqslant i \leqslant N)$ is the density of fluid i within the mixture. Other order parameters (e.g. volume fractions) can also be used to formulate the system. But the resulting form of the phase field equations (reflecting mass balance relations) will be considerably more complicated.

A prominent feature of the phase field equations (1c) is in the terms $\sum_{j=1}^{N-1}\lambda_{ij}\nabla^2\phi_j$, which, together with the $h_i(\vec{\phi})$ term, strongly couple together the $(N-1)$ phase field functions. Therefore, $\frac{1}{2}N(N-1)$ independent mixing energy density coefficients λ_{ij} are involved in the N-phase system. This is a major difference of our formulation from those of the existing studies of N-phase flows [9–11,34–38,40]. The coupling terms $\lambda_{ij}\nabla^2\phi_j$ result from the free energy form (3); see Appendix A for details. We note that similar free-energy forms have previously been used in literature for multicomponent materials (see e.g. [12–14,21,23,29]).

In the N-phase system represented by (1a)–(1c), the region of the fluid k $(1 \leqslant k \leqslant N-1)$ corresponds to the phase field variable values

$$\phi_i = \begin{cases} 1, & i = k, \\ \frac{\tilde{\rho}_N - \tilde{\rho}_i}{\tilde{\rho}_N + \tilde{\rho}_i}, & i \neq k, \end{cases} \quad 1 \leqslant i \leqslant N-1. \tag{13}$$

The region of the fluid N corresponds to the phase field variable values

$$\phi_i = -1, \quad 1 \leqslant i \leqslant N-1. \tag{14}$$

We will use the iso-surface

$$c_k(\vec{\phi}) = \frac{1}{2}, \tag{15}$$

where c_k is the volume fraction of fluid k given by (4), to mark the boundary of the region occupied by the fluid k $(1 \leqslant k \leqslant N)$.

It can be shown that $\rho(\vec{\phi})$ and $\tilde{\mathbf{J}}$ satisfies the relation (see Appendix A), assuming $g_i = 0$ in (1c),

$$\frac{\partial \rho}{\partial t} + \mathbf{u} \cdot \nabla \rho = -\nabla \cdot \tilde{\mathbf{J}}. \tag{16}$$

The above system admits the following energy relation, assuming that all surface flux terms vanish on the domain boundary and that $g_i = 0$ in (1c),

$$\frac{\partial}{\partial t} \int_{\Omega} \left[\frac{1}{2} \rho |\mathbf{u}|^2 + W(\vec{\phi}, \nabla\vec{\phi}) \right] = -\int_{\Omega} \frac{\mu}{2} \left\| \mathbf{D}(\mathbf{u}) \right\|^2 - \int_{\Omega} \sum_{i=1}^{N-1} m_i \left\| \nabla C_i(\vec{\phi}) \right\|^2 + \int_{\Omega} \mathbf{f} \cdot \mathbf{u}, \tag{17}$$

where $W(\vec{\phi}, \nabla\vec{\phi})$ is the free energy density function given by (3), and

$$C_i(\vec{\phi}) = \frac{\delta W}{\delta \phi_i} = -\sum_{j=1}^{N-1} \lambda_{ij} \nabla^2 \phi_j + \frac{\beta^2}{\eta^2} h_i(\vec{\phi}), \quad 1 \leqslant i \leqslant N-1, \tag{18}$$

is the chemical potential associated with ϕ_i.

The system of equations, (1a)–(1c), needs to be supplemented by appropriate boundary conditions for the velocity and the phase field functions. For the simplicity of algorithm development, on the domain boundary $\partial\Omega$ we will impose the Dirichlet condition for the velocity,

$$\mathbf{u} = \mathbf{w}(\mathbf{x}, t), \quad \text{on } \partial\Omega, \tag{19}$$

where $\mathbf{w}$ is the boundary velocity. For the phase field functions, we impose the conditions

$$\mathbf{n} \cdot \nabla \phi_i = 0, \quad \text{on } \partial\Omega,\ 1 \leqslant i \leqslant N-1, \tag{20}$$

$$\mathbf{n} \cdot \nabla\left(\nabla^2 \phi_i\right) = 0, \quad \text{on } \partial\Omega,\ 1 \leqslant i \leqslant N-1, \tag{21}$$

where $\mathbf{n}$ is the outward-pointing unit vector normal to $\partial\Omega$. The boundary conditions (20) and (21) correspond to the requirement that, if the interface between any two fluids i and j intersects the domain boundary $\partial\Omega$, then the contact angle between the fluid interface and the boundary shall be 90°.

In addition to the boundary conditions, appropriate initial conditions for the velocity and the phase field functions also need to be specified to supplement the system of equations.

2.2. *How to determine λ_{ij} based on pairwise surface tensions*

We next present a method for computing the mixing energy density coefficients λ_{ij} $(1 \leqslant i, j \leqslant N-1)$ based on the pairwise surface tensions among the N different fluids.

Let σ_{kl} $(1 \leqslant k < l \leqslant N)$ denote the surface tension associated with the interface formed between the fluid k and fluid l. There is a total of $\frac{1}{2}N(N-1)$ such pairwise surface tensions in the N-phase system. Suppose that all the pairwise surface tensions σ_{kl} are known. Our task is to determine the mixing energy density coefficients λ_{ij}. Note that there are $\frac{1}{2}N(N-1)$ independent λ_{ij} values due to symmetry of the matrix A defined in (2). We assume that the constants β^2 and η are also known in the free-energy density function $W(\vec{\phi}, \nabla\vec{\phi})$ defined by (3).

Our overall strategy is as follows. Given the N-phase system, we consider the configuration in which only a pair of fluids k and l is present (all other fluids are absent), assuming $k < l$ without loss of generality. Equivalently, this particular N-phase system can be regarded as a two-phase system consisting of fluids k and l. We impose the following requirement to the N-phase formulation: for such an N-phase system the N-phase formulation shall reduce to the equivalent two-phase formulation. In particular, the free energy density function for the N-phase system shall reduce to that for the equivalent two-phase system. We consider all such (k, l) fluid pairs in the N-phase system, and obtain a set of linear algebraic equations about λ_{ij}, which can be solved for the mixing energy density coefficients.

2.2.1. *Two fluid phases*

Let us first consider the two-phase system ($N = 2$). Then ϕ_1 is the only phase field variable, which is chosen such that (see Eq. (12))

$$\rho_1(\phi_1) - \rho_2(\phi_1) = \frac{1}{2}(\tilde{\rho}_1 - \tilde{\rho}_2) + \frac{1}{2}(\tilde{\rho}_1 + \tilde{\rho}_2)\phi_1. \tag{22}$$

The densities and volume fractions of the two fluids are, according to Eqs. (5) and (4),

$$\begin{cases} \rho_1(\phi_1) = \tilde{\rho}_1 \dfrac{1+\phi_1}{2}, & \rho_2(\phi_1) = \tilde{\rho}_2 \dfrac{1-\phi_1}{2}, \\ c_1(\phi_1) = \dfrac{1+\phi_1}{2}, & c_2(\phi_1) = \dfrac{1-\phi_1}{2}. \end{cases} \tag{23}$$

Based on (3), the free energy density function of the two-phase system is

$$W(\phi_1, \nabla\phi_1) = \frac{\lambda_{11}}{2}\nabla\phi_1 \cdot \nabla\phi_1 + \frac{\beta^2}{2\eta^2}\left[c_1^2(1-c_1)^2 + c_2^2(1-c_2)^2\right]. \tag{24}$$

In light of (23), the free energy density can be written as

$$W(\phi_1, \nabla\phi_1) = \frac{\lambda_{11}}{2}\nabla\phi_1 \cdot \nabla\phi_1 + \frac{\beta^2}{16\eta^2}\left(1-\phi_1^2\right)^2 = \frac{\lambda_{11}}{2}\nabla\phi_1 \cdot \nabla\phi_1 + \frac{\lambda_{11}}{4\epsilon^2}\left(1-\phi_1^2\right)^2, \tag{25}$$

where

$$\epsilon = \frac{2\eta}{\beta}\sqrt{\lambda_{11}}. \tag{26}$$

The free energy density in (25) has exactly the same form as those for two-phase flows well-developed in previous work; see e.g. [32,43,57].

Following the idea of [57], in a one-dimensional (1D) setting, we can derive the relationship between λ_{11} and the surface tension σ_{12} between the two fluids, by requiring that at equilibrium the integral of the free energy density function across the interface should equal the surface tension. This relation is given by [57],

$$\lambda_{11} = \frac{3}{2\sqrt{2}}\sigma_{12}\epsilon. \tag{27}$$

By combining Eqs. (26) and (27), we can determine λ_{11},

$$\lambda_{11} = \frac{9}{2}\frac{\eta^2}{\beta^2}\sigma_{12}^2. \tag{28}$$

Therefore, for a two-phase system with the free energy density given by Eq. (24), the mixing energy density coefficient is related to the surface tension between the two fluids by Eq. (28). This relation for two-phase systems will be used when determining the relationship between the mixing energy density coefficients λ_{ij} and the pairwise surface tensions σ_{kl} in the N-phase system.

2.2.2. N fluid phases

Let us now consider N fluid phases. We consider the following configuration. In this N-phase system only two fluids, fluid k and fluid l (assuming $k < l$), are present, that is,

$$\begin{cases} \rho_i(\vec{\phi}) \equiv 0, \\ c_i(\vec{\phi}) \equiv 0, \end{cases} \quad \text{if } i \neq k \text{ and } i \neq l, \ \text{for } 1 \leqslant i \leqslant N. \tag{29}$$

Therefore, the free energy density of this system becomes, based on (3),

$$W(\vec{\phi}, \nabla\vec{\phi}) = \sum_{i,j=1}^{N-1}\frac{\lambda_{ij}}{2}\nabla\phi_i \cdot \nabla\phi_j + \frac{\beta^2}{2\eta^2}\left[c_k^2(1-c_k)^2 + c_l^2(1-c_l)^2\right]. \tag{30}$$

Because this configuration is equivalent to a two-phase system, there exists only one independent phase field variable. In light of Eq. (22) and the discussions of Section 2.2.1, we choose this independent phase field variable (denoted by ϕ_a) such that

$$\rho_k(\vec{\phi}) - \rho_l(\vec{\phi}) = \frac{1}{2}(\tilde{\rho}_k - \tilde{\rho}_l) + \frac{1}{2}(\tilde{\rho}_k + \tilde{\rho}_l)\phi_a. \tag{31}$$

Our goal is to re-formulate the free energy density function (30) in terms of ϕ_a into the following form

$$W(\vec{\phi}, \nabla\vec{\phi}) = \frac{\Lambda^{kl}}{2}\nabla\phi_a \cdot \nabla\phi_a + \frac{\beta^2}{2\eta^2}\left[c_k^2(1-c_k)^2 + c_l^2(1-c_l)^2\right], \tag{32}$$

where Λ^{kl} is a function of the mixing energy density coefficients λ_{ij} ($1 \leqslant i, j \leqslant N-1$). Then by comparing the above form with (24), one can use Eq. (28) to relate Λ^{kl} to the surface tension σ_{kl} between fluid k and fluid l.

To find the relations between ϕ_i ($1 \leqslant i \leqslant N-1$) and ϕ_a, we differentiate two cases: (1) $l = N$, and (2) $l < N$. In the first case ($l = N$), we have $\phi_a \equiv \phi_k$ in light of (31) and (12). We have the following linear algebraic system about $\rho_i(\vec{\phi})$,

$$\tilde{\gamma}_k\rho_k + \tilde{\gamma}_N\rho_N = 1 \tag{33a}$$

$$\rho_k - \rho_N = \frac{1}{2}(\tilde{\rho}_k - \tilde{\rho}_N) + \frac{1}{2}(\tilde{\rho}_k + \tilde{\rho}_N)\phi_a \tag{33b}$$

$$-\rho_N = \frac{1}{2}(\tilde{\rho}_i - \tilde{\rho}_N) + \frac{1}{2}(\tilde{\rho}_i + \tilde{\rho}_N)\phi_i, \quad 1 \leqslant i \leqslant N-1, \ i \neq k. \tag{33c}$$

In the above system, Eq. (33a) comes from the condition (7) that the sum of the N volume fractions must be unity, and has taken into account the conditions (29). Eqs. (33b) and (33c) come from Eq. (12) by taking into account the conditions (29). The combination of Eqs. (33a) and (33b) leads to

$$\begin{cases} \rho_k = \dfrac{1}{\tilde{\gamma}_k + \tilde{\gamma}_N} + \dfrac{\tilde{\gamma}_N}{\tilde{\gamma}_k + \tilde{\gamma}_N}\left[\dfrac{1}{2}(\tilde{\rho}_k - \tilde{\rho}_N) + \dfrac{1}{2}(\tilde{\rho}_k + \tilde{\rho}_N)\phi_a\right] \\ \rho_N = \dfrac{1}{\tilde{\gamma}_k + \tilde{\gamma}_N} - \dfrac{\tilde{\gamma}_k}{\tilde{\gamma}_k + \tilde{\gamma}_N}\left[\dfrac{1}{2}(\tilde{\rho}_k - \tilde{\rho}_N) + \dfrac{1}{2}(\tilde{\rho}_k + \tilde{\rho}_N)\phi_a\right]. \end{cases} \tag{34}$$

In light of (33c) and (34), we obtain the following relation

$$\nabla\phi_i = L_i^{kN}\nabla\phi_a, \quad 1 \leqslant i \leqslant N-1, \tag{35}$$

where

$$L_i^{kN} = \begin{cases} 1, & \text{if } i = k, \\ \frac{\tilde{\rho}_N}{\tilde{\rho}_i + \tilde{\rho}_N}, & \text{if } i \neq k, \end{cases} \quad 1 \leqslant k < l = N. \tag{36}$$

In light of (34), the volume fractions are

$$\begin{cases} c_k = \tilde{\gamma}_k\rho_k = \dfrac{1}{2}(1 + \phi_a) \\ c_l = c_N = \tilde{\gamma}_N\rho_N = \dfrac{1}{2}(1 - \phi_a). \end{cases} \tag{37}$$

For the second case (i.e. $l < N$), we have a linear algebraic system consisting of Eq. (31) and the following equations,

$$\tilde{\gamma}_k\rho_k + \tilde{\gamma}_l\rho_l = 1 \tag{38a}$$

$$\rho_k = \frac{1}{2}(\tilde{\rho}_k - \tilde{\rho}_N) + \frac{1}{2}(\tilde{\rho}_k + \tilde{\rho}_N)\phi_k \tag{38b}$$

$$\rho_l = \frac{1}{2}(\tilde{\rho}_l - \tilde{\rho}_N) + \frac{1}{2}(\tilde{\rho}_l + \tilde{\rho}_N)\phi_l \tag{38c}$$

$$0 = \frac{1}{2}(\tilde{\rho}_i - \tilde{\rho}_N) + \frac{1}{2}(\tilde{\rho}_i + \tilde{\rho}_N)\phi_i, \quad 1 \leqslant i \leqslant N-1,\ i \neq k \text{ and } i \neq l. \tag{38d}$$

In this system, Eq. (38a) comes from the condition (7) and has taken into account the conditions (29). Eqs. (38b)–(38d) are a reformulation of Eq. (12) by taking into account the conditions (29). A combination of (38a) and (31) leads to

$$\begin{cases} \rho_k = \dfrac{1}{\tilde{\gamma}_k + \tilde{\gamma}_l} + \dfrac{\tilde{\gamma}_l}{\tilde{\gamma}_k + \tilde{\gamma}_l}\left[\dfrac{1}{2}(\tilde{\rho}_k - \tilde{\rho}_l) + \dfrac{1}{2}(\tilde{\rho}_k + \tilde{\rho}_l)\phi_a\right] \\ \rho_l = \dfrac{1}{\tilde{\gamma}_k + \tilde{\gamma}_l} - \dfrac{\tilde{\gamma}_k}{\tilde{\gamma}_k + \tilde{\gamma}_l}\left[\dfrac{1}{2}(\tilde{\rho}_k - \tilde{\rho}_l) + \dfrac{1}{2}(\tilde{\rho}_k + \tilde{\rho}_l)\phi_a\right]. \end{cases} \tag{39}$$

In light of (39) and Eqs. (38b)–(38d), we have the following relation

$$\nabla\phi_i = L_i^{kl}\nabla\phi_a, \quad 1 \leqslant i \leqslant N-1, \tag{40}$$

where

$$L_i^{kl} = \begin{cases} \frac{\tilde{\rho}_k}{\tilde{\rho}_k + \tilde{\rho}_N}, & i = k, \\ -\frac{\tilde{\rho}_l}{\tilde{\rho}_l + \tilde{\rho}_N}, & i = l, \\ 0, & \text{otherwise}, \end{cases} \quad 1 \leqslant k < l < N. \tag{41}$$

In light of Eq. (39), the volume fractions for this case are

$$\begin{cases} c_k = \tilde{\gamma}_k\rho_k = \dfrac{1}{2}(1 + \phi_a) \\ c_l = \tilde{\gamma}_l\rho_l = \dfrac{1}{2}(1 - \phi_a). \end{cases} \tag{42}$$

In light of Eqs. (35) and (40), the free energy density function (30) can be transformed into the form of (32), where

$$\Lambda^{kl} = \sum_{i,j=1}^{N-1}\lambda_{ij}L_i^{kl}L_j^{kl}, \tag{43}$$

and L_i^{kl} are given by (36) and (41). Comparing Eqs. (32) and (24), and in light of Eq. (28), we have the following relation

$$\sum_{i,j=1}^{N-1} L_i^{kl} L_j^{kl} \lambda_{ij} = \Lambda^{kl} = \frac{9}{2}\frac{\eta^2}{\beta^2}\sigma_{kl}^2, \tag{44}$$

where σ_{kl} is the surface tension between fluid k and fluid l. This is a linear algebraic equation about λ_{ij}.

We consider all such fluid pairs (k,l), $1 \leqslant k < l \leqslant N$, in the N-phase system, and therefore obtain the following system of linear algebraic equations about λ_{ij},

$$\sum_{i=1}^{N-1} \left(L_i^{kl}\right)^2 \lambda_{ii} + \sum_{j=1}^{N-1}\sum_{i=1}^{j-1} 2 L_i^{kl} L_j^{kl} \lambda_{ij} = \frac{9}{2}\frac{\eta^2}{\beta^2}\sigma_{kl}^2, \quad 1 \leqslant k < l \leqslant N, \tag{45}$$

where we have taken into account the symmetry, $\lambda_{ij} = \lambda_{ji}$. This system has $\frac{N(N-1)}{2}$ equations about $\frac{N(N-1)}{2}$ unknowns. It can be solved for the mixing energy density coefficients λ_{ij}, given all the pairwise surface tensions σ_{kl} in this N-phase system.

Two questions call for attention at this point. The first question concerns whether the coefficient matrix for the linear algebraic system (45) is non-singular. For a three-phase system ($N = 3$), one can show that the coefficient matrix for the system (45) has a determinant given by

$$2\left(1 - \frac{\tilde{\rho}_3}{\tilde{\rho}_1 + \tilde{\rho}_3}\frac{\tilde{\rho}_3}{\tilde{\rho}_2 + \tilde{\rho}_3}\right)^3 > 0$$

and therefore the system is non-singular. For a general N-phase system, it is difficult to prove the non-singularity of the coefficient matrix for this linear algebraic system. However, we have implemented the above method by solving the system using LAPACK, and performed a large number of numerical experiments with different combinations of density ratios and for various numbers of fluid phases. We observe that according to LAPACK this linear algebraic system has a unique solution in every case. It therefore seems reasonable to assume that, powered by the numerical experiments, this is a well-posed linear system. Very recently, an inquiry into a related but more general problem sheds light on the unique solvability of the linear system (45) from an unexpected perspective. We will fully address the unique solvability of (45) for general N-phase systems in a subsequent paper.

The other question concerns the positive-definiteness of the matrix **A** (see (2)) formed with the λ_{ij} values computed from the linear algebraic system (45). Note that, by requirement, the matrix **A** obtained from (45) will automatically be symmetric. Given an arbitrary set of positive values for the pairwise surface tensions $\sigma_{kl} > 0$ ($1 \leqslant k < l \leqslant N$), the matrix **A** so obtained is not necessarily positive definite. An important question is the following. For an N-phase system, under what conditions on the pairwise surface tensions σ_{kl}, and also possibly on the density ratios $\frac{\tilde{\rho}_i}{\tilde{\rho}_N}$ ($1 \leqslant i \leqslant N-1$), will the matrix **A** be positive definite? This is an open question at the moment, and much future research will be required for its resolution. The following observations seem to be true based on our numerical experiments:

- In the N-phase system, if there exists any 3-tuple of fluids, (i,j,k) ($1 \leqslant i,j,k \leqslant N$), whose pairwise surface tensions (σ_{ij}, σ_{ik} and σ_{jk}) violate the triangle inequality,

  $$|\sigma_{ij} - \sigma_{jk}| < \sigma_{ik} < \sigma_{ij} + \sigma_{jk}, \tag{46}$$

  then the matrix **A** will contain a zero or negative eigenvalue and thus will not be positive definite. Physically, the situation with $\sigma_{ik} > \sigma_{ij} + \sigma_{jk}$ corresponds to the total wetting [15], where the fluid j spreads completely on the interface between fluids i and k and its thickness becomes infinitely thin in a large enough domain.
- Change in the density ratio values, $\frac{\tilde{\rho}_i}{\tilde{\rho}_N}$ ($1 \leqslant i \leqslant N-1$), will modify the eigen-value magnitudes of the matrix **A**, but does not seem to change its positive-definiteness. It is however also observed in practice that, when there exists a zero eigen-value, its numerically computed values (while all below machine zero) may sometimes appear to change sign due to roundoff errors as the density ratio is varied.

For all the test problems in Section 3, the **A** matrices formed by λ_{ij} computed from the linear system (45) are symmetric positive definite.

2.3. Algorithm formulation

In this section we present an algorithm for simulating the N-phase system. The governing equations (1a)–(1c), the boundary conditions (19)–(21), and the appropriate initial conditions for the velocity and the $(N-1)$ phase field functions, together constitute the system that needs to be solved in numerical simulations.

We re-write (1a) into an equivalent form,

$$\frac{\partial \mathbf{u}}{\partial t} + \mathbf{u}\cdot\nabla\mathbf{u} + \frac{1}{\rho}\tilde{\mathbf{J}}\cdot\nabla\mathbf{u} = -\frac{1}{\rho}\nabla P + \frac{\mu}{\rho}\nabla^2\mathbf{u} + \frac{1}{\rho}\nabla\mu\cdot\mathbf{D}(\mathbf{u}) - \frac{1}{\rho}\sum_{i,j=1}^{N-1}\lambda_{ij}\nabla^2\phi_j\nabla\phi_i + \frac{1}{\rho}\mathbf{f}, \tag{47}$$

where

$$P = p + \sum_{i,j=1}^{N-1}\frac{\lambda_{ij}}{2}\nabla\phi_i\cdot\nabla\phi_j \tag{48}$$

is an auxiliary pressure and will also be loosely called pressure where no confusion arises.

A comparison between the N-phase governing equations, (47), (1b) and (1c), and those for two-phase systems [16,17,20] indicates that the primary difference lies in the set of phase field equations. On the other hand, the variable-density Navier–Stokes equation (1a) for N fluid phases is quite similar in form to that for two phases. This suggests that one might be able to deal with the computational challenges posed by the variable density and variable viscosity of the N-phase mixture in a similar fashion to the two-phase flows.

The following algorithm is for the N-phase system consisting of Eqs. (47), (1b) and (1c), together with the boundary conditions (19)–(21). Let $(\phi_i^n, P^n, \mathbf{u}^n)$ denote the $(N-1)$ phase field functions, pressure, and velocity at time step n, where n denotes the time step index. We successively solve for the phase field functions, the pressure, and the velocity at time step $(n+1)$ in a de-coupled fashion as follows.

For phase field functions ϕ_i^{n+1}:

$$\begin{aligned}
&\frac{\gamma_0\phi_i^{n+1}-\hat{\phi}_i}{\Delta t} + \mathbf{u}^{*,n+1}\cdot\nabla\phi_i^{*,n+1} \\
&\quad = m_i\nabla^2\left[-\sum_{j=1}^{N-1}\lambda_{ij}\nabla^2\phi_j^{n+1} + \sum_{j=1}^{N-1}\frac{S_{ij}}{\eta^2}\left(\phi_j^{n+1}-\phi_j^{*,n+1}\right) + \frac{\beta^2}{\eta^2}h_i\left(\vec{\phi}^{*,n+1}\right)\right] + g_i^{n+1}, \quad 1\leqslant i\leqslant N-1,
\end{aligned} \tag{49a}$$

$$\mathbf{n}\cdot\nabla\phi_i^{n+1} = 0, \quad \text{on } \partial\Omega,\ 1\leqslant i\leqslant N-1, \tag{49b}$$

$$\mathbf{n}\cdot\nabla\left(\nabla^2\phi_i^{n+1}\right) = 0, \quad \text{on } \partial\Omega,\ 1\leqslant i\leqslant N-1. \tag{49c}$$

In the above equations (and also the subsequent equations), if we use χ to denote a generic variable, then χ^n denotes χ at time step n. $\chi^{*,n+1}$ represents a J-order explicit approximation, where $J=1$ or 2 is the temporal order of accuracy, of χ^{n+1} defined by

$$\chi^{*,n+1} = \begin{cases}\chi^n, & J=1,\\ 2\chi^n-\chi^{n-1}, & J=2.\end{cases} \tag{50}$$

The expression $\frac{1}{\Delta t}(\gamma_0\chi^{n+1}-\hat{\chi})$ represents an approximation of $\frac{\partial\chi}{\partial t}\big|^{n+1}$ by the J-th order backward differentiation formula, where Δt is the time step size and $\hat{\chi}$ and γ_0 are given by

$$\hat{\chi} = \begin{cases}\chi^n, & J=1\\ 2\chi^n-\frac{1}{2}\chi^{n-1}, & J=2,\end{cases} \qquad \gamma_0 = \begin{cases}1, & J=1,\\ \frac{3}{2}, & J=2.\end{cases} \tag{51}$$

In Eq. (49a), $\vec{\phi}^{*,n+1} = (\phi_1^{*,n+1}, \phi_2^{*,n+1}, \ldots, \phi_{N-1}^{*,n+1})$, and S_{ij} $(1\leqslant i,j\leqslant N-1)$ are a set of $(N-1)^2$ constants to be determined later in Section 2.4.

For pressure P^{n+1}:

$$\begin{aligned}
&\frac{\gamma_0\tilde{\mathbf{u}}^{n+1}-\hat{\mathbf{u}}}{\Delta t} + \mathbf{u}^n\cdot\nabla\mathbf{u}^n + \frac{1}{\rho^{n+1}}\tilde{\mathbf{J}}^{n+1}\cdot\nabla\mathbf{u}^n + \frac{1}{\rho_0}\nabla P^{n+1} = \left(\frac{1}{\rho_0}-\frac{1}{\rho^{n+1}}\right)\nabla P^n - \frac{\mu^{n+1}}{\rho^{n+1}}\nabla\times\nabla\times\mathbf{u}^n \\
&\quad + \frac{1}{\rho^{n+1}}\nabla\mu^{n+1}\cdot\mathbf{D}\left(\mathbf{u}^n\right) - \frac{1}{\rho^{n+1}}\sum_{i,j=1}^{N-1}\lambda_{ij}\nabla^2\phi_j^{n+1}\nabla\phi_i^{n+1} + \frac{1}{\rho^{n+1}}\mathbf{f}^{n+1}
\end{aligned} \tag{52a}$$

$$\nabla\cdot\tilde{\mathbf{u}}^{n+1} = 0 \tag{52b}$$

$$\mathbf{n}\cdot\tilde{\mathbf{u}}^{n+1} = \mathbf{n}\cdot\mathbf{w}^{n+1}, \quad \text{on } \partial\Omega. \tag{52c}$$

In these equations, $\tilde{\mathbf{u}}^{n+1}$ is an auxiliary velocity and is an approximation of $\mathbf{u}^{n+1}$. $\tilde{\mathbf{J}}^{n+1}$ is an approximation of $\tilde{\mathbf{J}}$ at time step $(n+1)$ given by

$$\tilde{\mathbf{J}}^{n+1} = -\sum_{i=1}^{N-1}\left(1-\frac{N}{\Gamma}\tilde{\gamma}_i\right)\frac{\tilde{\rho}_i+\tilde{\rho}_N}{2}m_i\nabla\left[-\sum_{j=1}^{N-1}\lambda_{ij}\nabla^2\phi_j^{n+1}+\frac{\beta^2}{\eta^2}h_i\left(\vec{\phi}^{n+1}\right)\right], \tag{53}$$

where $h_i(\vec{\phi}^{n+1})$ is computed based on Eq. (8). The density ρ^{n+1} and the dynamic viscosity μ^{n+1} are computed based on Eqs. (10) and (11) once the phase field functions ϕ_i^{n+1} $(1 \leqslant i \leqslant N-1)$ are known. ρ_0 is a chosen positive constant that must satisfy the condition

$$0 < \rho_0 \leqslant \min(\tilde{\rho}_1, \tilde{\rho}_2, \dots, \tilde{\rho}_N). \tag{54}$$

For velocity $\mathbf{u}^{n+1}$:

$$\begin{aligned}
&\frac{\gamma_0\mathbf{u}^{n+1}-\gamma_0\tilde{\mathbf{u}}^{n+1}}{\Delta t}+\mathbf{u}^{*,n+1}\cdot\nabla\mathbf{u}^{*,n+1}+\frac{1}{\rho^{n+1}}\tilde{\mathbf{J}}^{n+1}\cdot\nabla\mathbf{u}^{*,n+1}-\nu_0\nabla^2\mathbf{u}^{n+1}\\
&\quad=\mathbf{u}^n\cdot\nabla\mathbf{u}^n+\frac{1}{\rho^{n+1}}\tilde{\mathbf{J}}^{n+1}\cdot\nabla\mathbf{u}^n+\left(\frac{1}{\rho_0}-\frac{1}{\rho^{n+1}}\right)\nabla\left(P^{n+1}-P^n\right)+\nu_0\nabla\times\nabla\times\mathbf{u}^{*,n+1}\\
&\qquad+\frac{\mu^{n+1}}{\rho^{n+1}}\nabla\times\nabla\times\left(\mathbf{u}^n-\mathbf{u}^{*,n+1}\right)+\frac{1}{\rho^{n+1}}\nabla\mu^{n+1}\cdot\left[\mathbf{D}\left(\mathbf{u}^{*,n+1}\right)-\mathbf{D}\left(\mathbf{u}^n\right)\right]
\end{aligned} \tag{55a}$$

$$\mathbf{u}^{n+1}=\mathbf{w}^{n+1}, \quad \text{on } \partial\Omega, \tag{55b}$$

where ν_0 is a chosen positive constant that is sufficiently large, and a conservative condition for ν_0 is

$$\nu_0 \geqslant \frac{1}{2}\frac{\max(\tilde{\mu}_1, \tilde{\mu}_2, \dots, \tilde{\mu}_N)}{\min(\tilde{\rho}_1, \tilde{\rho}_2, \dots, \tilde{\rho}_N)}. \tag{56}$$

We would like to make several comments on the formulations of the above algorithm, consisting of (49a)–(49c), (52a)–(52c), and (55a)–(55b). One can first note that the computations for the phase field functions are de-coupled from those for the pressure and the velocity, because of the explicit treatments of the convection terms in the discretized phase field equations (49a).

A prominent feature in the treatment of the coupled system of phase field equations lies in the $(N-1)^2$ extra terms, $\sum_{j=1}^{N-1}\frac{S_{ij}}{\eta^2}(\phi_j^{n+1}-\phi_j^{*,n+1})$ for $1 \leqslant i \leqslant N-1$, in the discrete form (49a). These extra terms are a crucial algorithmic construction. They will enable us to reformulate the $(N-1)$ semi-discretized fourth-order phase-field equations, which are strongly-coupled with one another, into $(N-1)$ individual fourth-order equations that are *completely de-coupled* from one another; see Section 2.4 for details. Then they further allow us to reformulate each individual fourth-order equation into two *de-coupled* Helmholtz-type equations using a technique developed previously for two-phase flows. Therefore, the discrete formulation in (49a) ultimately allows one to reformulate the $(N-1)$ coupled 4th-order phase field equations into $2(N-1)$ individual Helmholtz-type equations that are *completely de-coupled* from one another. This enables a successful treatment of the original fourth-order coupled system using C^0-continuous spectral elements (or finite elements); see Section 2.4 below for detailed discussions.

The computations for the pressure and for the velocity are also de-coupled in the above algorithm. One can recognize that the schemes in the discrete formulations of (52a) and (55a) for achieving this is a rotational velocity-correction type strategy; see [18,19,25]. The treatment for the variable density $\rho(\vec{\phi})$ follows a strategy first developed in [20] for two-phase flows, by introducing a constant ρ_0 in the discrete formulation. The condition on ρ_0, (54), is critical to the stability of the algorithm. This treatment of the variable density eventually gives rise to a pressure linear-algebraic system with a *constant* and *time-independent* coefficient matrix after discretization. Consequently, the pressure coefficient matrix can be pre-computed during pre-processing. This leads to an extremely efficient procedure for pressure computation, and effectively overcomes the performance bottleneck in N-phase flows caused by the variable coefficient matrix associated with the variable density.

The strategy for treating the variable dynamic viscosity $\mu(\vec{\phi})$ in the discrete formulation (55a) can be traced to the early ideas for variable diffusion coefficients in the 1970s (see e.g. [24]); see also the use of similar strategies in later studies [5,20] for two-phase flows. This treatment of the variable viscosity eventually gives rise to a velocity linear-algebraic system with a *constant* and *time-independent* coefficient matrix after discretization. This provides an efficient procedure for velocity computation. The lower bound on ν_0 in the condition (56) is a conservative estimation, and appears overly conservative based on numerical experiments. This condition can be relaxed. In the numerical simulations in Section 3, we will employ a value

$$\nu_0 = \max\left(\frac{\tilde{\mu}_1}{\tilde{\rho}_1}, \frac{\tilde{\mu}_2}{\tilde{\rho}_2}, \dots, \frac{\tilde{\mu}_N}{\tilde{\rho}_N}\right). \tag{57}$$

Let us next briefly comment on the treatments of different terms in the discrete formulation (52a). In particular, while the time derivative and the $\frac{1}{\rho_0}\nabla P$ term are approximated at time step $(n+1)$, the rest of terms are approximated at time step n. These approximations will not compromise the temporal accuracy of the velocity, due to the correction terms in (55a), such as $(\mathbf{u}^{*,n+1}\cdot\nabla\mathbf{u}^{*,n+1}-\mathbf{u}^n\cdot\nabla\mathbf{u}^n)$ and $\frac{1}{\rho^{n+1}}\nabla\mu^{n+1}\cdot[\mathbf{D}(\mathbf{u}^{*,n+1})-\mathbf{D}(\mathbf{u}^n)]$. On the other hand, according to the analysis in [25], they may slightly reduce the temporal accuracy of the pressure for certain error norms. This effect is however not quite obvious from our numerical experiments; see Section 3.2. Alternatively, one can also approximate all terms at time step $(n+1)$, which will improve the temporal accuracy of the pressure. Such an alternative scheme has been discussed in [20] for two-phase flows.

2.4. Solving coupled system of phase field equations

We employ high-order spectral elements [33,60] for spatial discretizations in the current paper. Let us now look into how to implement the algorithm with C^0 spectral elements. The formulations discussed below without any change also applies to low-order C^0 finite elements.

We first consider how to solve for the phase field functions ϕ_i^{n+1}. Eq. (49a) represents a system of $(N-1)$ coupled fourth-order equations about ϕ_i^{n+1}. We next present a method to reformulate this coupled system into $(N-1)$ individual fourth-order equations that are completely de-coupled from one another. We further reformulate each individual fourth-order equation into two *de-coupled* Helmholtz-type equations.

Re-write (49a) into

$$\sum_{j=1}^{N-1}\lambda_{ij}\nabla^2\left(\nabla^2\phi_j^{n+1}\right)-\frac{1}{\eta^2}\sum_{j=1}^{N-1}S_{ij}\nabla^2\phi_j^{n+1}+\frac{\gamma_0}{m_i\Delta t}\phi_i^{n+1}=Q_i=Q_i^{(1)}+\nabla^2R_i,\quad 1\leqslant i\leqslant N-1,\tag{58}$$

where

$$\begin{cases}Q_i^{(1)}=\dfrac{1}{m_i}\left(g_i^{n+1}-\mathbf{u}^{*,n+1}\cdot\nabla\phi_i^{*,n+1}+\dfrac{\hat{\phi}_i}{\Delta t}\right),\\[2ex] R_i=\dfrac{\beta^2}{\eta^2}h_i\left(\vec{\phi}^{*,n+1}\right)-\dfrac{1}{\eta^2}\displaystyle\sum_{j=1}^{N-1}S_{ij}\phi_j^{*,n+1}.\end{cases}\tag{59}$$

Note that S_{ij} are $(N-1)^2$ chosen constants to be determined below.

Let

$$\boldsymbol{\Phi}=\begin{bmatrix}\phi_1^{n+1}\\ \phi_2^{n+1}\\ \vdots\\ \phi_{N-1}^{n+1}\end{bmatrix},\qquad \mathbf{Q}=\begin{bmatrix}Q_1\\ Q_2\\ \vdots\\ Q_{N-1}\end{bmatrix},\qquad \mathbf{S}=[S_{ij}]_{(N-1)\times(N-1)},\qquad \mathbf{E}=\operatorname{diag}\left(\frac{\gamma_0}{m_1\Delta t},\frac{\gamma_0}{m_2\Delta t},\cdots,\frac{\gamma_0}{m_{N-1}\Delta t}\right).\tag{60}$$

Then Eq. (58) can be written into a compact matrix form

$$\mathbf{A}\nabla^2\left(\nabla^2\boldsymbol{\Phi}\right)-\frac{1}{\eta^2}\mathbf{S}\nabla^2\boldsymbol{\Phi}+\mathbf{E}\boldsymbol{\Phi}=\mathbf{Q}=\mathbf{Q}^{(1)}+\nabla^2\mathbf{R}\tag{61}$$

where the symmetric positive definite (SPD) matrix $\mathbf{A}$ is defined in Eq. (2), and

$$\mathbf{Q}^{(1)}=\begin{bmatrix}Q_1^{(1)}\\ Q_2^{(1)}\\ \vdots\\ Q_{N-1}^{(1)}\end{bmatrix},\qquad \mathbf{R}=\begin{bmatrix}R_1\\ R_2\\ \vdots\\ R_{N-1}\end{bmatrix}.\tag{62}$$

Multiplying both sides of Eq. (61) by the matrix

$$\mathbf{E}^{-\frac{1}{2}}=\operatorname{diag}\left(\sqrt{\frac{m_1\Delta t}{\gamma_0}},\sqrt{\frac{m_2\Delta t}{\gamma_0}},\cdots,\sqrt{\frac{m_{N-1}\Delta t}{\gamma_0}}\right),$$

we have

$$\mathbf{B}\nabla^2\left(\nabla^2\boldsymbol{\Psi}\right)-\frac{1}{\eta^2}\mathbf{S}_B\nabla^2\boldsymbol{\Psi}+\boldsymbol{\Psi}=\mathbf{E}^{-\frac{1}{2}}\mathbf{Q},\tag{63}$$

where

$$\boldsymbol{\Psi}=\mathbf{E}^{\frac{1}{2}}\boldsymbol{\Phi},\qquad \mathbf{B}=\mathbf{E}^{-\frac{1}{2}}\mathbf{A}\mathbf{E}^{-\frac{1}{2}},\qquad \mathbf{S}_B=\mathbf{E}^{-\frac{1}{2}}\mathbf{S}\mathbf{E}^{-\frac{1}{2}}.\tag{64}$$

One can note that matrix **B** is also SPD. Consequently, it can be diagonalized as follows,

$$\mathbf{P}^{-1}\mathbf{B}\mathbf{P} = \mathbf{K} = \operatorname{diag}(\hat{\lambda}_1, \hat{\lambda}_2, \cdots, \hat{\lambda}_{N-1}), \qquad \mathbf{B} = \mathbf{P}\mathbf{K}\mathbf{P}^{-1}, \tag{65}$$

where **K** is the diagonal matrix of the eigenvalues, $\hat{\lambda}_i$ (which are all positive), of the matrix **B**, and **P** is a non-singular matrix consisting of the eigen-vectors of matrix **B**. We can then transform Eq. (63) into

$$\mathbf{K}\nabla^2\big[\nabla^2\big(\mathbf{P}^{-1}\boldsymbol{\Psi}\big)\big] - \frac{1}{\eta^2}\big(\mathbf{P}^{-1}\mathbf{S}_B\mathbf{P}\big)\nabla^2\big(\mathbf{P}^{-1}\boldsymbol{\Psi}\big) + \mathbf{P}^{-1}\boldsymbol{\Psi} = \mathbf{P}^{-1}\mathbf{E}^{-\frac{1}{2}}\mathbf{Q}, \tag{66}$$

where we have used Eq. (65).

We choose $\mathbf{S}_B$ such that

$$\mathbf{P}^{-1}\mathbf{S}_B\mathbf{P} = \hat{\mathbf{S}} = \operatorname{diag}(\hat{s}_1, \hat{s}_2, \cdots, \hat{s}_{N-1}), \tag{67}$$

where $\hat{s}_i$ ($1 \leqslant i \leqslant N-1$) are constants to be determined below. Therefore, Eq. (66) is transformed into

$$\mathbf{K}\nabla^2\big(\nabla^2\mathbf{X}\big) - \frac{1}{\eta^2}\hat{\mathbf{S}}\nabla^2\mathbf{X} + \mathbf{X} = \mathbf{P}^{-1}\mathbf{E}^{-\frac{1}{2}}\mathbf{Q} = \mathbf{P}^{-1}\mathbf{E}^{-\frac{1}{2}}\mathbf{Q}^{(1)} + \mathbf{P}^{-1}\mathbf{E}^{-\frac{1}{2}}\nabla^2\mathbf{R}, \tag{68}$$

where $\mathbf{X} = \mathbf{P}^{-1}\boldsymbol{\Psi}$.

Eq. (68) represents a system of $(N-1)$ fourth-order equations that are completely de-coupled from one another. Let

$$\mathbf{X} = \begin{bmatrix} \xi_1^{n+1} \\ \xi_2^{n+1} \\ \vdots \\ \xi_{N-1}^{n+1} \end{bmatrix}, \qquad \mathbf{P}^{-1}\mathbf{E}^{-\frac{1}{2}}\mathbf{Q} = \begin{bmatrix} q_1 \\ q_2 \\ \vdots \\ q_{N-1} \end{bmatrix}, \qquad \mathbf{P}^{-1}\mathbf{E}^{-\frac{1}{2}}\mathbf{Q}^{(1)} = \begin{bmatrix} q_1^{(1)} \\ q_2^{(1)} \\ \vdots \\ q_{N-1}^{(1)} \end{bmatrix}, \qquad \mathbf{P}^{-1}\mathbf{E}^{-\frac{1}{2}}\mathbf{R} = \begin{bmatrix} r_1 \\ r_2 \\ \vdots \\ r_{N-1} \end{bmatrix}. \tag{69}$$

Then Eq. (68) is equivalent to,

$$\nabla^2\big(\nabla^2\xi_i^{n+1}\big) - \frac{\hat{s}_i}{\hat{\lambda}_i\eta^2}\nabla^2\xi_i^{n+1} + \frac{1}{\hat{\lambda}_i}\xi_i^{n+1} = \frac{1}{\hat{\lambda}_i}q_i, \quad 1 \leqslant i \leqslant N-1, \tag{70}$$

where $\hat{\lambda}_i$ ($1 \leqslant i \leqslant N-1$) are the eigenvalues of matrix **B**, $\hat{s}_i$ ($1 \leqslant i \leqslant N-1$) are chosen constants to be determined, and

$$q_i = q_i^{(1)} + \nabla^2 r_i, \quad 1 \leqslant i \leqslant N-1. \tag{71}$$

We have now transformed the $(N-1)$ coupled equations about ϕ_i^{n+1}, (58), into $(N-1)$ individual equations about ξ_i^{n+1} that are de-coupled from one another, (70).

Let us now consider the boundary conditions for the phase field functions. The conditions (49b) and (49c) can be written as

$$\mathbf{n} \cdot \nabla\boldsymbol{\Phi} = 0, \quad \text{on } \partial\Omega, \tag{72}$$

$$\mathbf{n} \cdot \nabla\big(\nabla^2\boldsymbol{\Phi}\big) = 0, \quad \text{on } \partial\Omega, \tag{73}$$

where $\boldsymbol{\Phi}$ is defined in (60). These two conditions can be transformed into

$$\mathbf{n} \cdot \nabla\mathbf{X} = 0, \quad \text{on } \partial\Omega, \tag{74}$$

$$\mathbf{n} \cdot \nabla\big(\nabla^2\mathbf{X}\big) = 0, \quad \text{on } \partial\Omega, \tag{75}$$

or equivalently

$$\mathbf{n} \cdot \nabla\xi_i^{n+1} = 0, \quad \text{on } \partial\Omega,\ 1 \leqslant i \leqslant N-1, \tag{76}$$

$$\mathbf{n} \cdot \nabla\big(\nabla^2\xi_i^{n+1}\big) = 0, \quad \text{on } \partial\Omega,\ 1 \leqslant i \leqslant N-1, \tag{77}$$

due to the relations

$$\mathbf{X} = \mathbf{P}^{-1}\mathbf{E}^{\frac{1}{2}}\boldsymbol{\Phi}, \qquad \boldsymbol{\Phi} = \mathbf{E}^{-\frac{1}{2}}\mathbf{P}\mathbf{X}, \tag{78}$$

and the fact that $\mathbf{E}^{-\frac{1}{2}}\mathbf{P}$ is a constant non-singular matrix.

Now let us consider how to solve the $(N-1)$ individual fourth-order equation (70). Each equation in (70) is similar in nature to the phase field equation encountered in two-phase flows [20]. Therefore we can reformulate this fourth-order equation into two *de-coupled* Helmholtz type equations using the technique developed previously; see [20,57].

Re-write (70) as

$$\nabla^2\left(\nabla^2\xi_i^{n+1} + \frac{\alpha_i}{\hat{\lambda}_i}\xi_i^{n+1}\right) - \frac{1}{\hat{\lambda}_i}\left(\alpha_i + \frac{\hat{s}_i}{\eta^2}\right)\left(\nabla^2\xi_i^{n+1} - \frac{1}{\alpha_i + \frac{\hat{s}_i}{\eta^2}}\xi_i^{n+1}\right) = \frac{1}{\hat{\lambda}_i}q_i, \tag{79}$$

where α_i is a constant to be determined. By requiring that

$$\frac{\alpha_i}{\hat{\lambda}_i} = -\frac{1}{\alpha_i + \frac{\hat{s}_i}{\eta^2}}, \tag{80}$$

we can determine the α_i value

$$\alpha_i = \frac{\hat{s}_i}{2\eta^2}\left(-1 - \sqrt{1 - 4\hat{\lambda}_i \frac{\eta^4}{\hat{s}_i^2}}\right), \quad \text{or} \quad \alpha_i = \frac{\hat{s}_i}{2\eta^2}\left(-1 + \sqrt{1 - 4\hat{\lambda}_i \frac{\eta^4}{\hat{s}_i^2}}\right), \tag{81}$$

and obtain the following condition about the chosen constant $\hat{s}_i$,

$$\hat{s}_i \geqslant 2\eta^2\sqrt{\hat{\lambda}_i}, \quad 1 \leqslant i \leqslant N-1. \tag{82}$$

Consequently, Eq. (79) can be reformulated into

$$\nabla^2\psi_i^{n+1} - \frac{1}{\hat{\lambda}_i}\left(\alpha_i + \frac{\hat{s}_i}{\eta^2}\right)\psi_i^{n+1} = \frac{1}{\hat{\lambda}_i}q_i, \quad 1 \leqslant i \leqslant N-1 \tag{83a}$$

$$\nabla^2\xi_i^{n+1} + \frac{\alpha_i}{\hat{\lambda}_i}\xi_i^{n+1} = \psi_i^{n+1}, \quad 1 \leqslant i \leqslant N-1, \tag{83b}$$

where ψ_i^{n+1} $(1 \leqslant i \leqslant N-1)$ are auxiliary phase-field variables. Eqs. (83a) and (83b) can be solved successively in an un-coupled fashion.

The boundary condition (77) can be transformed into, in light of (83b),

$$\mathbf{n} \cdot \nabla\psi_i^{n+1} = 0, \quad \text{on } \partial\Omega, \ 1 \leqslant i \leqslant N-1, \tag{84}$$

where we have used the condition (76).

In order to compute ξ_i^{n+1} from (70), we can successively solve (83a) for ψ_i^{n+1}, together with the boundary condition (84), and then solve (83b) for ξ_i^{n+1}, together with the boundary condition (76).

To facilitate the implementation with spectral elements, we next derive the weak forms for the phase field variables ξ_i^{n+1} and ψ_i^{n+1}. Let $\varphi \in H^1(\Omega)$ denote the test function. By taking the L^2 inner product between φ and Eq. (83a), we obtain the weak forms about ψ_i^{n+1},

$$\int_\Omega \nabla\psi_i^{n+1} \cdot \nabla\varphi + \frac{1}{\hat{\lambda}_i}\left(\alpha_i + \frac{\hat{s}_i}{\eta^2}\right)\int_\Omega \psi_i^{n+1}\varphi = -\frac{1}{\hat{\lambda}_i}\int_\Omega q_i^{(1)}\varphi + \frac{1}{\hat{\lambda}_i}\int_\Omega \nabla r_i \cdot \nabla\varphi, \quad \forall\varphi \in H^1(\Omega), \ 1 \leqslant i \leqslant N-1, \tag{85}$$

where we have used integration by part, boundary condition (84), and the fact that

$$\mathbf{n} \cdot \nabla R_i = \sum_{j=1}^{N-1} \frac{\partial R_i}{\partial\phi_j}\mathbf{n} \cdot \nabla\phi_j = 0, \quad \text{on } \partial\Omega, \ 1 \leqslant i \leqslant N-1, \tag{86}$$

because of the boundary condition (20). By taking the L^2 inner product between φ and Eq. (83b), we obtain the weak forms about ξ_i^{n+1},

$$\int_\Omega \nabla\xi_i^{n+1} \cdot \nabla\varphi - \frac{\alpha_i}{\hat{\lambda}_i}\int_\Omega \xi_i^{n+1}\varphi = -\int_\Omega \psi_i^{n+1}\varphi, \quad \forall\varphi \in H^1(\Omega), \ 1 \leqslant i \leqslant N-1, \tag{87}$$

where we have used integration by part and the boundary condition (76). Eqs. (85) and (87) can be discretized in space using C^0 spectral elements (or finite elements) in a straightforward fashion.

To summarize, in the pre-processing stage we need to compute the matrices **P** and **S** and the eigenvalues $\hat{\lambda}_i$ through the following procedure:

1. Compute matrix **B** in (64) based on the matrix **A** defined in (2) and the matrix **E** in (60).
2. Compute the eigenvalues $\hat{\lambda}_i$ and the eigenvectors of matrix **B**; Form the matrix **P** in (65) using the eigenvectors.
3. Choose $(N-1)$ constants $\hat{s}_i$ $(1 \leqslant i \leqslant N-1)$ that satisfy the conditions (82). Form the diagonal matrix $\hat{\mathbf{S}}$ defined in (67).
4. Compute matrix **S** in (60) as follows

$$\mathbf{S} = [S_{ij}] = \mathbf{E}^{\frac{1}{2}}\mathbf{P}\hat{\mathbf{S}}\mathbf{P}^{-1}\mathbf{E}^{\frac{1}{2}}. \tag{88}$$

At each time step, given $(\phi_i^n, \mathbf{u}^n)$, we compute $(\phi_i^{n+1}, \nabla^2\phi_i^{n+1})$ using the following procedure. We will refer to this procedure as **Advance-Phase** in subsequent sections. It consists of several steps.

Advance-Phase procedure:

1. Compute $Q_i^{(1)}$ and R_i $(1 \leqslant i \leqslant N-1)$ from Eq. (59); Form vectors $\mathbf{Q}^{(1)}$ and $\mathbf{R}$ in (62).
2. Compute vectors $\mathbf{P}^{-1}\mathbf{E}^{-\frac{1}{2}}\mathbf{Q}^{(1)}$ and $\mathbf{P}^{-1}\mathbf{E}^{-\frac{1}{2}}\mathbf{R}$ in (69). These will provide $q_i^{(1)}$ and r_i $(1 \leqslant i \leqslant N-1)$.
3. Solve Eq. (85) for ψ_i^{n+1} $(1 \leqslant i \leqslant N-1)$.
4. Solve Eq. (87) for ξ_i^{n+1} $(1 \leqslant i \leqslant N-1)$.
5. Compute $\boldsymbol{\Phi}$ based on Eq. (78). This will provide ϕ_i^{n+1} $(1 \leqslant i \leqslant N-1)$.
6. Compute $\nabla^2\boldsymbol{\Phi}$ based on the following, in light of Eq. (83b),

$$\begin{bmatrix} \nabla^2\phi_1^{n+1} \\ \nabla^2\phi_2^{n+1} \\ \vdots \\ \nabla^2\phi_{N-1}^{n+1} \end{bmatrix} = \nabla^2\boldsymbol{\Phi} = \mathbf{E}^{-\frac{1}{2}}\mathbf{P}\nabla^2\mathbf{X} = \mathbf{E}^{-\frac{1}{2}}\mathbf{P} \begin{bmatrix} \psi_1^{n+1} - \frac{\alpha_1}{\hat{\lambda}_1}\xi_1^{n+1} \\ \psi_2^{n+1} - \frac{\alpha_2}{\hat{\lambda}_2}\xi_2^{n+1} \\ \vdots \\ \psi_{N-1}^{n+1} - \frac{\alpha_{N-1}}{\hat{\lambda}_{N-1}}\xi_{N-1}^{n+1} \end{bmatrix}. \tag{89}$$

This will provide the data for $\nabla^2\phi_i^{n+1}$ $(1 \leqslant i \leqslant N-1)$, which will be needed for pressure and velocity computations.

2.5. Solving variable-density Navier–Stokes equations

Let us now assume that the phase field functions ϕ_i^{n+1} $(1 \leqslant i \leqslant N-1)$ have been computed and consider how to compute the pressure and velocity from the algorithm (52a)–(52c) and (55a)–(55b).

Apart from the term $\tilde{\mathbf{J}} \cdot \nabla\mathbf{u}$ and the surface tension terms $\sum_{i,j=1}^{N-1}\lambda_{ij}\nabla^2\phi_j\nabla\phi_i$, the issues encountered here for N-phase flows are similar to those encountered in two-phase flows [20]. The main difficulty lies in how to treat the second-derivative terms, such as $\nabla^2\phi_i\nabla\phi_j$, $\nabla \times \nabla \times \mathbf{u}$, which cannot be computed directly using C^0 spectral elements or finite elements. The numerical treatment of the $\nabla^2\phi_i$ terms has been provided in Eq. (89) in the previous section. The strategy for treating the $\nabla \times \nabla \times \mathbf{u}$ term using spectral elements was originally developed in [19,20] for single-phase and two-phase flows. We employ the same strategy here for N-phase implementations.

We will derive the weak forms for the pressure and the velocity in order to facilitate the implementation with C^0 spectral elements. In the process, the second-derivative terms will be dealt with in a natural way.

We re-write (52a) as

$$\frac{\gamma_0}{\Delta t}\tilde{\mathbf{u}}^{n+1} + \frac{1}{\rho_0}\nabla P^{n+1} = \mathbf{G}^{n+1} - \frac{\mu^{n+1}}{\rho^{n+1}}\nabla \times \nabla \times \mathbf{u}^n, \tag{90}$$

where

$$\begin{aligned} \mathbf{G}^{n+1} = {} & \frac{1}{\rho^{n+1}}\mathbf{f}^{n+1} - \left(\mathbf{u}^n + \frac{1}{\rho^{n+1}}\tilde{\mathbf{J}}^{n+1}\right) \cdot \nabla\mathbf{u}^n + \frac{\hat{\mathbf{u}}}{\Delta t} + \left(\frac{1}{\rho_0} - \frac{1}{\rho^{n+1}}\right)\nabla P^n + \frac{1}{\rho^{n+1}}\nabla\mu^{n+1} \cdot \mathbf{D}(\mathbf{u}^n) \\ & - \frac{1}{\rho^{n+1}}\sum_{i,j=1}^{N-1}\lambda_{ij}\nabla^2\phi_j^{n+1}\nabla\phi_i^{n+1}, \end{aligned} \tag{91}$$

and $\tilde{\mathbf{J}}^{n+1}$ is given by (53). Note that in both (91) and (53) the terms $\nabla^2\phi_j^{n+1}$ $(1 \leqslant j \leqslant N-1)$ shall be computed using Eq. (89). Therefore, $\mathbf{G}^{n+1}$ and $\tilde{\mathbf{J}}^{n+1}$ can be directly computed based on these expressions using C^0 elements.

Let $\varphi \in H^1(\Omega)$ denote the test function. Taking the L^2 inner product between Eq. (90) and $\nabla\varphi$, we obtain the weak form about the pressure P^{n+1},

$$\begin{aligned} \int_\Omega \nabla P^{n+1} \cdot \nabla\varphi = {} & \rho_0 \int_\Omega \left[\mathbf{G}^{n+1} + \nabla\left(\frac{\mu^{n+1}}{\rho^{n+1}}\right) \times \boldsymbol{\omega}^n\right] \cdot \nabla\varphi \\ & - \rho_0 \int_{\partial\Omega} \frac{\mu^{n+1}}{\rho^{n+1}}\mathbf{n} \times \boldsymbol{\omega}^n \cdot \nabla\varphi - \frac{\gamma_0\rho_0}{\Delta t}\int_{\partial\Omega}\mathbf{n} \cdot \mathbf{w}^{n+1}\varphi, \quad \forall\varphi \in H^1(\Omega), \end{aligned} \tag{92}$$

where $\mathbf{n}$ is the outward-pointing unit vector normal to $\partial\Omega$, $\boldsymbol{\omega} = \nabla \times \mathbf{u}$ is the vorticity, and we have used the integration by part, Eqs. (52b) and (52c), and the identity

$$\frac{\mu}{\rho}\nabla \times \boldsymbol{\omega} \cdot \nabla\varphi = \nabla \cdot \left[\frac{\mu}{\rho}\boldsymbol{\omega} \times \nabla\varphi\right] - \nabla\left(\frac{\mu}{\rho}\right) \times \boldsymbol{\omega} \cdot \nabla\varphi.$$

Sum up Eqs. (55a) and (52a), and we obtain the following equation about $\mathbf{u}^{n+1}$,

$$\frac{\gamma_0}{\nu_0 \Delta t}\mathbf{u}^{n+1} - \nabla^2 \mathbf{u}^{n+1} = \frac{1}{\nu_0}\mathbf{T}^{n+1} - \frac{1}{\nu_0}\left(\frac{\mu^{n+1}}{\rho^{n+1}} - \nu_0\right)\nabla \times \boldsymbol{\omega}^{*,n+1}, \tag{93}$$

where

$$\mathbf{T}^{n+1} = \frac{1}{\rho^{n+1}}\mathbf{f}^{n+1} - \left(\mathbf{u}^{*,n+1} + \frac{1}{\rho^{n+1}}\tilde{\mathbf{J}}^{n+1}\right)\cdot \nabla \mathbf{u}^{*,n+1} + \frac{\hat{\mathbf{u}}}{\Delta t} - \frac{1}{\rho^{n+1}}\nabla P^{n+1} + \frac{1}{\rho^{n+1}}\nabla \mu^{n+1}\cdot \mathbf{D}\big(\mathbf{u}^{*,n+1}\big) - \frac{1}{\rho^{n+1}}\sum_{i,j=1}^{N-1}\lambda_{ij}\nabla^2\phi_j^{n+1}\nabla\phi_i^{n+1}. \tag{94}$$

Note again that the $\nabla^2\phi_i^{n+1}$ involved in the above expression shall be computed based on Eq. (89). Therefore, $\mathbf{T}^{n+1}$ can be directly computed using C^0 spectral elements (or finite elements).

Let $H_0^1(\Omega) = \{\chi \in H^1(\Omega) : \chi|_{\partial\Omega} = 0\}$, and $\vartheta \in H_0^1(\Omega)$ denote the test function. Taking the L^2 inner product between Eq. (93) and ϑ, we obtain the weak form about $\mathbf{u}^{n+1}$,

$$\int_\Omega \nabla\vartheta \cdot \nabla \mathbf{u}^{n+1} + \frac{\gamma_0}{\nu_0 \Delta t}\int_\Omega \vartheta \mathbf{u}^{n+1} = \frac{1}{\nu_0}\int_\Omega \left[\mathbf{T}^{n+1} + \nabla\left(\frac{\mu^{n+1}}{\rho^{n+1}}\right)\times \boldsymbol{\omega}^{*,n+1}\right]\vartheta - \frac{1}{\nu_0}\int_\Omega \left(\frac{\mu^{n+1}}{\rho^{n+1}} - \nu_0\right)\boldsymbol{\omega}^{*,n+1}\times\nabla\vartheta, \quad \forall \vartheta \in H_0^1(\Omega), \tag{95}$$

where we have used integration by part, and the identity (χ denoting a scalar function)

$$\int_\Omega \chi \nabla\times\boldsymbol{\omega}\vartheta = \int_{\partial\Omega} \chi \mathbf{n}\times\boldsymbol{\omega}\vartheta - \int_\Omega \nabla\chi\times\boldsymbol{\omega}\vartheta + \int_\Omega \chi\boldsymbol{\omega}\times\nabla\vartheta. \tag{96}$$

The weak forms for the pressure and velocity, (92) and (95), involve no derivatives of order two or higher, noting that the $\nabla^2\phi_i^{n+1}$ terms in (91) and (94) shall be computed based on Eq. (89). These weak forms can be directly discretized in space using C^0 spectral elements (or finite elements). On can observe that both the pressure and velocity weak forms, after spatial discretization, give rise to linear algebraic systems with *constant* and *time-independent* coefficient matrices, which can be pre-computed during pre-processing. Note also that in Eq. (95) different velocity components are not coupled and therefore can be computed individually. In addition, one can observe that the auxiliary velocity $\tilde{\mathbf{u}}^{n+1}$ is absent from the final weak-form formulations. Therefore, it is not necessary to compute $\tilde{\mathbf{u}}^{n+1}$ in the implementation.

We finally briefly comment on the computations of the mixture density ρ^{n+1} and the mixture dynamic viscosity μ^{n+1}. Once ϕ_i^{n+1} ($1 \leqslant i \leqslant N-1$) are known, the density will be computed based on Eq. (10) and the dynamic viscosity will be computed based on Eq. (11). In practice we observe that the numerical values for ϕ_i may slightly go out of range ($-1 \leqslant \phi_i \leqslant 1$) at certain spatial points. If the maximum density ratio among the N fluids is large, this may give rise to unphysical (negative) density values at certain spatial points and thus cause numerical difficulties. Similar situation has also been observed in two-phase flows; see the discussions in this regard in [20] for two-phase flows. Therefore, when the maximum density ratio among the N fluids is large (typically beyond about 10^2), we will further use the following equation to clamp the values for the mixture density and mixture dynamic viscosity,

$$\rho^{n+1} = \begin{cases} \rho^{n+1}, & \text{if } \tilde{\rho}_{\min} \leqslant \rho^{n+1} \leqslant \tilde{\rho}_{\max} \\ \tilde{\rho}_{\max}, & \text{if } \rho^{n+1} > \tilde{\rho}_{\max} \\ \tilde{\rho}_{\min}, & \text{if } \rho^{n+1} < \tilde{\rho}_{\min} \end{cases} \qquad \mu^{n+1} = \begin{cases} \mu^{n+1}, & \text{if } \tilde{\mu}_{\min} \leqslant \mu^{n+1} \leqslant \tilde{\mu}_{\max} \\ \tilde{\mu}_{\max}, & \text{if } \mu^{n+1} > \tilde{\mu}_{\max} \\ \tilde{\mu}_{\min}, & \text{if } \mu^{n+1} < \tilde{\mu}_{\min}, \end{cases} \tag{97}$$

where $\tilde{\rho}_{\max} = \max(\tilde{\rho}_1, \cdots, \tilde{\rho}_N)$, $\tilde{\rho}_{\min} = \min(\tilde{\rho}_1, \cdots, \tilde{\rho}_N)$, $\tilde{\mu}_{\max} = \max(\tilde{\mu}_1, \cdots, \tilde{\mu}_N)$, and $\tilde{\mu}_{\min} = \min(\tilde{\mu}_1, \cdots, \tilde{\mu}_N)$.

Overall Solution procedure:

By combining the discussions from this section and the previous section, we arrive at the overall solution procedure for N-phase flow simulations. Given $(\phi_i^n, P^n, \mathbf{u}^n)$, our final algorithm consists of the following steps:

1. Employ the **Advance-Phase** procedure from Section 2.4 to compute ϕ_i^{n+1} and $\nabla^2\phi_i^{n+1}$ for $1 \leqslant i \leqslant N-1$.
2. Compute ρ^{n+1} based on Eq. (10), μ^{n+1} based on (11), and $\tilde{\mathbf{J}}^{n+1}$ based on (53). If the maximum density ratio among the N fluids is large, further apply Eq. (97) to ρ^{n+1} and μ^{n+1}.
3. Solve Eq. (92) for P^{n+1}.
4. Solve Eq. (95), together with the velocity Dirichlet condition (55b) on $\partial\Omega$, for $\mathbf{u}^{n+1}$.

One can observe that the above algorithm for N-phase flows has several characteristics that make it computationally very efficient:

- The computations for the $(N-1)$ phase field functions are completely de-coupled.
- The computations for different flow variables – pressure, velocity, and phase field functions – are completely de-coupled.
- The computations for different components of the velocity are completely de-coupled.
- Only linear algebraic systems are involved after discretization. No nonlinear algebraic solver is needed.
- The algorithm results in, after discretization, pressure and velocity linear algebraic systems with constant and time-independent coefficient matrices, which can be pre-computed during pre-processing.
- The algorithm results in, after discretization, constant and time-independent coefficient matrices for all the phase field functions ϕ_i^{n+1} and auxiliary phase field functions ψ_i^{n+1}. These coefficient matrices can be pre-computed.
- The algorithm involves the solution of only Helmholtz type (including Poisson) equations within a time step.

In addition, the resultant weak-form formulations can be directly implemented using C^0-continuous spectral elements or finite elements.

3. Representative numerical examples

We employ several numerical examples in this section in two dimensions, involving three to five fluid phases, to demonstrate the capabilities and performance of the N-phase algorithm we developed in the previous section. These test problems involve air, water, oil, and oil-like fluids with large density contrasts and large viscosity contrasts. We first briefly discuss the normalization of the flow variables, governing equations and boundary conditions. Then we demonstrate the spatial and temporal convergence rates of our algorithm using an analytic solution to the N-phase system. After that we consider the equilibrium configurations of oil drops or oil puddles floating on the air–water interface involving three or four fluid phases, and in particular we compare simulations results with the de Gennes theory. Finally, we simulate the dynamics of fluid drops and fluid interfaces with five fluid phases.

3.1. Normalization of flow variables and governing equations

To facilitate discussions in subsequent sections, we first briefly discuss the normalization of the flow variables, physical and numerical parameters, governing equations, and the boundary conditions.

Let L denote a characteristic length scale, and U_0 denote a characteristic velocity scale. We use the superscript in $(\cdot)^*$ to denote the non-dimensionalization of the variable $(\cdot)$. We normalize the flow variables and physical parameters as follows:

$$\begin{cases} \mathbf{x}^* = \dfrac{\mathbf{x}}{L}, \quad t^* = \dfrac{t}{L/U_0}, \quad p^* = \dfrac{p}{\tilde{\rho}_1 U_0^2}, \quad \mathbf{u}^* = \dfrac{\mathbf{u}}{U_0}, \quad \eta^* = \dfrac{\eta}{L}, \quad \beta^* = \dfrac{\beta}{\sqrt{\tilde{\rho}_1 U_0 L}}, \quad \mathbf{g}_r^* = \dfrac{\mathbf{g}_r}{U_0^2/L} \\ \tilde{\rho}_i^* = \dfrac{\tilde{\rho}_i}{\tilde{\rho}_1}, \quad \tilde{\mu}_i^* = \dfrac{\tilde{\mu}_i}{\tilde{\rho}_1 U_0 L}, \quad m_i^* = \dfrac{m_i \tilde{\rho}_1 U_0}{L}, \quad \tilde{\gamma}_i^* = \tilde{\rho}_1 \tilde{\gamma}_i, \quad \rho_i^*(\vec{\phi}) = \dfrac{\rho_i(\vec{\phi})}{\tilde{\rho}_1}, \quad 1 \leqslant i \leqslant N \\ \sigma_{ij}^* = \dfrac{\sigma_{ij}}{\tilde{\rho}_1 U_0^2 L}, \quad 1 \leqslant i < j \leqslant N \\ \lambda_{ij}^* = \dfrac{\lambda_{ij}}{\tilde{\rho}_1 U_0^2 L^2}, \quad 1 \leqslant i, j \leqslant N-1 \\ \rho^*(\vec{\phi}) = \dfrac{\rho(\phi)}{\tilde{\rho}_1}, \quad \mu^*(\vec{\phi}) = \dfrac{1}{\mathrm{Re}} \dfrac{\mu(\vec{\phi})}{\tilde{\mu}_1} = \dfrac{\tilde{\mu}_1}{\tilde{\rho}_1 U_0 L} \dfrac{\mu(\vec{\phi})}{\tilde{\mu}_1} \end{cases} \tag{98}$$

where $\mathbf{g}_r$ is the gravitational acceleration, and $\mathrm{Re} = \frac{\tilde{\rho}_1 U_0 L}{\tilde{\mu}_1}$ is the Reynolds number based on the properties of the first fluid.

Consequently, the governing equations (1a)–(1c) are transformed into the following non-dimensional form:

$$\rho^* \left(\frac{\partial \mathbf{u}^*}{\partial t^*} + \mathbf{u}^* \cdot \nabla^* \mathbf{u}^* \right) + \tilde{\mathbf{J}}^* \cdot \nabla^* \mathbf{u}^*$$

$$= -\nabla^* p^* + \nabla^* \cdot \left[\mu^* \mathbf{D}^* \left(\mathbf{u}^* \right) \right] - \sum_{i,j=1}^{N-1} \lambda_{ij}^* \nabla^* \cdot \left(\nabla^* \phi_i \nabla^* \phi_j \right) + \mathbf{f}^* \left(\mathbf{x}^*, t^* \right) \tag{99a}$$

$$\nabla^* \cdot \mathbf{u}^* = 0 \tag{99b}$$

$$\frac{\partial \phi_i}{\partial t^*} + \mathbf{u}^* \cdot \nabla^* \phi_i = m_i^* \nabla^{*2} \left[-\sum_{j=1}^{N-1} \lambda_{ij}^* \nabla^{*2} \phi_j + \frac{\beta^{*2}}{\eta^{*2}} h_i^*(\vec{\phi}) \right] + g_i^* \left(\mathbf{x}^*, t^* \right), \quad 1 \leqslant i \leqslant N-1, \tag{99c}$$

where $\nabla^* = \frac{\partial}{\partial \mathbf{x}^*}$, $\mathbf{D}^*(\mathbf{u}^*) = \nabla^* \mathbf{u}^* + (\nabla^* \mathbf{u}^*)^T$, and

$$\mathbf{f}^* = \frac{\mathbf{f} L}{\tilde{\rho}_1 U_0^2}, \quad g_i^* = \frac{L}{U_0} g_i, \quad 1 \leqslant i \leqslant N-1. \tag{100}$$

$h_i^*(\vec{\phi})$ is given by

$$h_i^*(\vec{\phi}) = \frac{\tilde{\rho}_i^* + \tilde{\rho}_N^*}{2} \sum_{k=1}^{N} \left(\tilde{\gamma}_k^* \delta_{ki} - \frac{\tilde{\gamma}_k^* \tilde{\gamma}_i^*}{\Gamma^*} \right) c_k(1-c_k)(1-2c_k), \quad 1 \leqslant i \leqslant N-1,$$

where $\Gamma^* = \sum_{i=1}^{N} \tilde{\gamma}_k^*$. $\tilde{\mathbf{J}}^*$ is given by

$$\tilde{\mathbf{J}}^* = -\sum_{i=1}^{N-1} \left(1 - \frac{N}{\Gamma^*} \tilde{\gamma}_i^* \right) \frac{\tilde{\rho}_i^* + \tilde{\rho}_N^*}{2} m_i^* \nabla^* \left[-\sum_{j=1}^{N-1} \lambda_{ij}^* \nabla^{*2} \phi_j + \frac{\beta^{*2}}{\eta^{*2}} h_i^*(\vec{\phi}) \right].$$

The boundary conditions for the velocity and phase field functions, (19)–(21), are transformed into

$$\begin{cases} \mathbf{u}^* = \mathbf{w}^*(\mathbf{x}^*, t^*), & \text{on } \partial\Omega, \\ \mathbf{n} \cdot \nabla^* \phi_i = 0, & \text{on } \partial\Omega, \ 1 \leqslant i \leqslant N-1, \\ \mathbf{n} \cdot \nabla^* (\nabla^{*2} \phi_i) = 0, & \text{on } \partial\Omega, \ 1 \leqslant i \leqslant N-1, \end{cases} \tag{101}$$

where $\mathbf{w}^* = \frac{\mathbf{w}}{U_0}$ is the normalized boundary velocity.

It is evident that, when the flow variables and parameters are normalized as given in (98) and (100), the forms for the non-dimensionalized governing equations and boundary conditions will remain the same. Therefore, hereafter we will drop the superscript $(\cdot)^*$ in the non-dimensionalized forms, with the understanding that all the flow variables and parameters have been appropriately normalized.

3.2. Convergence rates

The goal of this section is to demonstrate the spatial and temporal convergence rates of the N-phase algorithm from Section 2 using a contrived analytic solution to the system of N-phase governing equations.

Consider the flow domain, $0 \leqslant x \leqslant 2$ and $-1 \leqslant y \leqslant 1$, and the following analytic solutions to the governing equations, (47) and (1b)–(1c), with four fluid phases ($N = 4$):

$$\begin{cases} u = A \cos \pi y \sin ax \sin \omega t \\ v = -\dfrac{Aa}{\pi} \sin \pi y \cos ax \sin \omega t \\ P = A \sin \pi y \sin ax \cos \omega t \\ \phi_1 = A_1 \cos a_1 x \cos b_1 y \sin \omega_1 t \\ \phi_2 = A_2 \cos a_2 x \cos b_2 y \sin \omega_2 t \\ \phi_3 = A_3 \cos a_3 x \cos b_3 y \sin \omega_3 t \end{cases} \tag{102}$$

where (u, v) are the two components of velocity $\mathbf{u}$, and A, A_1, A_2, A_3, a, a_1, a_2, a_3, b_1, b_2, b_3, ω, ω_1, ω_2, and ω_3 are prescribed constants. In the governing equations we choose the body force $\mathbf{f}$ and the source terms g_i $(1 \leqslant i \leqslant 3)$ in such a way that the analytic expressions of (102) satisfy the system of governing equations of (47), (1b) and (1c). On the domain boundaries we impose the Dirichlet condition (19) for the velocity, and the boundary velocity $\mathbf{w}$ is chosen according to the analytic expressions from (102). For the phase field functions ϕ_i $(1 \leqslant i \leqslant 3)$, we choose the constants a_1, a_2, a_3, b_1, b_2 and b_3 such that the boundary conditions (20) and (21) are satisfied. The initial conditions for the velocity $\mathbf{u}$ and the phase field functions ϕ_i $(1 \leqslant i \leqslant 3)$ are chosen by setting $t = 0$ to the analytic expressions in (102).

We discretize the domain using two equal-sized quadrilateral spectral elements (partitioned along the x direction), while the element order is varied in the tests. The algorithm from Section 2 is employed to integrate the governing equations in time from $t = 0$ to a final time $t = t_f$, and then the error of the numerical solution is computed at $t = t_f$ against the analytic expression given in (102).

We have employed the following parameter values for this problem:

$$\begin{cases} A = 2.0, \quad A_1 = A_2 = A_3 = 1.0, \quad a = a_1 = a_2 = a_3 = \pi, \quad b_1 = b_2 = b_3 = \pi, \\ \omega = \omega_1 = 1.0, \quad \omega_2 = 1.2, \quad \omega_3 = 0.8, \\ \tilde{\rho}_1 = 1.0, \quad \tilde{\rho}_2 = 3.0, \quad \tilde{\rho}_3 = 2.0, \quad \tilde{\rho}_4 = 4.0, \\ \tilde{\mu}_1 = 0.01, \quad \tilde{\mu}_2 = 0.02, \quad \tilde{\mu}_3 = 0.03, \quad \tilde{\mu}_4 = 0.04, \\ m_1 = 10^{-3}, \quad m_2 = 2 \times 10^{-3}, \quad m_3 = 3 \times 10^{-3}, \quad \eta = 0.1, \quad \beta = 0.05, \\ \sigma_{12} = 4.656 \times 10^{-3}, \quad \sigma_{13} = 4.472 \times 10^{-3}, \quad \sigma_{14} = 1.356 \times 10^{-2}, \\ \sigma_{23} = 6.110 \times 10^{-3}, \quad \sigma_{24} = 1.559 \times 10^{-2}, \quad \sigma_{34} = 1.609 \times 10^{-2}, \\ \text{(integration order) } J = 2, \\ \nu_0 = \max\left(\dfrac{\tilde{\mu}_1}{\tilde{\rho}_1}, \dfrac{\tilde{\mu}_2}{\tilde{\rho}_2}, \dfrac{\tilde{\mu}_3}{\tilde{\rho}_3}, \dfrac{\tilde{\mu}_4}{\tilde{\rho}_4} \right), \quad \rho_0 = \min(\tilde{\rho}_1, \tilde{\rho}_2, \tilde{\rho}_3, \tilde{\rho}_4). \end{cases} \tag{103}$$

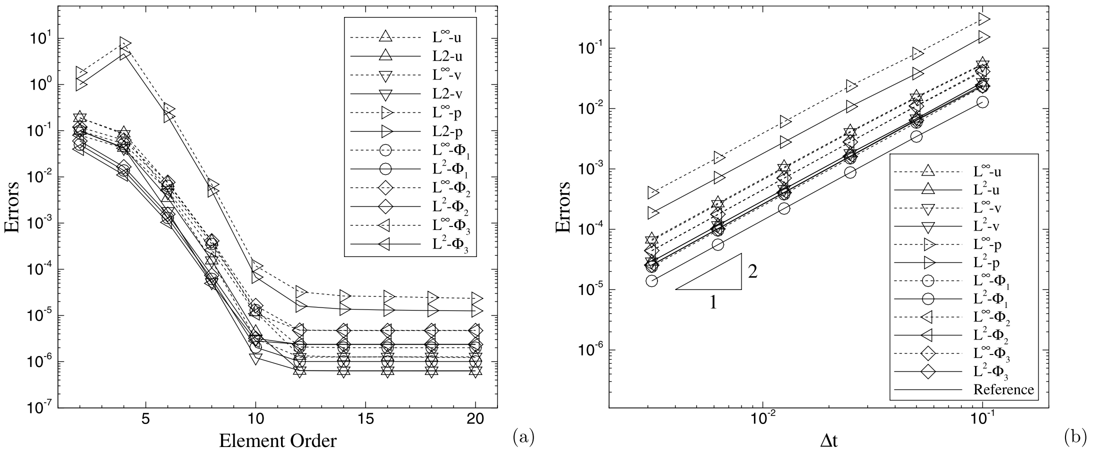

(a) (b)

Fig. 1. Convergence rates (4 fluid phases): (a) Numerical errors as a function of element order (fixed Δt) showing spatial exponential convergence rate and error saturation at large element orders due to temporal truncation error. (b) Numerical errors as a function of Δt (fixed element order) showing temporal 2nd-order convergence rate.

In the first set of tests, we fix the time step size at $\Delta t = 0.001$ and the final integration time at $t_f = 0.1$ (i.e. 100 time steps), and vary the element order systematically between 2 and 20. Fig. 1(a) shows the numerical errors in L^∞ and L^2 norms at $t = t_f$ for the velocity, pressure, and the three phase field functions, as a function of the element order. It can be observed that, as the element order increases (when below order 10 or 12), the numerical errors decrease exponentially, indicative of a spatial exponential convergence rate. As the element order increases beyond 12, the error curves level off with increasing element order, due to the saturation by the temporal truncation error.

In the second set of tests, we fix the final integration time at $t_f = 0.5$ and the element order at a high value 18, and then vary the time step size systematically between $\Delta t = 0.003125$ and $\Delta t = 0.1$. Fig. 1(b) shows the numerical errors of different flow variables at $t = t_f$ as a function of the time step size in logarithmic scales. The results clearly exhibit a second-order convergence rate in time.

The above results indicate that our algorithm presented in Section 2 has a spatial exponential convergence rate and a temporal second-order accuracy for different flow variables.

3.3. Floating liquid lens for three fluid phases and comparison with de Gennes theory

The goal of this section is to demonstrate the capability and accuracy of our method with the "floating liquid lens" problem involving three fluid phases by comparing with the theory of de Gennes [15].

We consider a drop of oil floating on the surface of water in ambient air. Depending on the relative importance of the gravity and the surface tensions, the oil may form a lens or a puddle on the water surface. The competition between the gravity and the surface tensions involves three characteristic length scales [15],

$$\begin{cases} \kappa_o = \sqrt{\dfrac{\sigma_{ao}}{\rho_o g_r}} & \text{(capillary length associated with air/oil interface)} \\ \kappa_w = \sqrt{\dfrac{\sigma_{aw}}{\rho_w g_r}} & \text{(capillary length associated with air/water interface)} \\ \kappa_{ow} = \sqrt{\dfrac{\sigma_{ow}}{(\rho_w - \rho_o) g_r}} & \text{(capillary length associated with oil/water interface)} \end{cases} \tag{104}$$

where g_r is the gravitational acceleration, ρ_a, ρ_w and ρ_o are respectively the densities of air, water and oil. σ_{ao}, σ_{aw} and σ_{ow} are respectively the surface tensions associated with the air/oil, air/water, and oil/water interfaces. Let R denote the characteristic size of the oil drop. If $R \ll \kappa_o$ and $R \ll \kappa_{ow}$, then the surface tension effect is dominant, and the oil-drop shape is made of two spherical caps (or in 2-D circular caps). If $R \gg \kappa_o$ and $R \gg \kappa_{ow}$, then the gravity effect is dominant, and the oil forms a puddle [15]. In this problem we simulate the equilibrium configurations of the oil drop floating on the air–water interface, and compare with the de Gennes theory.

The problem setup is as follows (Fig. 2). We consider a rectangular domain, $-L \leqslant x \leqslant L$ and $0 \leqslant y \leqslant \frac{4}{5}L$, where L is the characteristic length to be specified later. The gravity is assumed to be along the vertical $(-y)$ direction. The bottom and top sides of the domain ($y = 0$ and $\frac{4}{5}L$) are two solid walls. In the horizontal direction ($x = \pm L$) we assume that the problem is periodic. Initially, the bottom half the domain is filled with water and the top half is filled with air. In addition, a circular oil drop with radius $R_0 = \frac{L}{5}$ is placed on the air–water interface, with its center located at $\mathbf{x}_c = (x_c, y_c) = (0, \frac{2}{5}L)$. We assume that there is no initial flow. This three-phase system is then released, and it eventually evolves to an equilibrium state.

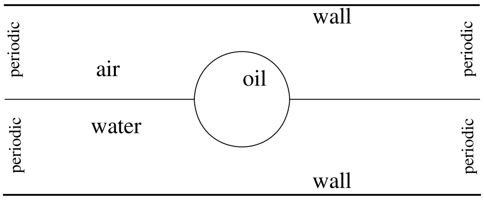

Fig. 2. Initial configuration of 3-phase air/water/oil problem.

We employ the following values for the physical parameters involved in this problem:

$$\begin{cases} \text{density [kg/m}^3\text{]:} \quad \text{air – 1.2041}, \quad \text{water – 998.207}, \quad \text{oil –577 (or varied)} \\ \text{dynamic viscosity [kg/(m}\cdot\text{s)]:} \quad \text{air – } 1.78\times10^{-5}, \quad \text{water – } 1.002\times10^{-3}, \quad \text{oil – } 9.15\times10^{-2} \\ \text{surface tensions [kg/s}^2\text{]:} \quad \text{air/water – 0.0728}, \quad \text{air/oil – 0.055}, \quad \text{oil/water – 0.04 (or varied)}, \\ \text{gravity [m/s}^2\text{]:} \quad \text{9.8 (or varied).} \end{cases} \tag{105}$$

The problem is non-dimensionalized with the characteristic length L and a characteristic velocity $U_0 = \sqrt{g_{r0}L}$, where $g_{r0} = 1$ m/s^2, using the procedure outlined in Section 3.1.

In the simulations we treat air, water and oil respectively as the first, second, and third fluid. We discretize the domain with 160 quadrilateral spectral elements, with 20 elements in the x direction and 8 elements in the y direction. We use an element order 14 within each element. On the top and bottom walls, we impose the Dirichlet boundary condition (19) with $\mathbf{w} = 0$ for the velocity, and the boundary conditions (20) and (21) for the phase field functions. In the horizontal direction we impose the periodic boundary conditions. The initial velocity is set zero. The initial conditions for the phase field functions are set as follows,

$$\phi_i(\mathbf{x}, t=0) = \frac{\tilde{\rho}_i}{\tilde{\rho}_i + \tilde{\rho}_N}(2c_i - 1) - \frac{\tilde{\rho}_N}{\tilde{\rho}_i + \tilde{\rho}_N}(2c_N - 1), \quad 1 \leqslant i \leqslant N-1, \tag{106}$$

where $N = 3$ and the initial volume fractions c_i are

$$\begin{aligned} c_1 &= \big[1 - \theta(x, x_c - R_0) + \theta(x, x_c + R_0)\big]\frac{1}{2}\left(1 + \tanh\frac{y - y_c}{\sqrt{2}\eta}\right) \\ &\quad + \big[\theta(x, x_c - R_0) - \theta(x, x_c + R_0)\big]\frac{1}{2}\left(1 + \tanh\frac{|\mathbf{x} - \mathbf{x}_c| - R_0}{\sqrt{2}\eta}\right)\theta(y, y_c), \\ c_2 &= \big[1 - \theta(x, x_c - R_0) + \theta(x, x_c + R_0)\big]\frac{1}{2}\left(1 - \tanh\frac{y - y_c}{\sqrt{2}\eta}\right) \\ &\quad + \big[\theta(x, x_c - R_0) - \theta(x, x_c + R_0)\big]\frac{1}{2}\left(1 + \tanh\frac{|\mathbf{x} - \mathbf{x}_c| - R_0}{\sqrt{2}\eta}\right)\big[1 - \theta(y, y_c)\big], \\ c_3 &= \frac{1}{2}\left(1 - \tanh\frac{|\mathbf{x} - \mathbf{x}_c| - R_0}{\sqrt{2}\eta}\right), \end{aligned}$$

and $\theta(x, a)$ is the Heaviside step function, taking unit value if $x \geqslant a$ and vanishing otherwise.

In the simulations we choose β in the free energy density expression (3) in a way such that η will correspond to the characteristic interfacial thickness of the interface between the pair of fluids with the smallest surface tension. Let $\sigma_{\min} = \min\{\sigma_{ij}\}_{1 \leqslant i < j \leqslant N}$ denote the smallest value among the $\frac{1}{2}N(N-1)$ surface tensions. Then this condition gives rise to

$$\beta = \sqrt{3\sqrt{2}\sigma_{\min}\eta}. \tag{107}$$

Therefore, once η is chosen, β can be determined from Eq. (107). The mixing energy density coefficients λ_{ij} $(1 \leqslant i, j \leqslant 2)$ are computed from the pair-wise surface tensions σ_{ij} $(1 \leqslant i < j \leqslant 3)$ using the method presented in Section 2.2.

We have employed the following numerical parameter values in the simulations:

$$\begin{cases} \dfrac{\eta}{L} = 0.0075, \\ \dfrac{m_1\tilde{\rho}_1 U_0}{L} = \dfrac{m_2\tilde{\rho}_1 U_0}{L} = \dfrac{10^{-7}}{\lambda^*_{\max}}, \quad \text{where } \lambda^*_{\max} = \dfrac{1}{\tilde{\rho}_1 U_0^2 L^2}\max\{\lambda_{ij}\}_{i,j=1,2}, \\ \nu_0 = \max\left(\dfrac{\tilde{\mu}_1}{\tilde{\rho}_1}, \dfrac{\tilde{\mu}_2}{\tilde{\rho}_2}, \dfrac{\tilde{\mu}_3}{\tilde{\rho}_3}\right), \\ \rho_0 = \min(\tilde{\rho}_1, \tilde{\rho}_2, \tilde{\rho}_3). \end{cases} \tag{108}$$

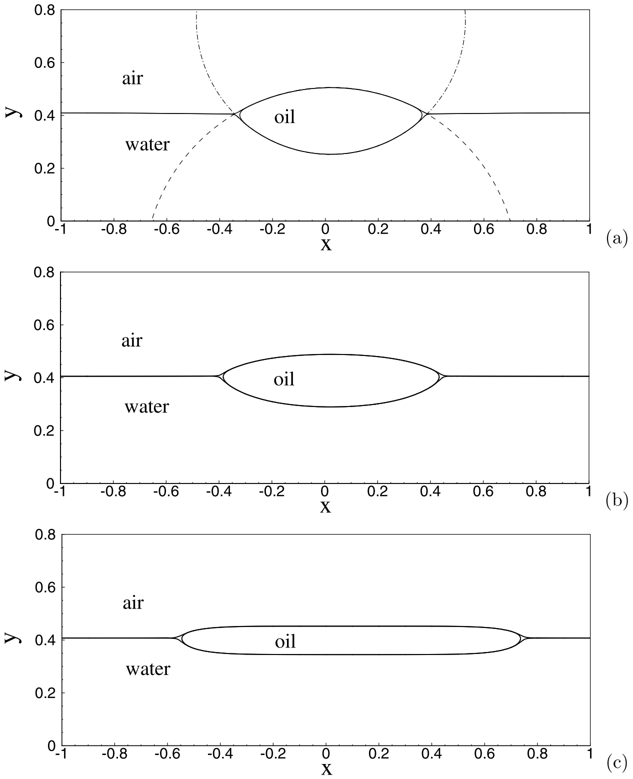

Fig. 3. Effect of gravity on the equilibrium configuration of an oil drop on air–water interface (3 fluid phases): (a) no gravity, (b) $g_r = 2$ m/s^2, (c) $g_r = 9.8$ m/s^2. In (a), dashed and dashed-dot curves are circular, showing that the oil drop consists of two circular caps in this case.

The time step size is $\Delta t = 10^{-5}$ in non-dimensional unit.

We now look into the case with a characteristic length $L = 4$ cm. This corresponds to an 8 cm × 3.2 cm domain, with an initial diameter 1.6 cm for the oil drop.

Let us first consider the effects of the gravity on the equilibrium oil-drop configurations. We systematically vary the value of the gravitational acceleration while fixing all the other physical parameters. In particular, the oil density is 577 kg/m^3 (air–oil density ratio ~ 479), the oil–water surface tension is 0.04 kg/s^2, and the other parameters are provided in (105). Due to the competition between the gravity and surface tension effects, the oil drop configuration changes dramatically as the gravity changes. Fig. 3 shows the equilibrium configurations of the oil drop corresponding to three gravitational acceleration values, $g_r = 0$, 2.0 m/s^2 and 9.8 m/s^2, from our simulations. Plotted are the contour levels $c_i = \frac{1}{2}$ $(1 \leqslant i \leqslant 3)$ for the three fluids, where c_i is the volume fraction of fluid i. At the three-phase contact lines in these plots, a "star-shaped" region can be observed. The presence of these regions is due to the fact that within them none of the three fluids has a volume fraction larger than $\frac{1}{2}$. Fig. 3(a) shows the oil drop configuration in the absence of gravity, where the surface tensions dominate. The dashed curve and the dashed-dot curve are two circles that respectively coincide with the upper and lower pieces that form the oil drop profile. They clearly show that the drop shape consists of two circular caps in this case. As the gravity magnitude increases, the oil drop becomes flatter (Fig. 3(b)). When the gravity is sufficiently large, the oil forms a puddle on the water surface (Fig. 3(c)). These simulation results are qualitatively consistent the de Gennes theory [15].

We next show quantitative comparisons with the de Gennes theory. Let us define the thickness of the oil drop/puddle as the largest distance between the upper and lower boundaries of the drop/puddle profile in the vertical direction. When the gravity effect dominates, the asymptotic thickness of the oil puddle can be obtained analytically by minimizing the total energy due to the surface tensions and the gravity [15]. Let e_c denote the asymptotic thickness of the oil puddle. Then it is given by [15,39],

$$e_c = \sqrt{\frac{2(\sigma_{ao} + \sigma_{ow} - \sigma_{aw})}{\frac{\rho_o}{\rho_w}(\rho_w - \rho_o) g_r}}. \tag{109}$$

Fig. 4 shows the oil drop/puddle thickness as a function of the gravitational acceleration obtained from our simulations (symbols). For comparison, the dashed curve in the plot shows the asymptotic puddle thickness (e_c) versus gravity (g_r) from the theory, see Eq. (109), where the gravity has been normalized by $g_{r0} = 1$ m/s^2. It can be observed that at large gravity values (beyond about 5 m/s^2 for this case), when the oil forms a puddle, the simulated puddle thickness agrees very well with that from the theory. At small gravity values, the drop shape markedly deviates from that of a puddle, and

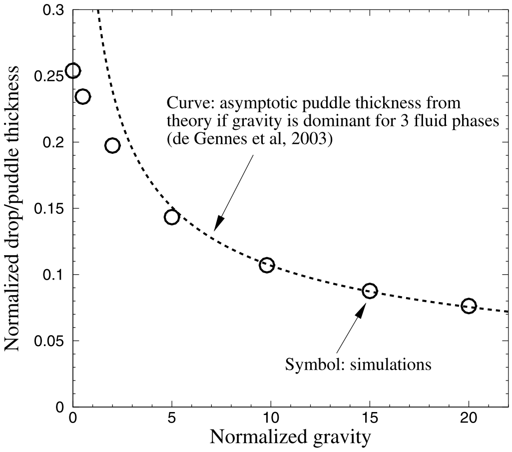

Fig. 4. Comparison of oil-drop/oil-puddle thickness (air–water–oil 3 phases) as a function of normalized gravity between current simulation and the de Gennes theory [15]. Gravity is varied while all other physical parameters are fixed.

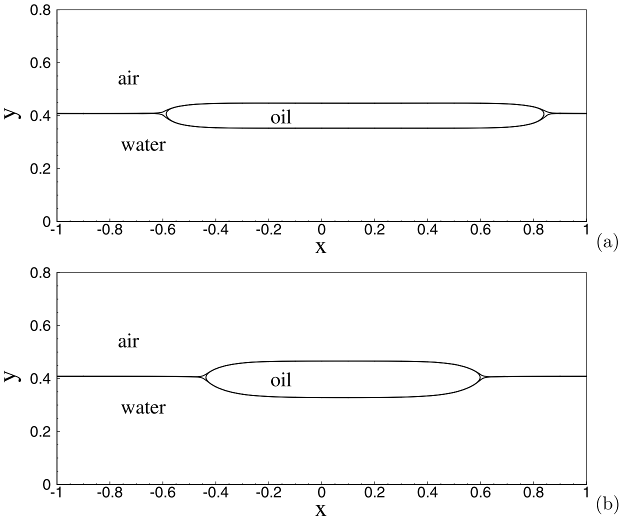

Fig. 5. Effect of oil–water surface tension on the equilibrium configuration of an oil drop floating on the air–water interface (3 fluid phases): (a) $\sigma_{ow} = 0.035$ kg/s^2, (b) $\sigma_{ow} = 0.055$ kg/s^2. Gravity is 9.8 m/s^2.

the theoretical asymptotic puddle thickness expression (109) is no longer valid. Therefore we observe a large discrepancy between the simulated drop thickness and the asymptotic theoretical thickness.

We next look into the effect of surface tensions on the equilibrium oil drop configurations. In this set of tests, we vary the surface tension of the oil–water interface (σ_{ow}) systematically, while fixing the gravitational acceleration at $g_r = 9.8$ m/s^2, the oil density at 577 kg/m^3, and the other physical parameters at those values given in (105). Fig. 5 shows the oil drop configurations corresponding to $\sigma_{ow} = 0.035$ kg/s^2 and $\sigma_{ow} = 0.055$ kg/s^2. One can observe that the oil forms a puddle in these cases, but the puddle size (diameter) and the puddle thickness strongly depend on the surface tension value. The puddle shrinks as the oil/water surface tension increases. These plots can be compared with Fig. 3(c), which corresponds to an oil/water surface tension $\sigma_{ow} = 0.04$ kg/s^2 while the other physical parameters are the same.

In Fig. 6 we show the puddle-thickness squared as a function of the oil/water surface tension obtained from our simulations (symbols). The asymptotic relation, $e_c^2 \sim \sigma_{ow}$, from the de Gennes theory (see Eq. (109)) is also shown in the plot as the dashed line for comparison. The simulation results are in good agreement quantitatively with the de Gennes theory.

Let us next consider the effect of the oil-drop size on the equilibrium configurations. We consider three characteristic length values: $L = 2$ cm, 4 cm and 5 cm. Respectively, they correspond to the domains 4 cm × 1.6 cm, 8 cm × 3.2 cm and 10 cm × 4 cm, with initial oil drop diameters 8 mm, 1.6 cm and 2 cm. In this set of tests, the oil density is 870 kg/m^3 (air–oil density ratio ~ 723), the oil/water surface tension and the gravity are respectively 0.04 kg/s^2 and 9.8 m/s^2, and the other physical parameter values are given in (105). Fig. 7 shows the equilibrium configurations of the oil for these three cases. Note that the length has been normalized in these plots. For a small drop size, the oil forms a bi-convex lens floating on the water surface (Fig. 7(a)). As the drop size increases, the oil may form a plano-convex lens, see Fig. 7(b), in which

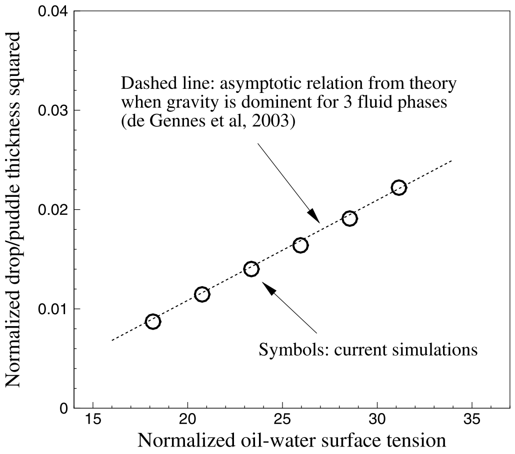

Fig. 6. Comparison of oil-puddle thickness squared (air–water–oil 3 phases) as a function of normalized oil–water surface tension between current simulations and the de Gennes theory [15]. The oil–water surface tension is varied while all other physical parameters are fixed.

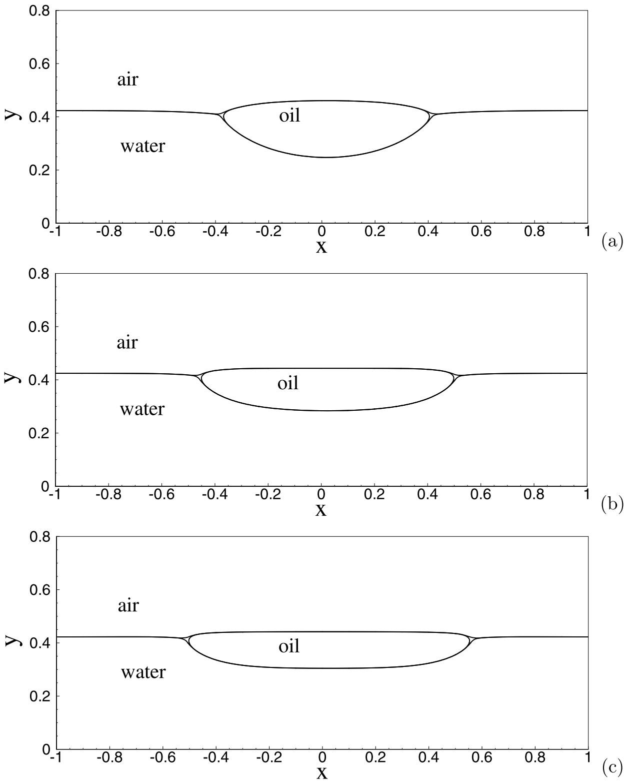

Fig. 7. Effect of oil drop size on equilibrium configurations (3 fluid phases): initial oil drop diameter: (a) 8 mm, (b) 1.6 cm, (c) 2 cm. Other parameters are fixed.

the air–oil interface is essentially flat while the oil–water interface is convex. For a sufficiently large drop size, the oil forms a puddle (Fig. 7(c)). Which type of floating lens the oil forms depends on the drop size relative to the capillary lengths κ_o and κ_{ow} defined in (104). For these three cases, we have $\kappa_o = 2.54$ mm and $\kappa_{ow} = 5.64$ mm. In the case of Fig. 7(a), the drop radius (4 mm) is larger, but not that significantly, than the air/oil capillary length (κ_o), and it is smaller than the oil/water capillary length (κ_{ow}). Consequently, both the air–oil interface and the oil–water interface are convex, and the air–oil interface is relatively flat. For Fig. 7(b), the drop radius (8 mm) is much larger than κ_o, but not that much larger than κ_{ow}. Consequently, the air–oil interface becomes essentially flat, while the oil–water interface is convex. For a sufficiently large oil drop, when the drop radius is much larger than both κ_o and κ_{ow}, both the air–oil interface and the oil–water interface will become flat and the oil will form a puddle.

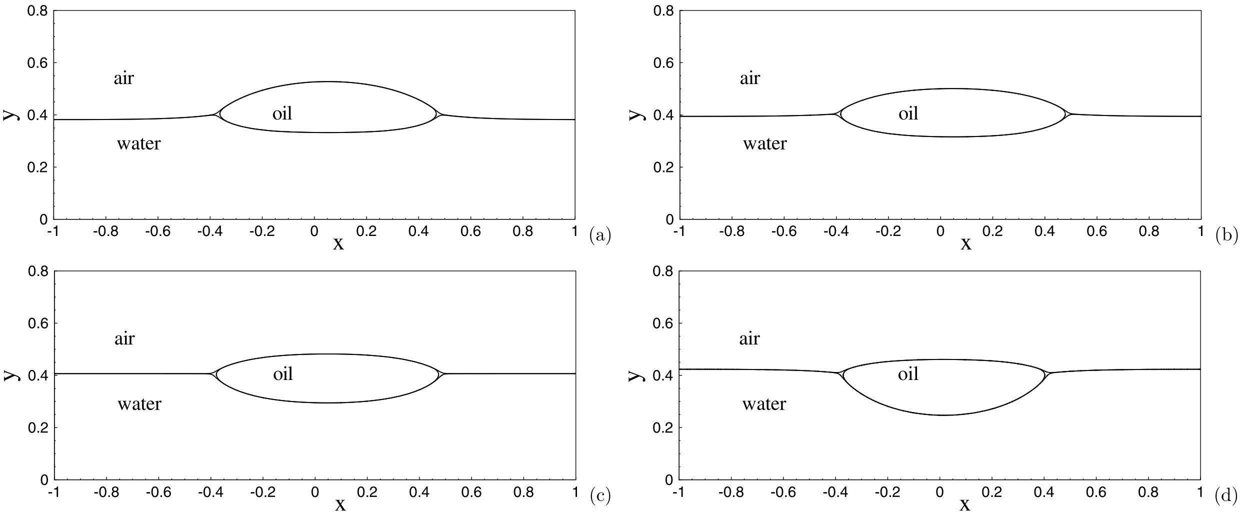

Fig. 8. Effect of density ratios (3 fluid phases): Equilibrium oil drop on air–water interface, with the air–oil density ratio (a) 166, (b) 332, (c) 498, and (d) 723. Gravity is 9.8 m/s^2.

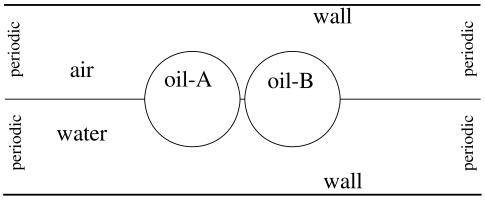

Fig. 9. Initial configuration of 4-phase air/water/oil-A/oil-B problem.

We next consider the effect of the oil density on the equilibrium configuration. In this set of tests, the characteristic length is $L = 2$ cm (domain: 4 cm × 1.6 cm; initial oil-drop diameter: 8 mm), and we vary the oil density systematically. We use a fixed gravitational acceleration $g_r = 9.8$ m/s^2 and oil–water surface tension $\sigma_{ow} = 0.04$ kg/s^2, and the other physical parameters are given in (105). We have simulated four oil density values, 200 kg/m^3, 400 kg/m^3, 600 kg/m^3 and 870 kg/m^3, which respectively correspond to the air–oil density ratios 166, 332, 498 and 723. Fig. 8 shows the equilibrium configurations of the oil drop for these cases. Both the drop shape and the depth of oil immersed under water have been affected by the density change. The oil-density change affects the drop shape because it modifies the capillary lengths κ_o and κ_{ow}. As a result, at a small oil density the oil–water interface becomes flatter (Fig. 8(a)), while at a large oil density the air–oil interface is flatter (Fig. 8(d)). The immersed depth of the oil is affected by the oil density due to the change in the density contrast between the oil and water.

The results of this section for three fluid phases, in particular the qualitative and quantitative comparisons with the de Gennes theory, show that the physical formulation and the numerical algorithm we presented in Section 2 have accurately captured the flow physics of the multiphase system. They also demonstrate that our method is suitable for large density contrasts and large viscosity contrasts among the multitude of fluids.

3.4. Equilibrium oil drops on air–water interface with four fluid phases

The goal of this section is to demonstrate the capability of our method with a flow problem involving four fluid phases. In particular, we will demonstrate the effects of the pair-wise surface tensions and the density contrasts on the four-phase system.

The problem setup has some similarity to the three-phase problem in the previous section. We consider the equilibrium drops of two types of immiscible oils floating on the water surface in ambient air. The initial configuration of this system is shown in Fig. 9. We consider the flow domain, $-L \leqslant x \leqslant L$ and $0 \leqslant y \leqslant \frac{4}{5}L$, where $L = 2$ cm. The domain has two solid walls on its bottom and top sides ($y = 0$ and $\frac{4}{5}L$). In the horizontal direction, we assume that all flow variables are periodic at $x = \pm L$. The domain is initially filled with water at the bottom half and air at the top half, and two circular drops of two different oils, referred to respectively as “oil-A” and “oil-B”, reside on the air–water interface. The two oil drops initially both have a radius $R_0 = \frac{L}{5}$, and their centers are located respectively at $\mathbf{x}_A = (x_A, y_A) = (-0.21L, 0.4L)$ and $\mathbf{x}_B = (x_B, y_B) = (0.21L, 0.4L)$. The gravity is assumed to be in the vertical direction, pointing downward. Upon release, the two oil drops, air and water interact with one another, and evolve under the influence of the gravity and surface tensions. The objective of this problem is to study the equilibrium configurations of this four-phase system.

The physical parameters involved in this problem take the following values:

$$\begin{cases} \text{density [kg/m}^3\text{]:} \quad \text{air – 1.2041}, \quad \text{water – 998.207}, \quad \text{oil-A – 870}, \quad \text{oil-B – 400 (or varied)} \\ \text{dynamic viscosity [kg/(m} \cdot \text{s)]:} \quad \text{air – } 1.78 \times 10^{-5}, \quad \text{water – } 1.002 \times 10^{-3}, \\ \quad \text{oil-A – } 9.15 \times 10^{-2}, \quad \text{oil-B – } 5.0 \times 10^{-2} \\ \text{surface tensions [kg/s}^2\text{]:} \quad \text{air/water – 0.0728}, \quad \text{air/oil-A – 0.055}, \quad \text{water/oil-A – 0.04}, \\ \quad \text{air/oil-B – 0.06 (or varied)}, \quad \text{water/oil-B – 0.045}, \quad \text{oil-A/oil-B – 0.032} \\ \text{gravity [m/s}^2\text{]:} \quad 9.8. \end{cases} \tag{110}$$

We choose a characteristic velocity $U_0 = \sqrt{g_{r0} L}$, where $g_{r0} = 1$ m/s^2, and use L and U_0 to non-dimensionalize the flow variables and the governing equations with the procedure discussed in Section 3.1.

To simulate this four-phase problem, we assign air, water, oil-A and oil-B respectively as the first, second, third and fourth fluids. We partition the domain using 160 quadrilateral spectral elements, with 20 elements in the x direction and 8 elements in the y direction. The element order is 14 for all elements in the simulations. We impose the velocity Dirichlet condition (19) with $\mathbf{w} = 0$, and the boundary conditions (20) and (21) for the phase field functions ϕ_i $(1 \leqslant i \leqslant 3)$, on the upper and lower walls. At $x = \pm L$ we impose periodic conditions for all flow variables. We set the initial velocity to zero, and the initial phase field functions according to Eq. (106) with $N = 4$ and the following initial volume fractions c_i,

$$\begin{aligned} c_1 &= \frac{1}{2}\left(1 + \tanh\frac{y - y_A}{\sqrt{2}\eta}\right)\left[1 - \frac{1}{2}\left(1 - \tanh\frac{|\mathbf{x} - \mathbf{x}_A| - R_0}{\sqrt{2}\eta}\right) - \frac{1}{2}\left(1 - \tanh\frac{|\mathbf{x} - \mathbf{x}_B| - R_0}{\sqrt{2}\eta}\right)\right], \\ c_2 &= \frac{1}{2}\left(1 - \tanh\frac{y - y_A}{\sqrt{2}\eta}\right)\left[1 - \frac{1}{2}\left(1 - \tanh\frac{|\mathbf{x} - \mathbf{x}_A| - R_0}{\sqrt{2}\eta}\right) - \frac{1}{2}\left(1 - \tanh\frac{|\mathbf{x} - \mathbf{x}_B| - R_0}{\sqrt{2}\eta}\right)\right], \\ c_3 &= \frac{1}{2}\left(1 - \tanh\frac{|\mathbf{x} - \mathbf{x}_A| - R_0}{\sqrt{2}\eta}\right), \\ c_4 &= \frac{1}{2}\left(1 - \tanh\frac{|\mathbf{x} - \mathbf{x}_B| - R_0}{\sqrt{2}\eta}\right). \end{aligned}$$

The numerical parameter values are as follows in the simulations:

$$\begin{cases} \frac{\eta}{L} = 0.01, \\ \beta \text{ computed based on Eq. (107)}, \\ \lambda_{ij}, \quad 1 \leqslant i, j \leqslant 3, \text{ computed based on linear system (45)}, \\ \frac{m_1 \tilde{\rho}_1 U_0}{L} = \frac{m_2 \tilde{\rho}_1 U_0}{L} = \frac{m_3 \tilde{\rho}_1 U_0}{L} = \frac{10^{-7}}{\lambda^*_{\max}}, \quad \text{where } \lambda^*_{\max} = \frac{1}{\tilde{\rho}_1 U_0^2 L^2} \max\{\lambda_{ij}\}_{1 \leqslant i,j \leqslant 3}, \\ \nu_0 \quad \text{chosen based on Eq. (57)}, \\ \rho_0 = \min(\tilde{\rho}_1, \tilde{\rho}_2, \tilde{\rho}_3, \tilde{\rho}_4). \end{cases} \tag{111}$$

The non-dimensional time step size is $\Delta t = 10^{-5}$ in the simulations.

Let us first look into the effects of the surface tensions on the equilibrium configuration of this four-phase system. In this set of tests, we vary the surface tension associated with the air/oil-B interface systematically, while the density of oil-B is fixed at 400 kg/m^3 and all the other physical parameters are given in (110). Fig. 10 shows the equilibrium configurations of the oil drops floating on the air/water interface, corresponding to five air/oil-B surface tensions: 0.04 kg/s^2, 0.05 kg/s^2, 0.06 kg/s^2, 0.07 kg/s^2 and 0.08 kg/s^2. Plotted are the contour levels of the volume fractions, $c_i = \frac{1}{2}$ $(1 \leqslant i \leqslant 4)$, for the four fluids. We can make several observations. First, the two oil drops touch each other, and a common interface between oil-A and oil-B is formed. Second, while much of oil-A is immersed under the water surface, the sinking depth of oil-B is notably smaller. This is because the density contrast between oil-B and water is much more significant than that between oil-A and water. Third, the surface tensions significantly influence the four-phase configurations. As the air/oil-B surface tension decreases, the drop of oil-B tends to spread out on the water surface (Figs. 10(a)–(b)), and the air/oil-B interface and the water/oil-B interface become quite flat (Fig. 10(a)). On the other hand, as the air/oil-B surface tension increases, the drop of oil-B becomes “fatter” (Figs. 10(d)–(e)), and the drop shape of oil-A is also notably affected at a large air/oil-B surface tension (Fig. 10(e)).

In the next set of tests we investigate the effect of density ratios on the four-phase equilibrium configurations. We vary the density of oil-B systematically, while the air/oil-B surface tension is fixed at 0.06 kg/s^2 and the other physical parameter values are given in (110). We have considered four oil-B density values, 240.82 kg/m^3, 400 kg/m^3, 602.05 kg/m^3 and 722.46 kg/m^3. They respectively lead to air/oil-B density ratios 200, 332.2, 500 and 600. Fig. 11 shows the configurations of

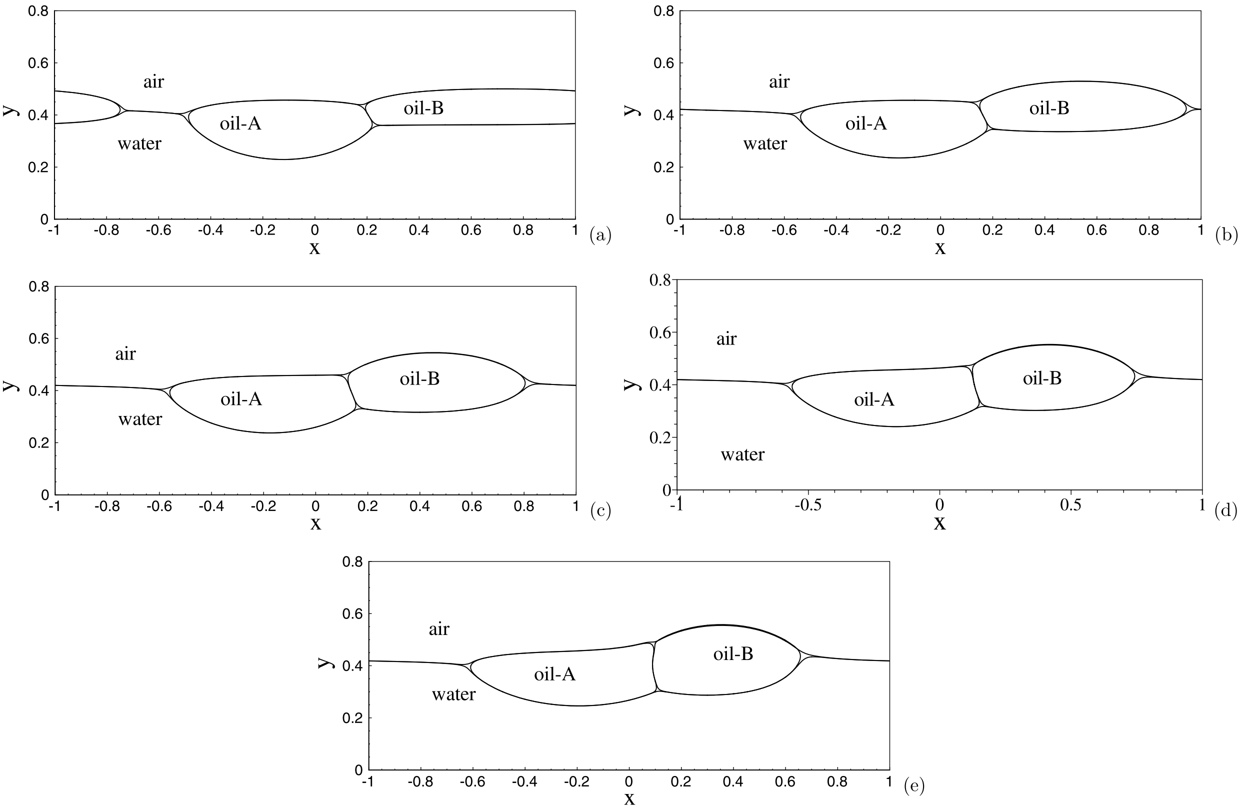

Fig. 10. Effect of air/oil-B surface tension on the equilibrium configuration of two types of oil drops at the air–water interface (4 fluid phases). Air/oil-B surface tensions (kg/s^2): (a) 0.04, (b) 0.05, (c) 0.06, (d) 0.07, (e) 0.08.

this four-phase system corresponding to these density ratios excluding 332.2, and Fig. 10(c) is the configuration corresponding to air/oil-B density ratio 332.2. The results show that the change in the oil-B density has several effects. First, the drop shape of oil-B changes notably. At a small oil-B density the air/oil-B interface tends to be more convex and the water/oil-B interface tends to be relatively flat (Fig. 11(a)), while at a large oil-B density the opposite tends to be the case (Fig. 11(c)). Second, the sinking depth of oil-B increases as the oil-B density increases, while that of oil-A appears little affected. Third, the orientation of oil-A/oil-B interface changes noticeably.

3.5. Dynamics of drops, bubbles and interfaces with five fluid phases

The goal of this section is to demonstrate the capabilities of our method with a dynamic problem involving five fluid phases.

The configuration of this test problem is as follows; see Fig. 12(a). We consider the flow domain, $-\frac{L}{2} \leqslant x \leqslant \frac{L}{2}$ and $0 \leqslant y \leqslant \frac{8}{5}L$, where $L = 2$ cm. The bottom and the top of the domain ($y = 0$ and $\frac{8}{5}L$) are two solid walls, and the domain is periodic in the horizontal direction ($x = \pm\frac{L}{2}$). The gravity is along the vertical direction, pointing downward. At $t = 0$, the domain is filled with water at the bottom half and air at the top half. Two liquid drops (initially circular, both with radius $R_0 = 0.15L$), of two different fluids referred to as "F1" and "F3", are suspended in the air at a certain distance above the water surface. An air bubble, and a liquid drop of another fluid referred to as "F2", both circular initially and also with radius $R_0 = 0.15L$, are trapped in the water. The three fluids F1, F2 and F3 are assumed to be all immiscible with one another and with air and water. The centers of the four drops/bubble are initially located respectively at:

$$\begin{cases} \mathbf{x}_{F1} = (x_{F1}, y_{F1}) = (-0.3L, 1.4L) \quad \text{(drop F1)}, \\ \mathbf{x}_{F2} = (x_{F2}, y_{F2}) = (0.3L, 0.2L) \quad \text{(drop F2)}, \\ \mathbf{x}_{F3} = (x_{F3}, y_{F3}) = (0.15L, 1.4L) \quad \text{(drop F3)}, \\ \mathbf{x}_{a} = (x_{a}, y_{a}) = (-0.2L, 0.2L) \quad \text{(air bubble)}. \end{cases} \tag{112}$$

The liquid drops/bubble are then released. They fall through the air or rise through the water, and impact the air–water interface. The objective of this problem is to simulate the dynamics of this five-phase system.

The physical parameters involved in this five-phase problem assume the following values:

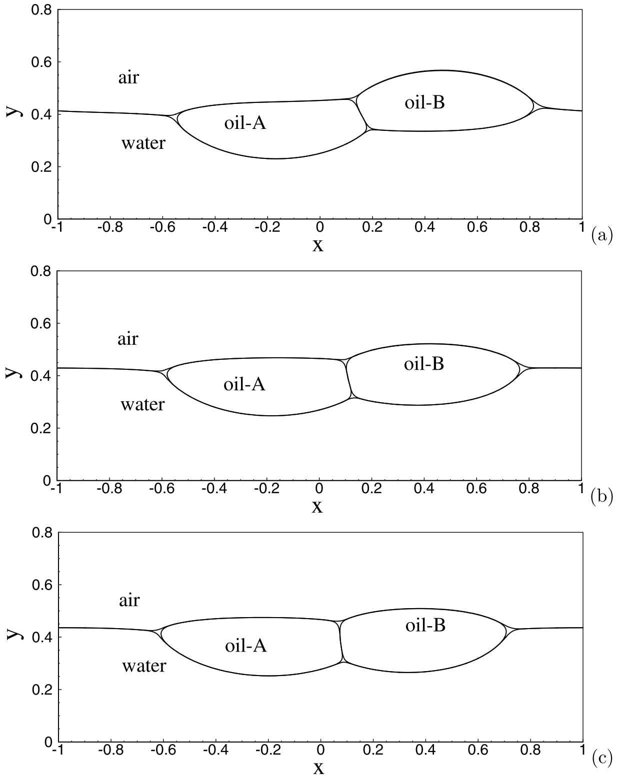

Fig. 11. Equilibrium configurations of two types of oil drops on air–water interface (4 fluid phases), with different air/oil-B density ratios (a) 200, (b) 500 and (c) 600. Other physical parameters are fixed. See Fig. 10(c) for the 4-phase configuration with air/oil-B density ratio 332.2.

$$\left\{\begin{array}{l}\text{density [kg/m}^3\text{]:}\quad \text{air} - 1.2041,\quad \text{water} - 998.207,\quad \text{F1} - 870,\quad \text{F2} - 400,\quad \text{F3} - 600\\ \text{dynamic viscosity [kg/(m}\cdot\text{s)]:}\quad \text{air} - 1.78\times 10^{-5},\quad \text{water} - 1.002\times 10^{-3},\\ \quad \text{F1} - 9.15\times 10^{-2},\quad \text{F2} - 2.0\times 10^{-2},\quad \text{F3} - 1.0\times 10^{-2}\\ \text{surface tensions [kg/s}^2\text{]:}\quad \text{air/water} - 0.0728,\quad \text{air/F1} - 0.055,\quad \text{water/F1} - 0.04,\\ \quad \text{air/F2} - 0.06,\quad \text{water/F2} - 0.045,\quad \text{F1/F2} - 0.032,\\ \quad \text{air/F3} - 0.05,\quad \text{water/F3} - 0.041,\quad \text{F1/F3} - 0.038,\quad \text{F2/F3} - 0.058\\ \text{gravity [m/s}^2\text{]:}\quad 9.8.\end{array}\right. \tag{113}$$

We choose a characteristic velocity $U_0 = \sqrt{g_{r0}L}$, where $g_{r0} = 1\ \text{m/s}^2$, and use L and U_0 to non-dimensionalize the problem.

In the simulations we assign air, water, F1, F2 and F3 respectively as fluids one to five. The flow domain is partitioned using 640 quadrilateral spectral elements, with 20 elements in the x direction and 32 elements in the y direction. The element order is 18 for all elements in the simulations. On the top and the bottom walls, the velocity Dirichlet condition (19) with $\mathbf{w} = 0$ is imposed, and the boundary conditions (20) and (21) are imposed for the phase field functions ϕ_i ($1 \leqslant i \leqslant 4$). At the horizontal boundaries $x = \pm\frac{L}{2}$, periodic boundary condition is imposed for all flow variables. The initial velocity field is set to zero. The initial phase field functions are set according to Eq. (106) with $N = 5$ and the following initial volume fractions c_i,

$$\begin{aligned} c_1 &= \frac{1}{2}\left(1 + \tanh\frac{y - y_{IF}}{\sqrt{2}\eta}\right)\left[1 - \frac{1}{2}\left(1 - \tanh\frac{|\mathbf{x} - \mathbf{x}_{F1}| - R_0}{\sqrt{2}\eta}\right) - \frac{1}{2}\left(1 - \tanh\frac{|\mathbf{x} - \mathbf{x}_{F3}| - R_0}{\sqrt{2}\eta}\right)\right] \\ &\quad + \frac{1}{2}\left(1 - \tanh\frac{|\mathbf{x} - \mathbf{x}_a| - R_0}{\sqrt{2}\eta}\right), \\ c_2 &= \frac{1}{2}\left(1 - \tanh\frac{y - y_{IF}}{\sqrt{2}\eta}\right)\left[1 - \frac{1}{2}\left(1 - \tanh\frac{|\mathbf{x} - \mathbf{x}_a| - R_0}{\sqrt{2}\eta}\right) - \frac{1}{2}\left(1 - \tanh\frac{|\mathbf{x} - \mathbf{x}_{F2}| - R_0}{\sqrt{2}\eta}\right)\right], \\ c_3 &= \frac{1}{2}\left(1 - \tanh\frac{|\mathbf{x} - \mathbf{x}_{F1}| - R_0}{\sqrt{2}\eta}\right), \end{aligned}$$

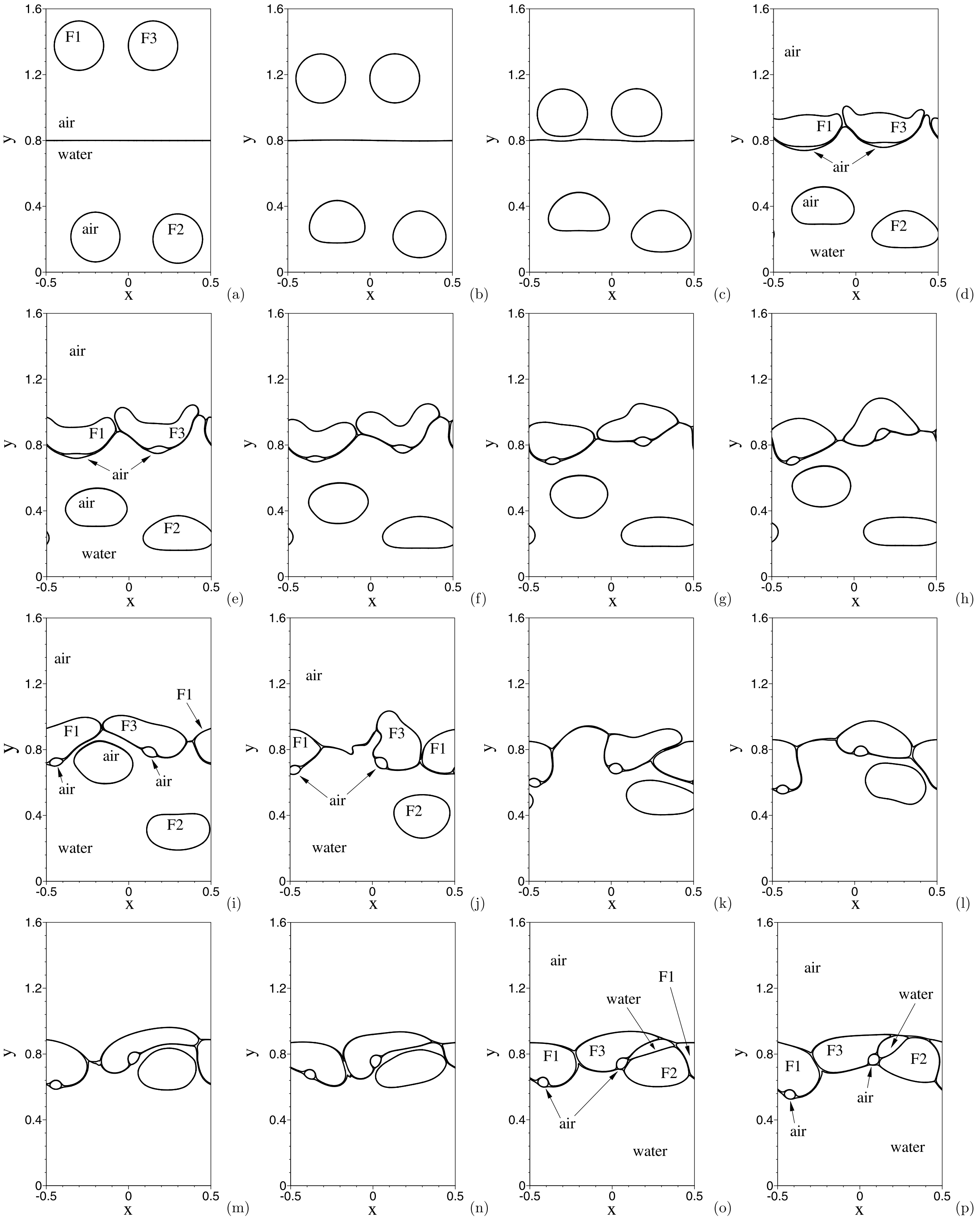

Fig. 12. Temporal sequence of snapshots of 5-phase fluid interfaces: (a) $t = 0.07$, (b) $t = 0.215$, (c) $t = 0.301$, (d) $t = 0.367$, (e) $t = 0.401$, (f) $t = 0.451$, (g) $t = 0.513$, (h) $t = 0.583$, (i) $t = 0.798$, (j) $t = 1.008$, (k) $t = 1.201$, (l) $t = 1.421$, (m) $t = 1.673$, (n) $t = 1.906$, (o) $t = 2.361$, (p) $t = 2.758$.

$$c_4 = \frac{1}{2}\left(1 - \tanh\frac{|\mathbf{x} - \mathbf{x}_{F2}| - R_0}{\sqrt{2}\eta}\right),$$
$$c_5 = \frac{1}{2}\left(1 - \tanh\frac{|\mathbf{x} - \mathbf{x}_{F3}| - R_0}{\sqrt{2}\eta}\right),$$

where $y_{IF} = \frac{4}{5}L$ is the initial position of the water surface.

The numerical parameters are set as follows in the simulations:

$$\begin{cases} \frac{\eta}{L} = 0.005, \\ \beta \text{ computed based on Eq. (107)}, \\ \lambda_{ij}, \quad 1 \leqslant i, j \leqslant 4, \text{ computed based on linear system (45)}, \\ \frac{m_i \tilde{\rho}_1 U_0}{L} = \frac{2 \times 10^{-8}}{\lambda^*_{\max}}, \quad 1 \leqslant i \leqslant 4, \text{ where } \lambda^*_{\max} = \frac{1}{\tilde{\rho}_1 U_0^2 L^2} \max\{\lambda_{ij}\}_{1 \leqslant i,j \leqslant 4}, \\ \nu_0 \text{ chosen based on Eq. (57)}, \\ \rho_0 = \min(\tilde{\rho}_1, \tilde{\rho}_2, \cdots, \tilde{\rho}_5). \end{cases} \tag{114}$$

We employ a non-dimensional time step size $\Delta t = 2.5 \times 10^{-6}$ in the simulations.

Let us next look into the dynamics of this five-phase system. Fig. 12 shows a temporal sequence of snapshots of the fluid interfaces. Plotted are the contour levels of the volume fraction $c_i = \frac{1}{2}$ $(1 \leqslant i \leqslant 5)$ for the five fluids. Upon release at $t = 0$, the fluid drops of F1 and F3 fall freely through the air, while the air bubble and the F2 drop rise through the water. The deformations of the air bubble and the F2 drop are evident (Figs. 12(b) and (c)). Around $t = 0.3$, the F1 and F3 drops are about to impact the water surface (Figs. 12(c)). Figs. 12(d)–(h) show the impact of the F1 and F3 fluids and the formation of floating drops on the water surface. The impact onto the water surface causes dramatic distortions in the F1 and F3 drops (Figs. 12(d)–(e)). Both F1 and F3 have trapped a small amount of air between these fluids and the water (Fig. 12(d)), which subsequently becomes two small air bubbles trapped between F1 and water and between F3 and water. One can observe the oscillation in the shape of the F1 and F3 drops and the undulation of the water surface (Figs. 12(e)–(h)). The floating F1 and F3 drops have covered the most part of the water surface. Simultaneously, the air bubble continues its rise through the water, and the F2 drop appears to be still during this time while exhibiting marked distortions in its shape (Figs. 12(d)–(h)). Fig. 12(i) shows that the rising air bubble approaches the water surface, which is now almost completely covered by fluids F1 and F3. Subsequently, the air bubble merges into the bulk of air above the water, leaving a section of open water surface free of F1 and F3 fluids (Figs. 12(j)–(k)). Meanwhile, the F2 drop rises through the water (Figs. 12(i)–(k)), and approaches the water surface which is covered by the F1 and F3 fluids (Figs. 12(l)–(m)). As the F2 drop rises further, a pocket of water is trapped in the cavity bounded by the air and the F2, F3, and F1 drops (Figs. 12(n)–(o)). The water surface is eventually completely covered by the F1, F3 and F2 fluids, which form a layer insulating the bulk of water from the bulk of air (Fig. 12(p)). Two small air bubbles are trapped at the underside of this layer, and a water drop is trapped by the bulk of air, one of the small air bubbles, the F2 and F3 fluids.

Fig. 13 shows a temporal sequence of snapshots of the velocity field of this problem, at identical time instants as the interface plots of Fig. 12. Figs. 13(a)–(c) indicate that the falling F1 and F3 drops have induced a velocity field in the air. In particular, a strong jet of air is produced between the two falling drops. The air jet moves upward, generating pairs of vortices in the wake of the falling drops (Fig. 13(c)). The two vortex pairs in the air appear to further intensify after the F1 and F3 drops impact the water surface (Figs. 13(d)–(e)). But over time, the velocity field of the air gradually dies down (Figs. 13(f)–(p)). On the other hand, in the water the rising air bubble induces a pair of vortices in its wake (Figs. 13(c)–(i)). So does the F2 drop as it rises through water (Figs. 13(g)–(k)). After the F2 drop contacts the F3 and F1 fluids on the water surface and they together form an insulating layer between the bulk of air and the bulk of water, the velocity field in the entire domain gradually dies down (Figs. 13(m)–(p)).

We can estimate a characteristic Reynolds number for this flow problem. The vertical velocity at the center of the F3 drop is $V_c \approx 2.75U_0$ at $t = 0.301\frac{L}{U_0}$ (corresponding to Fig. 13(c)) when the drop is about to impact the water surface. Let $D_0 = 0.3L$ denote the initial diameter of the F3 drop, and ρ_a and μ_a denote the density and dynamic viscosity of the air respectively. Then the Reynolds number based on the above quantities is $\mathrm{Re} = \frac{\rho_a V_c D_0}{\mu_a} \approx 158$.

4. Concluding remarks

In this paper we have presented a physical formulation, and an efficient numerical algorithm, within the phase field framework for simulating the mixture consisting of N $(N \geqslant 2)$ immiscible incompressible fluids. The physical formulation is developed by recourse to the conservations of mass and momentum, the second law of thermodynamics, and the Galilean invariance. In such a sense, this formulation is thermodynamically consistent.

We have also developed a method for computing the mixing energy density coefficients λ_{ij} $(1 \leqslant i, j \leqslant N - 1)$ based on the $\frac{1}{2}N(N-1)$ pairwise surface tensions σ_{ij} $(1 \leqslant i < j \leqslant N)$ among the N fluids. The basic idea lies in the following requirement for the N-phase formulation: if only two fluids i and j are present in the N-phase system, then the N-phase

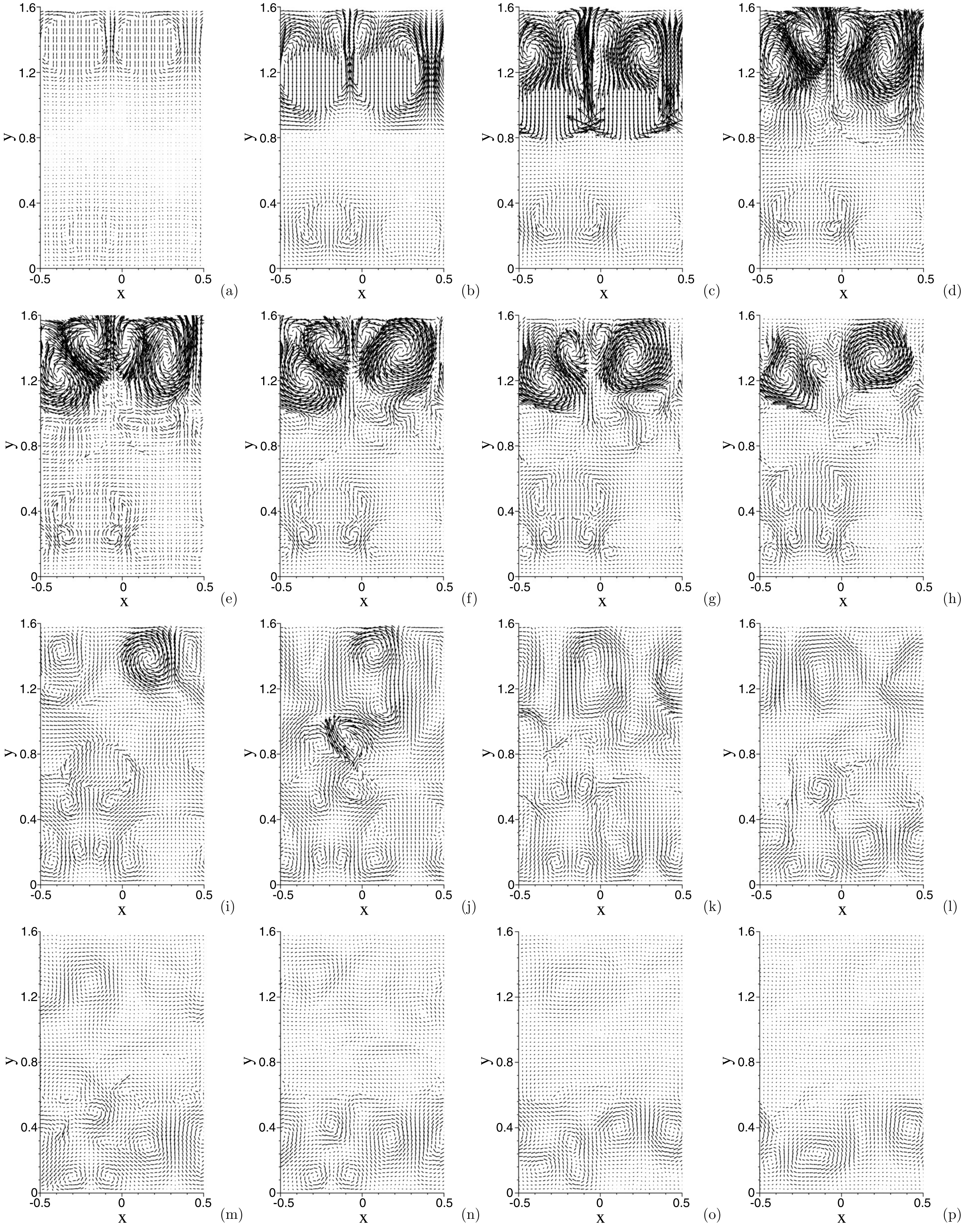

Fig. 13. Temporal sequence of snapshots of velocity fields (5 fluid phases): (a) $t = 0.07$, (b) $t = 0.215$, (c) $t = 0.301$, (d) $t = 0.367$, (e) $t = 0.401$, (f) $t = 0.451$, (g) $t = 0.513$, (h) $t = 0.583$, (i) $t = 0.798$, (j) $t = 1.008$, (k) $t = 1.201$, (l) $t = 1.421$, (m) $t = 1.673$, (n) $t = 1.906$, (o) $t = 2.361$, (p) $t = 2.758$. Velocity vectors are plotted on every ninth quadrature point in each direction within each element.

formulation should reduce to an equivalent two-phase formulation consisting of fluids i and j. Our method leads to a linear algebraic system about λ_{ij}, with the coefficient matrix depending only on the $(N-1)$ density ratios, $\frac{\tilde{\rho}_i}{\tilde{\rho}_N}$ $(1 \leqslant i \leqslant N-1)$. This system can be solved for λ_{ij}.

Our numerical algorithm for solving the N-phase system has several attractive properties that make it computationally very efficient. First, the computations for different flow variables (pressure, velocity, and phase field functions) are completely de-coupled. Second, the computations for the $(N-1)$ strongly-coupled phase field functions are also completely de-coupled. This is achieved by a combination of three ideas: (i) we introduce $(N-1)^2$ extra terms in the semi-discretized form of the coupled system of 4th-order phase field equations; (ii) we transform the coupled system, thanks to the extra terms, into $(N-1)$ 4th-order equations that are de-coupled from one another; (iii) we further re-formulate each individual 4th-order equation into two de-coupled Helmholtz-type equations, using a technique developed previously for two-phase flows. Third, the algorithm only involves the solution of linear algebraic systems after discretization, and no nonlinear algebraic solver is needed. Fourth, the linear algebraic system for each flow variable involves only *constant* and *time-independent* coefficient matrices, which can be pre-computed during pre-processing. The algorithm has therefore effectively overcome the performance bottleneck caused by the variable coefficient matrices associated with variable mixture density and variable mixture viscosity.

A comparison would be instructive between the current and several related works. In the literature there exist several studies involving three or more fluid components by other researchers; see e.g. [8–10,34,38,41], among others. For three fluid components, these simulations usually employ a decomposition of the three pairwise surface tensions in order to account for their effects on the flow [9,10,34]. See also [8] for an alternative form of the surface-tension force with three fluid phases for the volume of fluids approach. For more than three fluid components, a predominant issue lies in how to treat the multiple pairwise surface tensions, as mentioned in earlier sections. A phenomenological surface tension force is suggested in [35] for multiple fluid components; see its applications in e.g. [36,41]. The work of [50] assumes identical pairwise surface tensions for different fluid interfaces, and employs a surface-tension force in the level-set context that results in identical angles between fluid interfaces at triple junctions.

In contrast to the above works, the current formulation has implicitly incorporated the surface-tension effects through the free energy of the system. This naturally gives rise to the surface-tension terms in the momentum equation, thanks to the second law of thermodynamics. In addition, the mixing energy density coefficients are determined based on the pairwise surface tensions by solving a linear algebraic system. This linear system results from a consistency requirement on the N-phase formulation, namely, the N-phase formulation must reduce to the equivalent two-phase formulation if only a pair of fluids is present in the N-phase system. Thermodynamic consistency in the physical formulation is another distinguishing character of the current method, compared to the previous studies.

We have conducted extensive numerical experiments with problems involving multiple fluid phases to demonstrate the capabilities of the current method. In particular, for the three-phase floating liquid lens problem, we have performed qualitative and quantitative comparisons between our simulations and the de Gennes theory [15]. The results show that our N-phase formulation and algorithm have produced physically accurate results. We have also demonstrated the significant and sometimes dramatic effects of the gravity, pairwise surface tensions, fluid drop size, and fluid densities on the configurations of multi-phase systems. The numerical results have also shown the N-phase complex dynamics and the complex interactions among multiple fluid phases. They also show that our method is effective in dealing with large density ratios and large viscosity ratios among the multitude of fluid phases.

These results lend the confidence that our physical model and numerical algorithm can reasonably capture the physics of N-phase flows. The presented method can be a powerful tool for studying the interactions among multiple types of fluid interfaces, N-phase contact lines, and flows involving multiple immiscible incompressible components. On the other hand, we would also like to caution that, the usefulness of the model and the algorithm will ultimately be determined by the physical results and comparisons with experimental measurements. These all require much future research.

Acknowledgements

The author gratefully acknowledges the support from ONR (N000141110028) and NSF (DMS-1318820). Computer time was provided by XSEDE through an XRAC grant. The author would also like to thank the anonymous referees for the valuable comments and suggestions.

Appendix A. Development of N-phase formulation

In this appendix we briefly discuss how the physical formulation presented in Section 2.1 for the N-phase flows is developed based on the mass and momentum conservations and the second law of thermodynamics. This development has much been inspired by the work of [2] for two-phase flows.

Mass Balance In order to facilitate subsequent developments it is necessary in the following to introduce several forms about certain physical quantities, e.g. the density and the mass flux. It is crucial to distinguish the different forms, which have different physical meanings.

We take the same problem setting as outlined in Section 2.1. Consider the mixture of N ($N \geqslant 2$) immiscible incompressible fluids. Let $\tilde{\rho}_i$ ($1 \leqslant i \leqslant N$) denote the constant density of pure fluid i without mixing. Consider an arbitrary control volume V of the mixture, with a mass M. Let M_i ($1 \leqslant i \leqslant N$) denote the mass of fluid i contained in this volume. Let ρ_i denote the average density of the i-th fluid within the mixture, and ρ denote the average density of the mixture. Then, $\rho_i = \frac{M_i}{V}$, and

$$\rho = \frac{M}{V} = \frac{M_1 + M_2 + \cdots + M_N}{V} = \rho_1 + \rho_2 + \cdots + \rho_N. \tag{115}$$

We assume that, the volume occupied by a given amount of mass of any single fluid i ($1 \leqslant i \leqslant N$) does not change after mixing, in other words, there is no volume loss or volume addition after mixing of any of these N fluids. Let V_i denote the volume of pure fluid i before mixing. This assumption leads to

$$V = V_1 + V_2 + \cdots + V_N. \tag{116}$$

Let c_i denote the volume fraction of fluid i in the mixture,

$$c_i = \frac{V_i}{V} = \frac{M_i/\tilde{\rho}_i}{M_i/\rho_i} = \frac{\rho_i}{\tilde{\rho}_i}, \quad 1 \leqslant i \leqslant N. \tag{117}$$

Eq. (116) is equivalent to the condition (7) on the volume fractions.

Since the volume V is arbitrary, $\rho(\mathbf{x}, t)$, $\rho_i(\mathbf{x}, t)$, $c_i(\mathbf{x}, t)$ defined above are field variables, while $\tilde{\rho}_i$ are constants. Eqs. (115), (117) and (7) will be extensively used in subsequent discussions.

Let $\hat{\mathbf{J}}_i$ ($1 \leqslant i \leqslant N$) denote the mass flux of fluid i in the mixture. Then the mass balance for fluid i is given by

$$\frac{\partial \rho_i}{\partial t} + \nabla \cdot \hat{\mathbf{J}}_i = 0, \quad 1 \leqslant i \leqslant N. \tag{118}$$

One can define the velocity of the individual fluids, $\mathbf{u}_i$ ($1 \leqslant i \leqslant N$), based on the mass flux,

$$\hat{\mathbf{J}}_i = \rho_i \mathbf{u}_i, \quad 1 \leqslant i \leqslant N. \tag{119}$$

Note that if fluid i does not exist at a point in space (i.e. $\rho_i = 0$ at that point), then $\hat{\mathbf{J}}_i = 0$ at that point, and we assume that $\mathbf{u}_i = 0$ at that point.

Following [2], we define the mixture velocity $\mathbf{u}$ as the *volume-averaged* velocities of the individual fluids,

$$\mathbf{u} = \sum_{i=1}^{N} c_i \mathbf{u}_i = \sum_{i=1}^{N} \frac{\rho_i}{\tilde{\rho}_i} \mathbf{u}_i = \sum_{i=1}^{N} \frac{\hat{\mathbf{J}}_i}{\tilde{\rho}_i}. \tag{120}$$

Note that this mixture velocity is divergence free,

$$\nabla \cdot \mathbf{u} = \sum_{i=1}^{N} \frac{1}{\tilde{\rho}_i} \nabla \cdot \hat{\mathbf{J}}_i = -\frac{\partial}{\partial t} \sum_{i=1}^{N} \frac{\rho_i}{\tilde{\rho}_i} = -\frac{\partial}{\partial t}(c_1 + c_2 + \cdots + c_N) = -\frac{\partial}{\partial t} 1 = 0, \tag{121}$$

where we have used Eqs. (118), (117) and (7). We would like to mention that the velocity in the formulations of [27,38] is the *mass-averaged* mixture velocity and is not divergence free. This is a key difference between our formulation and those of [27,38]. One notes that the mixture models of two-phase flows historically used density or mass-averaged equations, which led to non-zero velocity divergence; see e.g. [7,31]. We note that in the model of [42] the velocity also has a non-zero divergence.

Define the differential flux, $\mathbf{J}_i$, of fluid i relative to the bulk mixture motion,

$$\mathbf{J}_i = \hat{\mathbf{J}}_i - \rho_i \mathbf{u}, \quad 1 \leqslant i \leqslant N. \tag{122}$$

Then the mass balance equation (118) can be transformed into

$$\frac{\partial \rho_i}{\partial t} + \mathbf{u} \cdot \nabla \rho_i = -\nabla \cdot \mathbf{J}_i, \quad 1 \leqslant i \leqslant N, \tag{123}$$

where we have used (121). Note that $\mathbf{J}_i$ ($1 \leqslant i \leqslant N$) satisfies the relation

$$\sum_{i=1}^{N} \frac{\mathbf{J}_i}{\tilde{\rho}_i} = \sum_{i=1}^{N} \frac{\hat{\mathbf{J}}_i}{\tilde{\rho}_i} - \sum_{i=1}^{N} \frac{\rho_i}{\tilde{\rho}_i} \mathbf{u} = \mathbf{u} - \left(\sum_{i=1}^{N} c_i \right) \mathbf{u} = \mathbf{u} - \mathbf{u} = 0, \tag{124}$$

where we have used (122), (120) and (7). This relation between $\mathbf{J}_i$ will be extensively used in subsequent discussions.

We now reformulate the set of N mass balance equations (123) into an equivalent set, in order to facilitate the subsequent discussions. In (123), subtract the N-th equation from the i-th one ($1 \leqslant i \leqslant N-1$), and we can get

$$\frac{\partial}{\partial t}(\rho_i - \rho_N) + \mathbf{u} \cdot \nabla(\rho_i - \rho_N) = -\nabla \cdot \mathbf{J}_{ai}, \quad 1 \leqslant i \leqslant N-1, \tag{125}$$

where

$$\mathbf{J}_{ai} = \mathbf{J}_i - \mathbf{J}_N. \tag{126}$$

is the relative differential flux between fluids i and N. Summing up the N equations in (123), we get the mass balance about the mixture

$$\frac{\partial \rho}{\partial t} + \mathbf{u}\cdot\nabla\rho = -\nabla\cdot\tilde{\mathbf{J}}, \tag{127}$$

where

$$\tilde{\mathbf{J}} = \mathbf{J}_1 + \mathbf{J}_2 + \cdots + \mathbf{J}_N. \tag{128}$$

The set of mass balance equations consisting of (125) and (127) are equivalent to the N mass balance equations of (123).

We next show that the mixture mass-balance equation (127) is redundant from the $(N-1)$ equations of (125), because of the relations (7) and (124). Define

$$\varphi_i \equiv \rho_i - \rho_N, \quad 1 \leqslant i \leqslant N-1. \tag{129}$$

We will find the relation between ρ and φ_i $(1 \leqslant i \leqslant N-1)$, and also the relation between $\tilde{\mathbf{J}}$ and $\mathbf{J}_{ai}$ $(1 \leqslant i \leqslant N-1)$.

Consider the following linear algebraic system about $\mathbf{J}_i$ $(1 \leqslant i \leqslant N)$:

$$\tilde{\gamma}_1\mathbf{J}_1 + \tilde{\gamma}_2\mathbf{J}_2 + \cdots + \tilde{\gamma}_N\mathbf{J}_N = 0 \tag{130a}$$

$$\mathbf{J}_i - \mathbf{J}_N = \mathbf{J}_{ai}, \quad 1 \leqslant i \leqslant N-1, \tag{130b}$$

where $\tilde{\gamma}_i$ is defined in (6), Eq. (130a) is a restatement of (124), and Eq. (130b) is restatement of the definition for $\mathbf{J}_{ai}$ in (126). One can obtain from this system

$$\mathbf{J}_N = -\frac{1}{\Gamma}\sum_{i=1}^{N-1}\tilde{\gamma}_i\mathbf{J}_{ai}, \quad \text{and} \quad \mathbf{J}_i = \mathbf{J}_N + \mathbf{J}_{ai}, \quad 1 \leqslant i \leqslant N-1, \tag{131}$$

where Γ is defined in (6). Therefore, one can express $\tilde{\mathbf{J}}$ in (127) in terms of $\mathbf{J}_{ai}$ as follows,

$$\tilde{\mathbf{J}} = \sum_{i=1}^{N}\mathbf{J}_i = \sum_{i=1}^{N-1}\left(1 - \frac{N}{\Gamma}\tilde{\gamma}_i\right)\mathbf{J}_{ai}. \tag{132}$$

Next we consider the following linear algebraic system about ρ_i $(1 \leqslant i \leqslant N)$:

$$\tilde{\gamma}_1\rho_1 + \tilde{\gamma}_2\rho_2 + \cdots + \tilde{\gamma}_N\rho_N = 1 \tag{133a}$$

$$\rho_i - \rho_N = \varphi_i, \quad 1 \leqslant i \leqslant N-1, \tag{133b}$$

where Eq. (133a) is a restatement of (7) by using the definition (117), and Eq. (133b) is a restatement of (129). One can obtain from this system

$$\rho_N = \frac{1}{\Gamma}\left(1 - \sum_{i=1}^{N-1}\tilde{\gamma}_i\varphi_i\right), \quad \text{and} \quad \rho_i = \rho_N + \varphi_i, \quad 1 \leqslant i \leqslant N-1. \tag{134}$$

Therefore, one can express the mixture density ρ in terms of φ_i as follows

$$\rho = \sum_{i=1}^{N}\rho_i = \frac{N}{\Gamma} + \sum_{i=1}^{N-1}\left(1 - \frac{N}{\Gamma}\tilde{\gamma}_i\right)\varphi_i. \tag{135}$$

It is straightforward to verify, with the relations (132) and (135), that the $(N-1)$ equations of (125) imply the mixture mass-balance equation (127). Therefore, the mass balance of this N-phase system can be represented by the $(N-1)$ equations of (125). We will determine the forms for the relative differential flux $\mathbf{J}_{ai}$ $(1 \leqslant i \leqslant N-1)$ by invoking the second law of thermodynamics in subsequent discussions.

Momentum Balance Following [2], we assume that the inertia and kinetic energy due to the motion of the fluids relative to the bulk motion is negligible. So the mixture can be considered as a single fluid with velocity $\mathbf{u}$, which satisfies the linear-momentum conservation with respect to the volume-averaged velocity. For simplicity we assume that there is no external body force.

The development for the momentum equation below closely follows [2] for two-phase flows. The momentum conservation leads to

$$\frac{\partial}{\partial t}(\rho\mathbf{u}) + \nabla\cdot(\rho\mathbf{u}\mathbf{u}) = \nabla\cdot\tilde{\mathbf{T}}, \tag{136}$$

where ρ is the mixture density, $\mathbf{u}$ is the volume-averaged mixture velocity, and $\tilde{\mathbf{T}}$ is a stress tensor whose form has to be specified based on constitutive assumptions.

Eq. (136) is equivalent to

$$\rho\left(\frac{\partial \mathbf{u}}{\partial t}+\mathbf{u}\cdot\nabla\mathbf{u}\right)+\left(\frac{\partial \rho}{\partial t}+\mathbf{u}\cdot\nabla\rho\right)\mathbf{u}=\nabla\cdot\tilde{\mathbf{T}}. \tag{137}$$

In the above equation, the stress tensor $\tilde{\mathbf{T}}$ cannot be an objective stress tensor (i.e. invariant under Galilean transform), because otherwise the above equation will not be Galilean invariant due to the $(\frac{\partial\rho}{\partial t}+\mathbf{u}\cdot\nabla\rho)\mathbf{u}$ term.

In light of Eq. (127), we can transform (137) into

$$\rho\left(\frac{\partial \mathbf{u}}{\partial t}+\mathbf{u}\cdot\nabla\mathbf{u}\right)+\tilde{\mathbf{J}}\cdot\nabla\mathbf{u}=\nabla\cdot(\tilde{\mathbf{T}}+\tilde{\mathbf{J}}\mathbf{u})=\nabla\cdot\mathbf{T}, \tag{138}$$

where we have used the relation $(\nabla\cdot\tilde{\mathbf{J}})\mathbf{u}=\nabla\cdot(\tilde{\mathbf{J}}\mathbf{u})-\tilde{\mathbf{J}}\cdot\nabla\mathbf{u}$. Now the momentum equation admits an objective stress tensor $\mathbf{T}=\tilde{\mathbf{T}}+\tilde{\mathbf{J}}\mathbf{u}$.

While the term $\tilde{\mathbf{J}}\cdot\nabla\mathbf{u}$ in (138) mathematically results from the Galilean invariance requirement and the mixture mass balance equation (127), its physical meaning can be understood as follows. The mass flux of a phase consists of two contributions: a transport due to the mixture bulk velocity $\mathbf{u}$, and a transport at the scale of the diffuse interfacial layer driven by the effective chemical potentials between the phases (see subsequent discussions, and Eqs. (156), (157c) and (132)). There is a momentum flux associated with the latter mass transport, and the term $\tilde{\mathbf{J}}\cdot\nabla\mathbf{u}$ represents the effect of this momentum flux.

Thanks to the fact that $\mathbf{u}$ is divergence-free, see (121), we can introduce a pressure p,

$$\mathbf{T}=-p\mathbf{I}+\mathbf{S}, \tag{139}$$

where $\mathbf{I}$ is the identity tensor, and $\mathbf{S}$ is a trace-free stress tensor. The momentum equation then becomes

$$\rho\left(\frac{\partial \mathbf{u}}{\partial t}+\mathbf{u}\cdot\nabla\mathbf{u}\right)+\tilde{\mathbf{J}}\cdot\nabla\mathbf{u}=-\nabla p+\nabla\cdot\mathbf{S}. \tag{140}$$

The constitutive form for the stress tensor $\mathbf{S}$ will be determined subsequently by invoking the second law of thermodynamics.

Specifying Constitutive Relations Let us now consider how to specify the forms for the flux vectors $\mathbf{J}_{ai}$ $(1\leqslant i\leqslant N-1)$ in (125) and the stress tensor $\mathbf{S}$ in (140) based on the second law of thermodynamics.

Suppose that we have chosen a set of $(N-1)$ order parameters $\vec{\phi}=(\phi_1,\phi_2,\cdots,\phi_{N-1})$ to characterize this N-phase system, and then the relation

$$\rho_i-\rho_N=\varphi_i=\varphi_i(\vec{\phi}) \tag{141}$$

will be known. As a result, the relations $\rho=\rho(\vec{\phi})$ and $\rho_i=\rho_i(\vec{\phi})$ can be determined thanks to Eqs. (135) and (134).

We assume that the relative motion of any two fluids is diffusive. In the spirit of the phase field approach, we introduce a free energy density function $W(\vec{\phi},\nabla\vec{\phi})$, which plays the role of the interfacial energy for the diffuse interfaces. The total energy density function is then

$$e(\mathbf{u},\vec{\phi},\nabla\vec{\phi})=\frac{1}{2}\rho(\vec{\phi})|\mathbf{u}|^2+W(\vec{\phi},\nabla\vec{\phi}), \tag{142}$$

where the first term on the right hand side denotes the kinetic energy.

We invoke the following form of the second law of thermodynamics for isothermal systems [26],

$$\frac{d}{dt}\int\limits_{\Omega(t)} e(\mathbf{u},\vec{\phi},\nabla\vec{\phi})\leqslant P_c \tag{143}$$

where $\Omega(t)$ is an arbitrary volume that is transported with the mixture velocity $\mathbf{u}$, and P_c is the conventional power expended on $\Omega(t)$. Intuitively, this means that not all conventional power expended on a system can be converted into changes in the net free- and kinetic-energy of the system, because a portion of that power must go into dissipation.

The power expended on $\Omega(t)$ consists of several components (see also [2]):

- Work done to the system due to the objective stress tensor $\mathbf{T}=-p\mathbf{I}+\mathbf{S}$,

  $$\int\limits_{\partial\Omega(t)} \mathbf{n}\cdot\mathbf{T}\cdot\mathbf{u}\,dA$$

  where $\mathbf{n}$ is the outward-pointing unit vector normal to $\partial\Omega(t)$, and dA denotes integration with respect to the surface.

- Kinetic energy transport into $\Omega(t)$ due to the relative motion with respect to the mixture velocity,

$$-\int_{\partial\Omega(t)} \sum_{i=1}^{N} \frac{1}{2}|\mathbf{u}|^2 \mathbf{n}\cdot\mathbf{J}_i dA = -\int_{\partial\Omega(t)} \frac{1}{2}|\mathbf{u}|^2 \mathbf{n}\cdot\left(\sum_{i=1}^{N}\mathbf{J}_i\right)dA = -\int_{\partial\Omega(t)} \frac{1}{2}|\mathbf{u}|^2\mathbf{n}\cdot\tilde{\mathbf{J}}dA,$$

  where $\mathbf{n}\cdot\mathbf{J}_i dA$ represents the mass transport of fluid i in unit time due to relative motion with respect to the mixture velocity, and we have used Eq. (128).
- Free energy transport into $\Omega(t)$ due to diffusion. Note our assumption about the diffusiveness of the relative motion between any two fluids. The term $\mathbf{n}\cdot(\mathbf{J}_i - \mathbf{J}_j)dA$ represents the mass change due to diffusion between fluids i and j, assuming $1 \leqslant i < j \leqslant N$. Let $\tilde{C}_{ij}$ denote the chemical potential associated with this diffusive flux. Then the total free energy transport due to diffusion is

$$-\int_{\partial\Omega(t)} \sum_{\substack{i,j=1\\ i<j}}^{N} \mathbf{n}\cdot(\mathbf{J}_i - \mathbf{J}_j)\tilde{C}_{ij} dA$$

  In light of Eq. (126), we have

$$\sum_{\substack{i,j=1\\ i<j}}^{N} \mathbf{n}\cdot(\mathbf{J}_i - \mathbf{J}_j)\tilde{C}_{ij} = \sum_{\substack{i,j=1\\ i<j}}^{N-1} \mathbf{n}\cdot(\mathbf{J}_{ai} - \mathbf{J}_{aj})\tilde{C}_{ij} + \sum_{i=1}^{N-1}\mathbf{n}\cdot\mathbf{J}_{ai}\tilde{C}_{iN} = \sum_{i=1}^{N-1}\mathbf{n}\cdot\mathbf{J}_{ai}C_i,$$

  where we have used $\mathbf{J}_i - \mathbf{J}_j = \mathbf{J}_{ai} - \mathbf{J}_{aj}$, and C_i denotes an effective chemical potential associated with $\mathbf{J}_{ai}$ and is a linear combination of $\tilde{C}_{ij}$. Therefore, the total free energy transport into $\Omega(t)$ due to diffusion can be represented by

$$-\int_{\partial\Omega(t)} \sum_{i=1}^{N-1}\mathbf{n}\cdot\mathbf{J}_{ai}C_i dA. \tag{144}$$

- Similar to [2], we assume the existence a generalized surface force $\boldsymbol{\Upsilon}_i$ $(1 \leqslant i \leqslant N-1)$ associated with ϕ_i such that

$$\sum_{i=1}^{N-1}\int_{\partial\Omega(t)} \mathbf{n}\cdot\boldsymbol{\Upsilon}_i\left(\frac{\partial\phi_i}{\partial t} + \mathbf{u}\cdot\nabla\phi_i\right)dA$$

  represents the associated work done on the system.

Therefore, the inequality (143) becomes

$$\begin{aligned}\frac{d}{dt}\int_{\Omega(t)} e(\mathbf{u},\vec{\phi},\nabla\vec{\phi}) \leqslant{}& \int_{\partial\Omega(t)} \mathbf{n}\cdot\mathbf{T}\cdot\mathbf{u}dA - \int_{\partial\Omega(t)} \frac{1}{2}|\mathbf{u}|^2\mathbf{n}\cdot\tilde{\mathbf{J}}dA \\ &- \int_{\partial\Omega(t)} \sum_{i=1}^{N-1}\mathbf{n}\cdot\mathbf{J}_{ai}C_i dA + \sum_{i=1}^{N-1}\int_{\partial\Omega(t)} \mathbf{n}\cdot\boldsymbol{\Upsilon}_i\left(\frac{\partial\phi_i}{\partial t} + \mathbf{u}\cdot\nabla\phi_i\right)dA\end{aligned} \tag{145}$$

Noting the Leibnitz theorem and the arbitrariness of $\Omega(t)$, one can obtain

$$-\mathcal{D} \equiv \frac{\partial e}{\partial t} + \nabla\cdot(e\mathbf{u}) + \sum_{i=1}^{N-1}\nabla\cdot(C_i\mathbf{J}_{ai}) + \nabla\cdot\left(\frac{1}{2}|\mathbf{u}|^2\tilde{\mathbf{J}}\right) - \sum_{i=1}^{N-1}\nabla\cdot(\dot{\phi}_i\boldsymbol{\Upsilon}_i) - \nabla\cdot(\mathbf{T}\cdot\mathbf{u}) \leqslant 0, \tag{146}$$

where $\mathcal{D}$ denotes a non-negative quantity, and $\dot{\phi}_i$ represents the material derivative $(\frac{\partial\phi_i}{\partial t} + \mathbf{u}\cdot\nabla\phi_i)$.

We transform (146) into

$$-\mathcal{D} = \frac{\partial W}{\partial t} + \mathbf{u}\cdot\nabla W + \sum_{i=1}\nabla\cdot(C_i\mathbf{J}_{ai}) - \sum_{i=1}^{N-1}\nabla\cdot(\dot{\phi}_i\boldsymbol{\Upsilon}_i) - \mathbf{T}^T : \nabla\mathbf{u} \leqslant 0 \tag{147}$$

by noting (125), (138), and the relation

$$\frac{\partial}{\partial t}\left(\frac{1}{2}\rho|\mathbf{u}|^2\right) + \mathbf{u}\cdot\nabla\left(\frac{1}{2}\rho|\mathbf{u}|^2\right) = -(\nabla\cdot\tilde{\mathbf{J}})\frac{1}{2}\rho|\mathbf{u}|^2 + (\nabla\cdot\mathbf{T})\cdot\mathbf{u} - (\tilde{\mathbf{J}}\cdot\nabla\mathbf{u})\cdot\mathbf{u}.$$

Then by noting the relations

$$\begin{cases} \nabla\cdot(C_i\mathbf{J}_{ai}) = \nabla C_i\cdot\mathbf{J}_{ai} - \displaystyle\sum_{j=1}^{N-1} C_i\frac{\partial\varphi_i}{\partial\phi_j}\dot{\phi}_j \\ \dfrac{\partial W}{\partial t} + \mathbf{u}\cdot\nabla W = \displaystyle\sum_{i=1}^{N-1}\frac{\partial W}{\partial\phi_i}\dot{\phi}_i + \sum_{i=1}^{N-1}(\nabla\phi_i)^{\bullet}\cdot\frac{\partial W}{\partial(\nabla\phi_i)} \\ \boldsymbol{\Upsilon}_i\cdot\nabla\dot{\phi}_i = \boldsymbol{\Upsilon}_i\cdot(\nabla\phi_i)^{\bullet} + (\nabla\phi_i\otimes\boldsymbol{\Upsilon}_i):\nabla\mathbf{u} \end{cases}$$

where $(\nabla\phi_i)^{\bullet} = \frac{\partial}{\partial t}(\nabla\phi_i) + \mathbf{u}\cdot\nabla(\nabla\phi_i)$ and $\otimes$ denotes the tensor product, we can transform (147) into

$$\begin{aligned} -\mathcal{D} = {} & \sum_{i=1}^{N-1}\left(\frac{\partial W}{\partial\phi_i} - \sum_{j=1}^{N-1}\frac{\partial\varphi_j}{\partial\phi_i}C_j - \nabla\cdot\boldsymbol{\Upsilon}_i\right)\dot{\phi}_i + \sum_{i=1}^{N-1}\left(\frac{\partial W}{\partial(\nabla\phi_i)} - \boldsymbol{\Upsilon}_i\right)\cdot(\nabla\phi_i)^{\bullet} \\ & - \left(\mathbf{S}^T + \sum_{i=1}^{N-1}\nabla\phi_i\otimes\boldsymbol{\Upsilon}_i\right):\nabla\mathbf{u} + \sum_{i=1}^{N-1}\nabla C_i\cdot\mathbf{J}_{ai} \leqslant 0 \end{aligned} \tag{148}$$

where we have used (125), (121), and (139).

Let us next consider specifying constitutive relations for $\mathbf{J}_{ai}$, $\mathbf{S}$, $\boldsymbol{\Upsilon}_i$, and C_i such that the inequality (148) will always be satisfied. We assume that $\mathbf{J}_{ai}$, $\mathbf{S}$, $\boldsymbol{\Upsilon}_i$ $(1\leqslant i\leqslant N-1)$ are functions of $\vec{\phi}$, $\nabla\vec{\phi}$, $\nabla\mathbf{u}$, C_k, and ∇C_k $(1\leqslant k\leqslant N-1)$ only, and that C_i do not depend on $\dot{\phi}_k$ $(1\leqslant k\leqslant N-1)$. Furthermore, we assume that $\mathbf{S}$ is a symmetric tensor. Since $\dot{\phi}_i$ and $(\nabla\phi_i)^{\bullet}$ can attain arbitrary values, and that the expressions in the first and second parentheses behind the equality sign in (148) do not depend on $\dot{\phi}_i$ and $(\nabla\phi_i)^{\bullet}$ respectively, we conclude that

$$\frac{\partial W}{\partial(\nabla\phi_i)} - \boldsymbol{\Upsilon}_i = 0, \quad 1\leqslant i\leqslant N-1, \tag{149}$$

$$\frac{\partial W}{\partial\phi_i} - \sum_{j=1}^{N-1}\frac{\partial\varphi_j}{\partial\phi_i}C_j - \nabla\cdot\boldsymbol{\Upsilon}_i = 0, \quad 1\leqslant i\leqslant N-1. \tag{150}$$

Therefore, one obtains a linear algebraic system about the chemical potentials C_i,

$$\sum_{j=1}^{N-1}\frac{\partial\varphi_j}{\partial\phi_i}C_j = \frac{\partial W}{\partial\phi_i} - \nabla\cdot\frac{\partial W}{\partial(\nabla\phi_i)}, \quad 1\leqslant i\leqslant N-1, \tag{151}$$

which can be solved for C_i $(1\leqslant i\leqslant N-1)$ once the free energy $W(\vec{\phi},\nabla\vec{\phi})$ is chosen.

The inequality (148) is reduced to

$$\begin{aligned} -\mathcal{D} = {} & -\left(\mathbf{S} + \sum_{i=1}^{N-1}\nabla\phi_i\otimes\frac{\partial W}{\partial\nabla\phi_i}\right):\frac{1}{2}\mathbf{D}(\mathbf{u}) \\ & - \frac{1}{2}\left(\sum_{i=1}^{N-1}\nabla\phi_i\otimes\frac{\partial W}{\partial\nabla\phi_i} - \sum_{i=1}^{N-1}\frac{\partial W}{\partial\nabla\phi_i}\otimes\nabla\phi_i\right):\frac{1}{2}\left(\nabla\mathbf{u} - \nabla\mathbf{u}^T\right) \\ & + \sum_{i=1}^{N-1}\nabla C_i\cdot\mathbf{J}_{ai} \leqslant 0, \end{aligned} \tag{152}$$

where $\mathbf{D}(\mathbf{u}) = \nabla\mathbf{u} + \nabla\mathbf{u}^T$. Since $\frac{1}{2}(\nabla\mathbf{u} - \nabla\mathbf{u}^T)$ is independent of $\mathbf{D}(\mathbf{u})$ and can attain arbitrary values, we conclude that

$$\sum_{i=1}^{N-1}\nabla\phi_i\otimes\frac{\partial W}{\partial\nabla\phi_i} = \sum_{i=1}^{N-1}\frac{\partial W}{\partial\nabla\phi_i}\otimes\nabla\phi_i, \tag{153}$$

which is a condition that the free energy density function $W(\vec{\phi},\nabla\vec{\phi})$ must satisfy.

The inequality (152) is then reduced to

$$-\mathcal{D} = -\left(\mathbf{S} + \sum_{i=1}^{N-1}\nabla\phi_i\otimes\frac{\partial W}{\partial\nabla\phi_i}\right):\frac{1}{2}\mathbf{D}(\mathbf{u}) + \sum_{i=1}^{N-1}\nabla C_i\cdot\mathbf{J}_{ai} \leqslant 0. \tag{154}$$

Motivated by the constitutive relation for Newtonian fluids, we assume that

$$\mathbf{S}+\sum_{i=1}^{N-1}\nabla\phi_i\otimes\frac{\partial W}{\partial\nabla\phi_i}=\mu(\vec{\phi})\mathbf{D}(\mathbf{u}) \tag{155}$$

where $\mu(\vec{\phi})\geqslant 0$ plays the role of viscosity. We further assume that

$$\mathbf{J}_{ai}=-\tilde{m}_i(\vec{\phi})\nabla C_i,\quad 1\leqslant i\leqslant N-1 \tag{156}$$

for some function $m_i(\vec{\phi})\geqslant 0$.

Therefore, the constitutive relations given by (155) and (156), where the chemical potentials C_i are given by the linear algebraic system (151), satisfy the second law of thermodynamics. The free energy density function $W(\vec{\phi},\nabla\vec{\phi})$ for the N-phase system must be chosen in a form such that the condition (153) is satisfied.

Physical Formulation Substituting the constitutive relations (155) and (156) for $\mathbf{S}$ and $\mathbf{J}_{ai}$ into Eqs. (140) and (125), we obtain the following phase field formulation for the N-phase system:

$$\rho\left(\frac{\partial\mathbf{u}}{\partial t}+\mathbf{u}\cdot\nabla\mathbf{u}\right)+\tilde{\mathbf{J}}\cdot\nabla\mathbf{u}=-\nabla p+\nabla\cdot\left[\mu(\vec{\phi})\mathbf{D}(\mathbf{u})\right]-\sum_{i=1}^{N-1}\nabla\cdot\left(\nabla\phi_i\otimes\frac{\partial W}{\partial\nabla\phi_i}\right), \tag{157a}$$

$$\nabla\cdot\mathbf{u}=0, \tag{157b}$$

$$\sum_{j=1}^{N-1}\frac{\partial\varphi_i}{\partial\phi_j}\left(\frac{\partial\phi_j}{\partial t}+\mathbf{u}\cdot\nabla\phi_j\right)=\nabla\cdot\left[\tilde{m}_i(\vec{\phi})\nabla C_i\right],\quad 1\leqslant i\leqslant N-1, \tag{157c}$$

where $\varphi_i(\vec{\phi})$ is defined in (141), $C_i(\vec{\phi})$ is given by the linear algebraic system (151), and $W(\vec{\phi},\nabla\vec{\phi})$ is the free energy density function that satisfies the condition (153). This is the general form, in which the order parameters $\vec{\phi}$ and the free energy density function $W(\vec{\phi},\nabla\vec{\phi})$ still need to be specified.

In order to simplify the form of the phase field equations (157c), we choose the set of order parameters ϕ_i such that

$$\varphi_i=\rho_i-\rho_N=\frac{1}{2}(\tilde{\rho}_i-\tilde{\rho}_N)+\frac{1}{2}(\tilde{\rho}_i+\tilde{\rho}_N)\phi_i,\quad \phi_i\in[-1,1],\ 1\leqslant i\leqslant N-1. \tag{158}$$

This choice greatly simplifies the phase field equations because $\frac{\partial\varphi_i}{\partial\phi_j}=\frac{1}{2}(\tilde{\rho}_i+\tilde{\rho}_N)\delta_{ij}$. Note that other quantities (e.g. volume fraction, mass fraction, density) can also be used as order parameters, but the resulting phase field equations will be considerably more complicated because of the matrix $[\frac{\partial\varphi_i}{\partial\phi_j}]_{(N-1)\times(N-1)}$. With the above set of order parameters, the chemical potential is given by, according to (151),

$$C_i=\frac{2}{\tilde{\rho}_i+\tilde{\rho}_N}\left[\frac{\partial W}{\partial\phi_i}-\nabla\cdot\frac{\partial W}{\partial(\nabla\phi_i)}\right],\quad 1\leqslant i\leqslant N-1. \tag{159}$$

The mixture density $\rho(\vec{\phi})$ is given by (10). We assume that the dynamic viscosity $\mathbf{u}(\vec{\phi})$ has a form given by (11).

We further choose the free energy density function $W(\vec{\phi},\nabla\vec{\phi})$ in a form given by (3). One can verify that it satisfies the condition (153) if the matrix A defined in (2) is symmetric. By assuming that all model parameters involved herein are constants and by re-scaling the parameters $\tilde{m}_i$, one can arrive at the formulation given by Eqs. (1a)–(1c) in Section 2.1.

References

[1] Federal on-scene coordinator (FOSC) report on deepwater horizon oil spill, Technical report, www.uscg.mil/foia/docs/DWH/FOSC_DWH_Report.pdf, September 2011.

[2] H. Abels, H. Garcke, G. Grün, Thermodynamically consistent, frame indifferent diffuse interface models for incompressible two-phase flows with different densities, Math. Models Methods Appl. Sci. 22 (2012) 1150013.

[3] D.M. Anderson, G.B. McFadden, A.A. Wheeler, Diffuse-interface methods in fluid mechanics, Annu. Rev. Fluid Mech. 30 (1998) 139–165.

[4] M.V. Ariyapadi, E.B. Nauman, Free energy of an inhomogeneous polymer–polymer–solvent system II, J. Polym. Sci., Part B 30 (1992) 533–538.

[5] V.E. Badalassi, H.D. Ceniceros, S. Banerjee, Computation of multiphase systems with phase field models, J. Comput. Phys. 190 (2003) 371–397.

[6] J.W. Barrett, J.F. Blowey, Finite element approximation of a model for phase separation of a multi-component alloy with nonsmooth free energy and a concentration dependent mobility matrix, Math. Models Methods Appl. Sci. 9 (1999) 627–663.

[7] G.K. Batchelor, Transport properties of 2-phase materials with random structure, Annu. Rev. Fluid Mech. 6 (1974) 227–255.

[8] R. Bonhomme, J. Magnaudet, F. Duval, B. Piar, Inertial dynamics and air bubbles crossing a horizontal fluid–fluid interface, J. Fluid Mech. 707 (2012) 405–443.

[9] F. Boyer, C. Lapuerta, Study of a three component Cahn–Hilliard flow model, ESAIM: Math. Model. Numer. Anal. 40 (2006) 653–687.

[10] F. Boyer, C. Lapuerta, S. Minjeaud, B. Piar, M. Quintard, Cahn–Hilliard/Navier–Stokes model for the simulation of three-phase flows, Transp. Porous Media 82 (2010) 463–483.

[11] F. Boyer, S. Minjeaud, Numerical schemes for a three component Cahn–Hilliard model, ESAIM: Math. Model. Numer. Anal. 45 (2011) 697–738.

[12] D.A. Cogswell, W.C. Carter, Thermodynamic phase-field model for microstructure with multiple components and phases: the possibility of metastable phases, Phys. Rev. E 83 (2011) 061602.

[13] D. de Fontaine, A computer simulation of the evolution of coherent composition variations in solid solutions, PhD thesis, Northwestern University, 1967.

[14] D. de Fontaine, An analysis of clustering and ordering in multicomponent solid solutions, I stability criteria, J. Phys. Chem. Solids 33 (1972) 297–310.

[15] P.G. de Gennes, F. Brochard-Wyart, D. Quere, Capillarity and Wetting Phenomena, Springer, 2003.
[16] S. Dong, On imposing dynamic contact-angle boundary conditions for wall-bounded liquid–gas flows, Comput. Methods Appl. Mech. Eng. 247–248 (2012) 179–200.
[17] S. Dong, An outflow boundary condition and algorithm for incompressible two-phase flows with phase field approach, J. Comput. Phys. 266 (2014) 47–73.
[18] S. Dong, G.E. Karniadakis, C. Chryssostomidis, A robust and accurate outflow boundary condition for incompressible flow simulations on severely-truncated unbounded domains, J. Comput. Phys. 261 (2014) 83–105.
[19] S. Dong, J. Shen, An unconditionally stable rotational velocity-correction scheme for incompressible flows, J. Comput. Phys. 229 (2010) 7013–7029.
[20] S. Dong, J. Shen, A time-stepping scheme involving constant coefficient matrices for phase field simulations of two-phase incompressible flows with large density ratios, J. Comput. Phys. 231 (2012) 5788–5804.
[21] C.M. Elliott, H. Garcke, Diffusional phase transition in multicomponent systems with concentration dependent mobility matrix, Physica D 109 (1997) 242–256.
[22] C.M. Elliott, S. Luckhaus, A generalized diffusion equation for phase separation of a multicomponent mixture with interface free energy, IMA preprint, 887, 1991.
[23] D.J. Eyre, Systems of Cahn–Hilliard equations, SIAM J. Appl. Math. 53 (1993) 1686–1712.
[24] D. Gottlieb, S.A. Orszag, Numerical Analysis of Spectral Methods: Theory and Applications, SIAM–CMBS, 1977.
[25] J.L. Guermond, J. Shen, Velocity-correction projection methods for incompressible flows, SIAM J. Numer. Anal. 41 (2003) 112–134.
[26] M.E. Gurtin, E. Fried, L. Anand, The Mechanics and Thermodynamics of Continua, Cambridge University Press, 2010.
[27] M. Heida, J. Malek, K.R. Rajagopal, On the development and generalization of Cahn–Hilliard equations within a thermodynamic framework, Z. Angew. Math. Phys. 63 (2012) 145–169.
[28] J.J. Hoyt, Spinodal decomposition in ternary alloys, Acta Metall. 38 (1989) 2489–2497.
[29] J.J. Hoyt, The continuum theory of nucleation in multicomponent systems, Acta Metall. 38 (1990) 1405–1412.
[30] Y. Inoue, Y. Chen, H. Ohashi, A mesoscopic simulation model for immiscible multiphase fluids, J. Comput. Phys. 201 (2004) 191–203.
[31] R. Jackson, Dynamics of Fluidized Particles, Cambridge University Press, 2000.
[32] D. Jacqmin, Calculation of two-phase Navier–Stokes flows using phase-field modeling, J. Comput. Phys. 155 (1999) 96–127.
[33] G.E. Karniadakis, S.J. Sherwin, Spectral/hp Element Methods for Computational Fluid Dynamics, 2nd ed., Oxford University Press, 2005.
[34] J. Kim, Phase field computations for ternary fluid flows, Comput. Methods Appl. Mech. Eng. 196 (2007) 4779–4788.
[35] J. Kim, A generalized continuous surface tension force formulation for phase-field models for multi-component immiscible fluid flows, Comput. Methods Appl. Mech. Eng. 198 (2009) 3105–3112.
[36] J. Kim, Phase-field models for multi-component fluid flows, Commun. Comput. Phys. 12 (2012) 613–661.
[37] J. Kim, K. Kang, J. Lowengrub, Conservative multigrid methods for ternary Cahn–Hilliard systems, Commun. Math. Sci. 2 (2004) 53–77.
[38] J. Kim, J. Lowengrub, Phase field modeling and simulation of three-phase flows, Interfaces Free Bound. 7 (2005) 435–466.
[39] I. Langmuir, Oil lenses on water and the nature of monomolecular expanded films, J. Chem. Phys. 1 (1933) 756.
[40] H.G. Lee, J.-W. Choi, J. Kim, A practically unconditionally gradient stable scheme for the n-component Cahn–Hilliard system, Physica A 391 (2012) 1009–1019.
[41] H.G. Lee, J. Kim, Buoyancy-driven mixing of multi-component fluids in two-dimensional tilted channels, Eur. J. Mech. B, Fluids 42 (2013) 37–46.
[42] J. Li, Q. Wang, A class of conservative phase field models for multiphase fluid flows, J. Appl. Mech. 81 (2014) 021004.
[43] C. Liu, J. Shen, A phase field model for the mixture of two incompressible fluids and its approximation by a Fourier-spectral method, Physica D 179 (2003) 211–228.
[44] J. Lowengrub, L. Truskinovsky, Quasi-incompressible Cahn–Hilliard fluids and topological transitions, Proc. R. Soc. Lond. A 454 (1998) 2617–2654.
[45] S. Matsutani, K. Nakano, K. Shinjo, Surface tension of multi-phase flow with multiple junctions governed by the variational principle, Math. Phys. Anal. Geom. 14 (2011) 237–278.
[46] B. Merriman, J.K. Bence, S.J. Osher, Motion of multiple junctions – a level set approach, J. Comput. Phys. 112 (1994) 334–363.
[47] J.E. Morral, J.W. Cahn, Spinodal decomposition in ternary systems, Acta Metall. 19 (1971) 1037–1045.
[48] S.J. Osher, J.A. Sethian, Fronts propagating with curvature dependent speed: algorithms based on Hamilton–Jacobi formulations, J. Comput. Phys. 79 (1988) 12–49.
[49] S.U. Pickering, Emulsions, J. Chem. Soc. 91 (1907) 2001–2021.
[50] R.I. Saye, J.A. Sethian, The Voronoi implicit interface method for computing multiphase physics, Proc. Natl. Acad. Sci. USA 108 (2011) 19498–19503.
[51] R. Scardovelli, S. Zaleski, Direct numerical simulation of free-surface and interfacial flow, Annu. Rev. Fluid Mech. 31 (1999) 567–603.
[52] J.A. Sethian, P. Semereka, Level set methods for fluid interfaces, Annu. Rev. Fluid Mech. 35 (2003) 341–372.
[53] K.A. Smith, F.J. Solis, D.L. Chopp, A projection method for motion of triple junctions by level sets, Interfaces Free Bound. 4 (2002) 263–276.
[54] G.I. Taylor, The formation of emulsions in definable fields of flow, Proc. R. Soc. Lond. A 146 (1934) 501–523.
[55] G. Tryggvason, B. Bunner, A. Esmaeeli, et al., A front-tracking method for computations of multiphase flow, J. Comput. Phys. 169 (2001) 708–759.
[56] A. Villa, L. Formaggia, Implicit tracking for multi-fluid simulations, J. Comput. Phys. 229 (2010) 5788–5802.
[57] P. Yue, J.J. Feng, C. Liu, J. Shen, A diffuse-interface method for simulating two-phase flows of complex fluids, J. Fluid Mech. 515 (2004) 293–317.
[58] H.-K. Zhao, T. Chan, B. Merriman, S. Osher, A variational level set approach to multiphase motion, J. Comput. Phys. 127 (1996) 179–195.
[59] W. Zheng, J.-H. Yong, J.-C. Paul, Visual simulation of multiple unmixable fluids, J. Comput. Sci. Technol. 22 (2007) 156–160.
[60] X. Zheng, S. Dong, An eigen-based high-order expansion basis for structured spectral elements, J. Comput. Phys. 230 (2011) 8573–8602.
[61] S. Zlotnik, P. Diez, Hierarchical X-FEM for n-phase flow ($n > 2$), Comput. Methods Appl. Mech. Eng. 198 (2009) 2329–2338.